Facoltà di Scienze Matematiche, Fisiche e Naturali
Dipartimento di Biologia
Scuola Dottorale in Biologia
Sezione di Biologia Applicata alla Salute dell'Uomo

XXIV ciclo

THE BINDING VERSATILITY OF HUMAN SERUM ALBUMIN AND ITS ALLOSTERIC MODULATION

MODULAZIONE ALLOSTERICA DELLE PROPRIETA' LEGANTI DELLA SIERO ALBUMINA UMANA

PhD student
Dr. Cao Yu

Tutor
Prof. Paolo Ascenzi

Coordinator of the PhD School Section
"Biology Applied to Human Health"
Prof. Paolo Visca

A.A. 2010/2011

Index

1. Abstract

Human serum albumin (HSA), the most prominent protein in plasma, is best known for its exceptional ligand binding capacity. Seven binding sites for fatty acids (FA; FA1-FA7) have been found to be common for FAs ranging from C10:0 to C18:0; however, nine clefts can bind C10:0 FAs. Moreover, defatted HSA binds four thyroxine molecules at FA3-FA4, FA5, and FA7; on the other hand, the HSA-FA complex binds one thyroxine molecule at the II-III interdomain region (*i.e.*, FA9). Furthermore, HSA binds the GA module of the bacterial protein PAB at domain II; this seems to add selective advantages to the bacterium in terms of growth, increasing its virulence by providing to the bacteria FAs and, possibly, other nutrients transported by HSA. Lastly, HSA displays three binding sites endowed with appropriate residues to coordinate metal ions. Remarkably, HSA participates in heme scavenging by binding the macrocycle at the FA1 site. In turn, heme endows HSA with globin-like reactivity and spectroscopic properties. Notably, ligand binding to HSA is competitively and allosterically modulated. To highlight the molecular bases of the allosteric and competitive binding properties of HSA, the following aspects have been investigated. (*i*) The reductive nitrosylation of ferric human serum heme-albumin (HSA-heme-Fe(III)) has been investigated from the kinetic and thermodynamic viewpoints. At pH = 5.5, HSA-heme-Fe(III) binds NO reversibly, leading to the formation of nitrosylated HSA-heme-Fe(III) (HSA-heme-Fe(III)-NO). By contrast, at pH≥6.5, the addition of NO to HSA -heme-Fe(III) leads to the transient formation of HSA-heme-Fe(III)-NO that precedes the formation of ferrous nitrosylated human serum heme-albumin (HSA-heme-Fe(II)-NO). The rate-limiting step for reductive nitrosylation of HSA-heme-Fe(III) is represented by the OH^--mediated reduction of HSA-heme-Fe(II)-NO^+ to HSA-heme-Fe(II). (*ii*) Carbonylation of ferrous heme-albumin (HSA-heme-Fe(II)) has been studied from both kinetic and spectroscopic

viewpoints. The heme-Fe(II) atom is a mixture of a four-coordinate intermediate-spin species (predominant at pH 5.8 and 7.0), a five-coordinate high-spin form (mainly at pH 7.0), and a six-coordinate low-spin species (predominant at pH 10.0). The acidic-to-alkaline reversible transition reflects conformational changes leading to the coordination of the heme-Fe(II) atom by the His146 residue. The presence of several HSA-heme-Fe(II) species accounts for the complex, multi-exponential kinetics observed, and reflects the very slow interconversion between the different species observed both for CO association and dissociation as a function of pH. (*iii*) HSA-heme-Fe(II) nitrosylation has been investigated from the kinetic viewpoint. Ibuprofen and warfarin binding to FA2 and FA7 sites, respectively, inhibit allosterically HSA-heme-Fe(II) nitrosylation. Remarkably, the affinity of ibuprofen and warfarin for HSA-heme-Fe(II) is different from that for drug binding to HSA and HSA-heme-Fe(III), indicating that both heme binding and the redox state of the heme-Fe atom affect allosterically HSA(-heme-Fe) properties. (*iv*) Δ9-tetrahydrocannabinol (THC) and diazepam binding to HSA and HSA-heme-Fe(III) has been investigated from both thermodynamic and spectrophotometric viewpoints. THC binds to the FA2 and FA7 sites of HSA with very different affinity without affecting diazepam association. THC binding to the high-affinity FA2 site accounts for the low free fraction of the drug in plasma, and increases allosterically the heme-Fe(III) affinity for the FA1 site. Possibly, the HSA conformational transition(s) induced by THC binding could account for drug delivery to the liver through receptor-mediated endocytosis. As a whole, the present data highlight: (*ii*) the binding mode of drugs to HSA(-heme-Fe), (*ii*) the reactivity of HSA-heme-Fe(III) and HSA-heme-Fe(II), and (*iii*) the allosteric modulation mechanism(s) of HSA(-heme-Fe).

2. Riassunto

L’albumina umana (HSA) è la più abbondante proteina plasmatica, infatti la sua concentrazione è pari a circa 700 μM, e rappresenta il 60% di tutte le proteine plasmatiche. Bassi valori plasmatici della HSA riflettono una ridotta produzione della proteina da parte del fegato. La capacità di sintetizzare la HSA è compromessa nelle epatopatie gravi quali l'emocromatosi, le epatiti croniche e la cirrosi epatica. Nel corso di tali patologie, la variazioni della concentrazione plasmatica della HSA costituiscono un importante indice diagnostico e prognostico. Inoltre, la presenza della HSA nell'urina è un importante marcatore di disfunzioni renali.

La HSA è essenziale per la regolazione ed il mantenimento della pressione oncotica. Inoltre, la HSA è caratterizzata da una straordinaria capacità di legare sostanze di origine endogena ed esogena. Pertanto, la HSA svolge la funzione di deposito e di trasporto di numerosi composti fra cui gli ormoni, la bilirubina, l’eme e gli acidi grassi (FA). Inoltre, la HSA influenza la solubilità e le proprietà farmacocinetiche di molti farmaci, coopera all’inattivazione di composti tossici, svolge un ruolo anti-ossidante e possiede proprietà enzimatiche.

La HSA è una proteina caratterizzata da una singola catena polipeptidica non-glicosilata composta da 585 amino acidi. La HSA è caratterizzata da una struttura secondaria di sola α-elica ed ha una forma detta “a cuore”. La HSA è costituita da tre domini omologhi (I, II e III) ciascun dominio formato da due sottodomini (A e B). Le regioni che uniscono i sottodomini non hanno struttura secondaria definita. Le regioni che uniscono i domini I-II (residui 173-205) e II-III (residui 336-398) sono regioni ad α-elica ciascuna caratterizzata da circa 9 spire. Nonostante la somiglianza strutturale, ciascun dominio interagisce con i domini vicini con diverse modalità, pertanto l’orientazione dei domini I-II rispetto ai domini II-III è

nettamente diversa e ciò comporta un'organizzazione strutturale altamente asimmetrica.

L'HSA presenta numerosi siti di legame con proprietà molto diverse. Infatti, la HSA è in grado di legare sette equivalenti di FA a catena lunga nei siti FA1-FA7 e nove equivalenti di FA a catena corta nei siti FA1-FA9. Secondo la nomenclatura di Sudlow, gli anioni eterociclici si legano preferenzialmente al sito I (localizzato nel sottodominio IIA; FA7), mentre il sito II (localizzato nel sottodominio IIIA; FA3-FA4) lega composti aromatici caratterizzati da almeno un gruppo carbossilico. Il warfarin, un farmaco ad azione anti-coagulante, e l'ibuprofene, un agente anti-infiammatorio non-steroideo, sono considerati, rispettivamente, i leganti modello dei siti Sudlow I e II. Inoltre, in assenza di FA, la HSA è in grado di legare quattro equivalenti di tiroxina nei siti FA3-FA4, FA5 e FA7. Viceversa, la HSA lega un solo equivalente di tiroxina in presenza di FA nella cavità compresa fra domini I e III (FA9). La HSA lega anche proteine di batteri patogeni con funzioni di trasportatori. Tali macromolecule sottraggono alla HSA FA e metaboliti indispensabili per la crescita dei batteri, pertanto sono considerate fattori di virulenza. Infine, la HSA lega i metalli a diversi siti. Il primo sito è localizzato nella regione *N*-terminale dove gli ioni Cu(II), Co(II) e Ni(II) sono coordinati dagli atomi di azoto dei residui Asp1, Ala2, e His3. Il secondo sito è rappresentato dall'atomo di zolfo del residuo Cys34 in grado di legare gli ioni Au(I), Hg(II) e Pt(II). Il terzo sito di legame è detto "multimetal binding site" o sito A del cadmio (MBS-A) e vede la partecipazione dei residui His67, Asn99, His247 e Asp249. Recentemente, la presenza di un sito secondario per il legame dello ione Cd(II), detto sito B del cadmio (MBS-B), è stata ipotizzata. Infine, non si può escludere la presenza di altri siti per il legame di ioni metallici nella HSA.

Il legame di composti endogeni ed esogeni alla HSA è modulato da meccanismi di tipo allosterico e competitivo. In particolare, gli acidi grassi, di cui la HSA è considerate un

importante trasportatore sono in grado di modularne la reattività. Parimenti, la HSA va incontro a molteplici variazioni conformazionali in funzione del pH.

Fra le diverse funzioni della HSA merita ricordare il ruolo svolto nella rimozione dell'eme dal circolo, cedendolo all'emopessina che lo trasporta al fegato. In particolare, poiché la concentrazione plasmatica dell'emopessina (circa 10 μM) è nettamente inferiore a quella della HSA, quest'ultima funge da deposito dell'eme soprattutto nei soggetti affetti da patologie, quali l'anemia emolitica grave e la sindrome da schiacciamento, che sono caratterizzate dal notevole aumento dell'eme libero nel sangue.

Il sito primario di legame dell'eme alla HSA è detto FA1, una cavità idrofobica posta nel sotto-dominio IB. L'eme è stabilizzato da interazioni π-π con i residui Tyr138 e Tyr161, l'atomo di ferro dell'eme è debolmente coordinato dal gruppo fenolico del residuo Tyr161, e i propionati dell'eme formano ponti salini con i residui Arg114 e Lys190. Inoltre, l'eme è legato alla HSA per effetto della regione polipeptidica che unisce i sottodomini IA e IB.

Il legame dell'eme alla HSA rende tale complesso (noto come emoalbumina; HSA-eme) non dissimile dalle emoproteine, quali la mioglobina, dal punto di vista spettroscopico e funzionale. E' interessante osservare come il legame dell'eme alla HSA e la reattività della HSA-eme siano modulate da molecole endogene ed esogene (quali metaboliti e farmaci).

Al fine di chiarire le basi molecolari dei meccanismi di natura allosterica della HSA, in assenza ed in presenza di eme sono stati studiati: (1) il processo di nitrosilazione dell derivato ferrico della HSA-eme (HSA-eme-Fe(III)), (2) la reattività verso il CO del derivato ferroso della HSA-eme (HSA-eme-Fe(II)), (3) la reattività verso il NO della HSA-eme-Fe(II), e (4) il legame del Δ9-tetraidrocannabinolo (TIC) e del diazepam alla HSA e alla HSA-eme-Fe(III).

La reazione del NO con la HSA-eme-Fe(III) è stata studiata dal punto di vista cinetico e termodinamico. A pH = 5.5, la HSA-eme-Fe(III) reagisce reversibilmente con il NO dando luogo alla specie nitrosilata HSA-eme-Fe(III)-NO. Viceversa, a pH $\geq$6.5, il legame del NO alla HSA -eme-Fe(III) comporta la formazione della specie transiente HSA-eme-Fe(III)-NO che precede la formazione della specie stabile HSA-eme-Fe(II)-NO. Lo stadio limitante la reazione di riduzione della HSA-eme-Fe(III) da parte del NO è rappresentato dalal riduzione dell'atomo di ferro dell'eme da parte della specie OH^- del derivato HSA-eme-Fe(II)-NO^+ a HSA-eme-Fe(II).

Il processo di carbonilazione della HSA-eme-Fe(II) è stato studiato dal punto di vista cinetico e spettroscopico. Il centro di reazione della HSA-eme-Fe(II) rappresentato dall'atomo Fe(II) dell'eme è presente sotto forma di un insieme di diversi stati di coordinazione. Pertanto, a pH = 5.8 prevale la forma tetra-coordinata, a pH = 5.8 e 7.0 sono presenti entrambe le forme tetra-coordinata e penta-coordinata e a pH = 10.0 prevale la forma esa-coordinata. La transizione reversibile acido-base riflette le variazioni conformazionali che comportano la coordinazione dell'atomo di Fe(II) dell'eme da parte del residuo His146. La coesistenza di diverse specie della HSA-eme-Fe(II) è presupposto del complesso quadro cinetico, inatteso per un'emoproteina monomerica, e riflette la lenta interconversione fra le diverse specie sia nel corso dei processi di associazione e dissociazione del CO sia per effetto delle variazioni del pH.

Il processo di nitrosilazione della HSA-eme-Fe(II) è stato studiato dal punto di vista cinetico, in assenza ed in presenza dell'ibuprofene e del warfarin. L'ibuprofene ed il warfarin si legano rispettivamente ai siti FA2 and FA7, inibendo con meccanismi di tipo allosterico il processo di nitrosilazione della HSA-eme-Fe(II). E' interessante osservare come l'affinità dell'ibuprofene e del warfarin per la HSA-eme-Fe(II) sia diversa da quella di entrambi i farmaci per la HSA e la HSA-eme-Fe(III). Ciò implica che sia il legame dell'eme alla HSA sia lo stato redox

dell'atomo di Fe dell'eme modulino con meccanismi di tipo allosterico le proprietà della HSA(-eme-Fe).

Il legame del TIC e del diazepam alla HSA e alla HSA-eme-Fe(III) è stato studiato dal punto di vista termodinamico e spettrofotometrico. Il TIC si lega ai siti FA2 e FA7 della HSA e della HSA-eme-Fe(III) con affinità molto diverse senza influenzare il legame del diazepam. Il legame del TIC al sito FA2 a maggiore affinità è in accordo con il fatto che la frazione libera del farmaco nel plasma è molto bassa. Inoltre, il legame del TIC alla HSA aumenta l'affinità dell'eme-Fe(III) per il sito FA1 mediante un meccanismo di tipo allosterico. Le variazioni conformazionali indotte dal legame del TIC alla HSA potrebbero essere rilevanti in relazione ai meccanismi di rilascio del farmaco agli epatociti mediante il processo di endocitosi dipendente da recettori ancorché aspecifici.

L'insieme di questi studi ha permesso di descrivere a livello atomico i meccanismi allosterici che modulano la reattività dei siti FA1, FA2, FA6, e FA7 localizzati nei domini I e II della HSA. In particolare, a seguito dell'interazione dei leganti, la α-elica che unisce i siti FA1, FA2, FA6 e FA7 va incontro ad una rotazione di circa 16° modificando i contatti che hanno luogo fra il dominio I ed il dominio II. Inoltre, a seguito dell'interazione dei leganti, il residuo Tyr150 (presente nel sito FA7) induce una variazione conformazionale del residuo Phe149 (presente nel sito FA1). Ciò è in accordo con l'evidenza sperimentale secondo cui la regione della HSA la cui reattività è modulata da meccanismi di tipo allosterico è formata dai domini I e II (in cui sono contenuti i siti FA1, FA2, FA6 e FA7), ma non dal dominio III (in cui è presente il sito FA3-FA4).

In conclusione, alcune considerazioni di ordine bio-medico. Le variazioni della concentrazione plasmatica dell'eme, dei metaboliti e dei farmaci, ovvero la reattività della HSA-eme-Fe, possono variare in modo anche drastico per effetto della modulazione reciproca delle proprietà di legame, con conseguenze indesiderate. In particolare, l'aumento dei livelli

plasmatici dell'eme (dovuti ad esempio ad una grave anemia emolitica) può indurre il rilascio di metaboliti e farmaci legati alla HSA, determinando un aumento della loro bio-disponibilità e quindi il rischio di intossicazione dei pazienti. Analogamente, la concentrazione plasmatica dell'eme potrebbe aumentare nei pazienti a seguito di somministrazione di farmaci quali il warfarin e l'ibuprofene. Pertanto, la modulazione della reattività della HSA da parte di farmaci e metabolici è rilevante nella terapia clinica. Infine, la capacità della HSA di legare l'eme ha suggerito la possibilità di sviluppare forme ingegnerizzate di tale emoproteina in grado di legare reversibilmente lo O_2 per scopi terapeutici. Ciò rappresenta un'alternativa all'emotrasfusione, senza il limite dell'isto-compatibilità ed il rischio della contaminazione da agenti patogeni.

3. Who's who ?

The name *albumin* derives from the early German term *albumen*, generally indicating proteins. *Albumen*, on the other hand, derives from the Latin word *albus* (white) indicating the white part of the cooked egg surrounding the yolk. The protein component of the egg white makes part of a heterogeneous group of proteins, broadly indicated as albumins, including serum albumin (SA), milk albumin, urinary proteins, and the secretion of the snail. More specifically, SA is a member of a family of homologous proteins characterized by distinctive structural features and peculiar ligand binding properties. Members of this family are α-fetoprotein, afamin (also named α-albumin), and vitamin D binding protein [1-3].

Human serum albumin (HSA), one of the most abundant protein in plasma (~ 7.5×10^{-4} M), is characterized by an extraordinary ligand binding capacity. HSA provides a depot and carrier for many compounds (including drugs), affects pharmacokinetics of many drugs, facilitates the metabolic modification of some ligands, renders potential toxins harmless by transporting them to disposal sites, accounts for most of the antioxidant capacity of human serum, and displays (pseudo-) enzymatic properties [1,3-20].

Some physiological and pathological properties of HSA were recognized in 400 BC by Hippocrates of Cos, who reported in *Aphorisms* that a foamy urine, in all likelihood caused by the presence of HSA, indicates kidney disease. SA was named a century and half ago and deeply investigated over the last century. In particular: in 1932, HSA was separated from plasma proteins; in 1934, HSA was crystallized; in 1939, the neutral-to-acid (*i.e.*, N-to-F) conformational transition was detected; in 1940, HSA was purified for intravenous use as a blood substitute; in 1954, the first two cases of analbuminemia were reported; in 1960, the HSA "domain" structure was proposed; in 1975, the primary structure of HSA was deduced, and the characterization of

specific drug binding sites started; in 1979, the HSA gene was isolated; in 1981, the nucleotide sequence of HSA cDNA was reported; in 1986, the complete gene sequence of HSA was determined, and the expression, the accompanying cleavage, and the secretion of HSA from cultured yeast *Saccharomyces cerevisiae* was reported; starting from 1989, many HSA mutations were localized; in 1992, the "heart-shaped" three-dimensional structure of HSA was determined; in 1995, the ferrous tetraphenylporphirinatoiron (FeP(II)) was incorporated in HSA to obtain a red blood cell substitute; in 1999, the role of HSA in heme scavenging was highlighted, and HSA-heme was engineered to become a O_2 carrier; starting from 2001, the detoxifying role of HSA-heme towards nitrogen and oxygen reactive species was underlined (see [1,3]).

4. The HSA structure

HSA is a α-helical protein (67% α-helix) consisting of a single polypeptide chain of 585 amino acids residues arranged in a globular heart-shaped conformation containing three homologous domains (labeled I, II, and III). Each domain is made up by two separate helical sub-domains (named A and B), connected by random coils. Terminal regions of sequential domains contribute to the formation of inter-domain, 9-turn-long helices linking sub-domain IB to IIA (residues 173-205), and sub-domain IIB to IIIA (residues 336-398), respectively. Despite their structural similarity, each domain interacts with the neighbor domain(s) in different ways. Therefore, the orientation of domains I-II with respect to domains II-III constitutes a highly asymmetric environment where a variety of ligand binding sites are distributed (Fig. 1) [3,7,13,19-21].

The extraordinary ligand binding properties of HSA reflect its multidomain organization. The complex mechanism modulating ligand binding to HSA represents one of the most

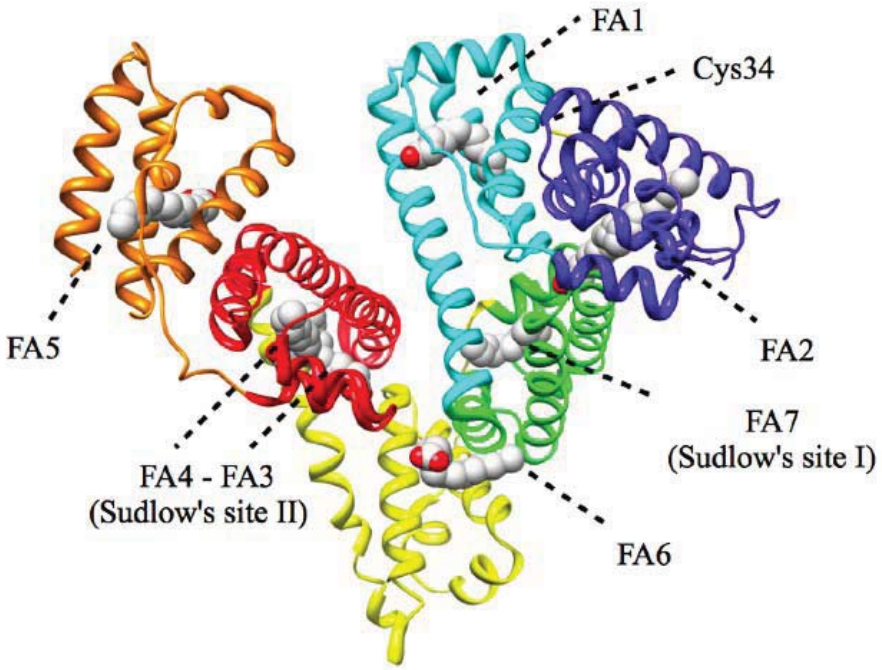

Fig. 1. FA-bound HSA structure. HSA is rendered with ribbons colored as follows: subdomain IA, blue; subdomain IB, cyan; subdomain IIA, green; subdomain IIB, yellow; subdomain IIIA, red; subdomain IIIB, orange. The 8 myristate ions are rendered as spacefill in gray. The FA binding sites and the Cys34 residue are labeled. The atomic coordinates have been retrieved from the PDB entry 1E7G [22]. The picture was drawn with Chimera [86].

important structure-function correlations ever reported for monomeric proteins. Thus, it is a potential contender for being a molecular cargo/or nanovehicle for clinical, biophysical and industrial purposes [3,13,15,20,21].

4.1. The fatty acid binding sites

HSA serves as a main FA binding protein which overcomes the low aqueous solubility of FAs, hence greatly amplifies transporting capacity of the plasma. The structural and functional aspects of FAs binding to HSA as the primary endogenous ligand have been intensively studied over half of the century [3].

Seven binding sites, namely FA1-7, are found to be common for FAs ranging from C10:0 to C18:0, as revealed by crystallographic analysis (Fig. 1). Up to nine binding sites are found to occur only upon the co-crytallisation with C10:0 FA (*i.e.*, FA1-FA9). However, the binding sites FA8 and FA9 do not appear to be physiologically relevant [22].

Studies by NMR, combining mutagenesis, and drug competition have revealed FA2, FA4 and FA5 as the highest affinity sites for long chain FAs such as palmitic acid (C16:0), and the secondary binding sites corresponding to FA1, FA3, FA6 and FA7 [23]. From a structural point of view, the highest affinity binding sites not only provide the more enclosed hydrophobic environment to secure the methylene tails, but also offers more basic amino acid to anchor the carboxylate head of FAs via salt bridges. Couriously, even if FA3 provides greater coordination for carboxyl group, the obglided bent conformation for the methylene unfavors energetically the FA binding. Instead for FA6 and FA7, there's not a specific coordination of the carboxylate group and basic or polar side chains. Notably, the cavity of FA1 is structurally well-adapted to bind heme with high affinity, so FA binding maybe serve as secondary function [22,23].

The seven binding sites are distributed asymetrically across the homologos domains of HSA and display considerable

topological differences: FA1, FA4, FA5 and FA7 are contained within a single sub-domain; FA2 and FA3 are at the interface between two domains; instead FA6 locates at interface of IIA and IIB within the same domain [19]. These binding sites also provide accommodation for a large number of endogenous and exogenous ligands, including heme, thyroxine, and a wide variety of drugs, displaying appreciable affinity for one or more binding sites [13]. The effects of FAs occupancy on the binding of other ligands, involving both competition and allostery, is of great physiological and pharmakinetic importance [3].

4.1.1. The FA1 cleft (heme pocket)

The FA1 cleft (heme pocket) is located in a cavity in the centre of the four-helix bundle of sub-domain IB. In the absence of FA, the L-shaped binding pocket is closed by Tyr138 that stacks with Tyr161, whereas upon FA binding the Tyr side-chains rotate through about 90° and their phenyl rings hold the lipid in a hydrophobic clamp. All FAs bind to FA1 in the same orientation with the carboxylate group hydrogen-bonded to Arg117 and to a water molecule that is also coordinated by the side-chain hydroxyl group of Tyr161 and the carbonyl oxygen atom of Leu182. For long-chain saturated FAs, the tail curls around the inside surface of the cavity so that the tip of the hydrophobic tail gradually approaches His146 at the lower end of the cavity opening [22].

FA1 partially corresponds to the heme binding site. Heme binding induces a dramatic conformational change(s) of the FA1 cleft (which appears D-shaped) with the reorientation of Tyr138 and Tyr161 residues that provide π-π stacking interaction with the porphyrin and supply a donor oxygen (from Tyr161) for the pentacoordinate iron. Heme-Fe(III) is secured by the long IA-IB connecting loop that fits into the cleft opening. Heme-Fe(III) propionates point toward the interface between domains I and III and are stabilized by salt bridges with Arg114, His146, and Lys190 residues (Fig. 2) [3,24,25].

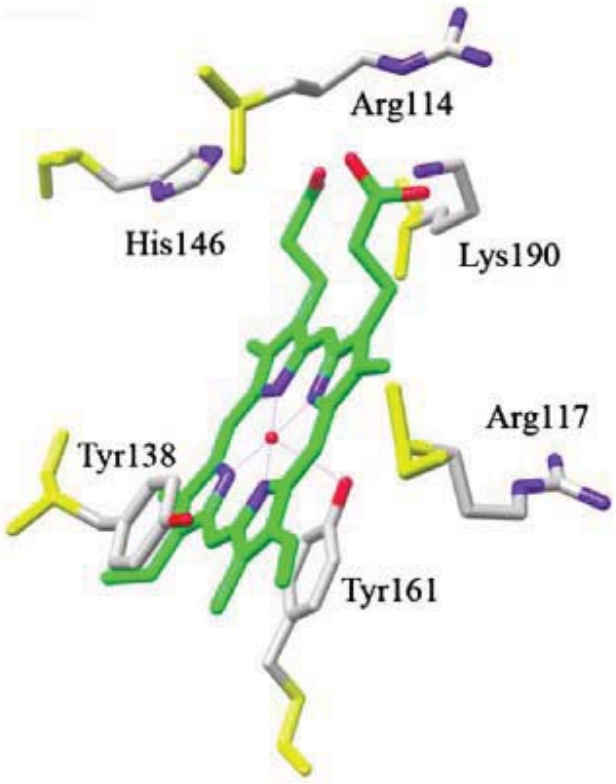

Fig. 2. Schematic representation of the heme cleft (FA1) of HSA. The heme cleft is presented in the same orientation as Fig. 1. Heme carbon atoms are colored in green and backbone atoms of the residues building up the site are colored in yellow. The atomic coordinates have been retrieved from the PDB entry IN5U [24]. The picture was drawn with Chimera [86].

Values of thermodynamic and kinetic parameters for heme-Fe(III) binding to HSA are $K_d = 1.2\times10^{-8}$ M, $k_{on} = 7.4\times10^{5}$ M^{-1} s^{-1}, and $k_{off} = 9.6\times10^{-3}$ s^{-1} [12]. Remarkably, heme-Fe(III) binding to HSA is modulated allosterically and inhibited competitively [3,12,20].

HSA binds also bilirubin and fusidic acid in sub-domain IB, in close proximity to the heme site. However, bilirubin and fusidic acid do not induce the large conformational changes as reported for heme binding [26].

4.1.2. The FA2 cleft

The FA2 cleft is located between sub-domains IA and IIA and it is one of the most enclosed FA binding sites of HSA. FA binding to FA2 stabilizes the HSA B-conformation modulating allosteric properties [3,20,27,28]. The carboxylate head-groups of FAs are anchored in sub-domain IIA by hydrogen bond interactions to the side-chains of Tyr150, Arg257 and Ser287. The methylene tail extends linearly within the narrow hydrophobic cavity formed by realignment of sub-domains IA and IIA [22]. Eventually, FA2 has been suggested to be a third binding site of ibuprofen [3,18,29,30].

4.1.3. The FA3-FA4 cleft (Sudlow's site II)

The FA3 and FA4 clefts are composed of six helices and are located in a large cavity in sub-domain IIIA that as a whole constitutes Sudlow's site II. This cleft is preferred by aromatic carboxylates with an extended conformation, the non-steroideal anti-inflammatory drug ibuprofen representing the prototypical ligand [1,3-5,7,14,19,31-35].

In FA3, the head-groups of FAs are hydrogen bonded to Ser342 and Arg348 from the IIB sub-domain, and Arg485 from the IIIA sub-domain. In FA4, the carboxylate head-groups of FAs are hydrogen bonded by Arg410, Tyr411 and Ser489. The methylene tails of FA bound to FA3 and FA4 are located in hydrophobic tunnels within domain III [14,19,22].

Drugs (*e.g.*, ibuprofen) cluster in the center of Sudlow's site II, interacting with the hydroxyl group of Tyr411; Arg410 and Ser489 residues also contribute with salt-bridge and hydrogen-bond interactions to drug binding (Fig. 3) [14,19]. The values of the dissociation equilibrium constant for ibuprofen binding to FA3-FA4 is $K_d = 1\times10^{-6}$ M [36,37]. Remarkably, ibuprofen binding to HSA is inhibited competitively [14].

4.1.4. The FA5 cleft

FA5 is formed by a hydrophobic channel located in sub-domain IIIB. A single FA molecule binds in an extended conformation; the carboxylate head-group of the bound FA interacts with the side chains of Lys525 and Tyr401, while the methylene tail extends into the tunnel [22].

4.1.5. The FA6 cleft

The FA6 cleft is located at the interface between sub-domains IIA and IIB and is occupied by both medium and long-chain FAs. This cleft is significantly different from FA1-FA5 sites; in fact, there is not a cluster of amino acid side-chains that stabilize electrostatically the FA carboxylate. The middle portion of the methylene tail is well anchored by salt-bridges from Arg209 to both Asp324 and Glu354 [22,23]. Noteworthy, FA6 has been reported to be the ibuprofen secondary binding site [14].

4.1.6. The FA7 cleft (Sudlow's site I)

The hydrophobic cavity of sub-domain IIA hosts the seventh FA binding site (*i.e.*, FA7 or Sudlow's site I). This site binds preferentially bulky heterocyclic anions, the prototypical ligand being warfarin [1,3,4,5,7,14,19,31,32,34,35].

The FA carboxylate is stabilized by polar interaction(s) with the Arg257 residue, thus providing a bridge between FA2 and FA7 sites. The basic residues Lys199, Arg218, Arg222, and His242 do not appear to be directly involved in FA binding, but could actively participate to the stabilization of other ligands in

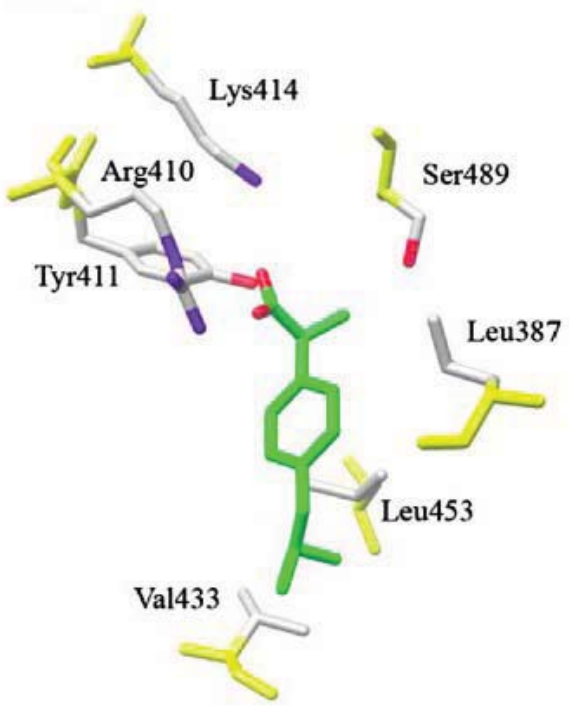

Fig. 3. Schematic representation of Sudlow's site II (FA3-FA4) of HSA. The FA3-FA4 cleft is presented in the same orientation as Fig. 1. Ibuprofen carbon atoms are colored in green and backbone atoms of the residues building up the site are colored in yellow. The atomic coordinates have been retrieved from the PDB entry 2BXG [14]. The picture was drawn with Chimera [86].

the cavity. FAs bind to FA7 in a curved configuration with the tail co-planar with aromatic drugs bound to this site, thus suggesting that FA7 is a low affinity cleft [22,23].

Drugs (*e.g.*, warfarin) cluster in the center of Sudlow's site I, having a planar group pinned snugly between the apolar side-chains of Leu238 and Ala291 (Fig. 4) [14,19,34]. Values of thermodynamic and kinetic parameters for warfarin binding to HSA are $K_d = 3\times10^{-7}$ M, $k_{on} = 3\times10^{6}$ M^{-1} s^{-1} and $k_{off} = 10$ s^{-1} [14,19,34,38]. Remarkably, warfarin binding to HSA is modulated allosterically and competitively [3,39-41].

4.1.7. The FA8 and FA9 clefts

The FA8 and FA9 sites bind small FAs (such as capric acid) with low affinity. Therefore, it is debatable if they are physiologically relevant [3].

FA8 is located at the base of the gap between sub-domains IA-IB-IIA on one side and sub-domains IIB-IIIA-IIIB on the other side. The methylene tail of capric acid bound to FA6 contributes to the formation of the hydrophobic end of FA8. At the other end of the cavity some polar residues (*i.e.*, Lys195, Lys199, Arg218, Asp451, and Ser454) form an open ring that stabilizes the polar head of the ligand [22].

FA9 lies in an upper region of the gap between sub-domains IA-IB-IIA on one side and sub-domains IIB-IIIA-IIIB on the other side, thus providing a rather open binding environment. A salt-bridge between Glu187 of domain I and Lys432 of domain III contributes to keep the ligand in place [22].

4.2. The thyroxine binding sites

Thyroxine (3,3',5,5'-tetraiodo-L-thyronine; T_4) binds to FA-free HSA at four sites, which are labeled Tr-1 to Tr-4. Tr-1 binds to sub-domain IIA, Tr-2 binds to sub-domain IIIA, and Tr-3 and Tr-4 bind to sub-domain IIIB. The T_4 binding clefts partially overlap the FA7, FA3-FA4, and FA5 binding sites, respectively

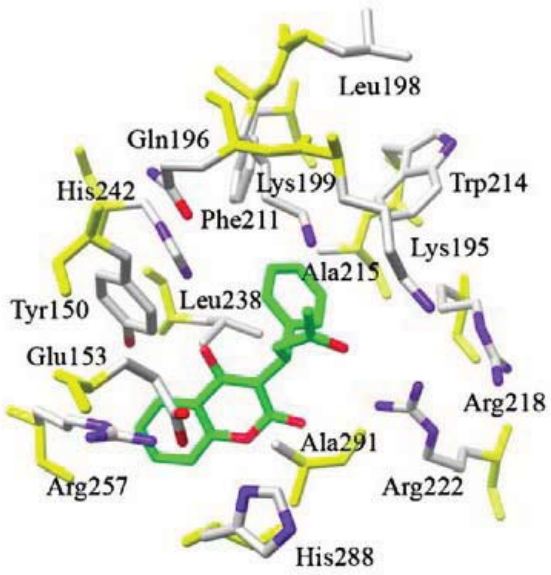

Fig. 4. Schematic representation of Sudlow's site I (FA7) of HSA. The FA7 cleft is presented in the same orientation as Fig. 1. Warfarin carbon atoms are colored in green and backbone atoms of the residues building up the site are colored in yellow. The atomic coordinates have been retrieved from the PDB entry 2BXD [14]. The picture was drawn with Chimera [86].

(Fig. 5A) [42]. Notebly, FAs compete with T_4 at all four Tr sites, eccesive FAs could induce structural rearrangement of HSA resulting the formation of the fifth T_4 binding site which is located in the cleft between domains I and III (*i.e.*, FA9) [7,19,32]. This open site, called Tr-5, is composed by the long helix connecting domains I and II and by a pair of helices from sub-domain IIIA (see 4.1.7) (Fig. 5B). T_4 binds to Tr-5 with a dissociation equilibrium constant ($K_d = 4.9\times10^{-6}$ M) similar to that observed for the primary binding site (*i.e.*, Tr-1) in defatted HSA [42].

Natural mutants of HSA Arg218Pro and Arg218His within sub-domain IIA were reported to be associated with familial dysalbuminemic hyperthyroxinemia. Structural studies revealed that the point mutants posses a high affinity for T_4 by relaxing the steric restriction on the binding site which causes an elevated serum thyroxin level [3,42].

4.3. The bacterial protein binding site

HSA has been reported to bind the bacterial surface of *Finegoldia magna*. As many bacterial species express surface protein domains for binding to host serum proteins, *Finegoldia magna* expresses a surface protein called PAB, which contains a protein G-related albumin binding module, shortly GA module [43]. GA domain shows high sequence similarity (60%) to albumin binding domains of protein G, a bacterial protein that binds the FC domain of IgGs [44].

The interaction occurs between residues from the second α-helix and the two surrounding loops on the GA module, and the HSA domain II region delimited by h2-h3 and h7-h8 with the loop region preceeding h7 (Fig. 6). Although the biological function(s) of the GA module is not known in detail, the acquisition of the GA module seems to add selective advantages to the bacterium in terms of growth and also increases its virulence, probably by providing growing bacteria with FAs and, possibly, other nutrients transported by HSA [3,45].

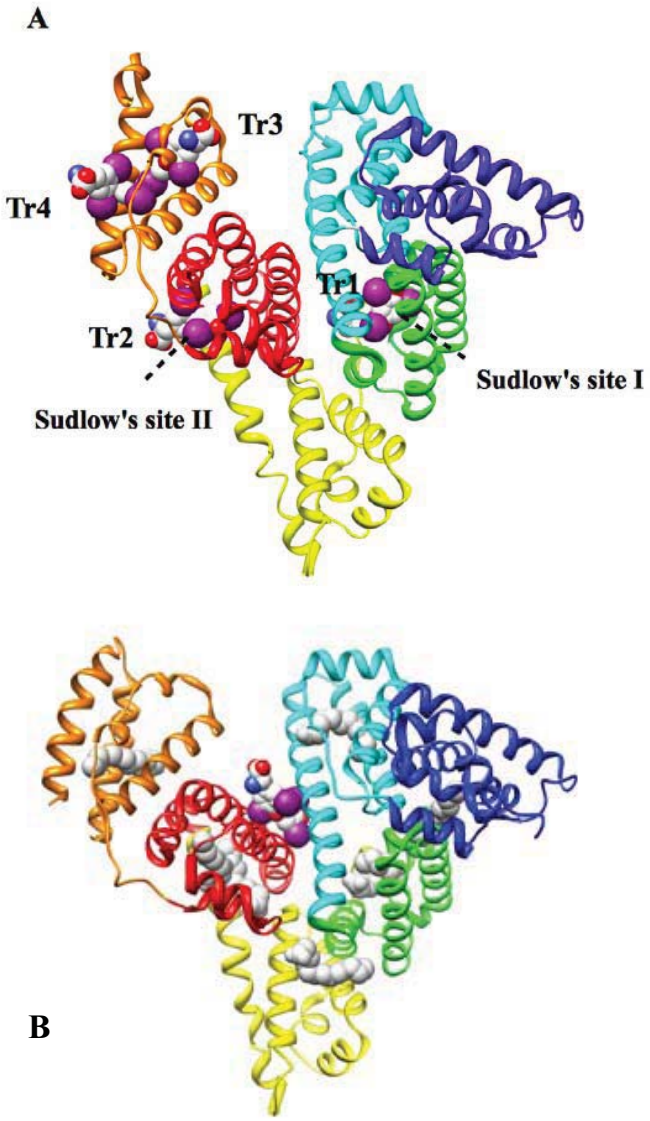

Fig. 5. T_4 binding to HSA in the absence (panel A) and presence (panel B) of myristate ions. HSA is rendered with ribbons colored as in Fig. 1. The myristate ions are rendered as spacefill in gray. The T_4 molecules are rendered as spacefill and colored by atom type. The atomic coordinates have been retrieved from PDB entries 1HK1 and 1HK4 [42]. The picture was drawn with UCSF Chimera [86]

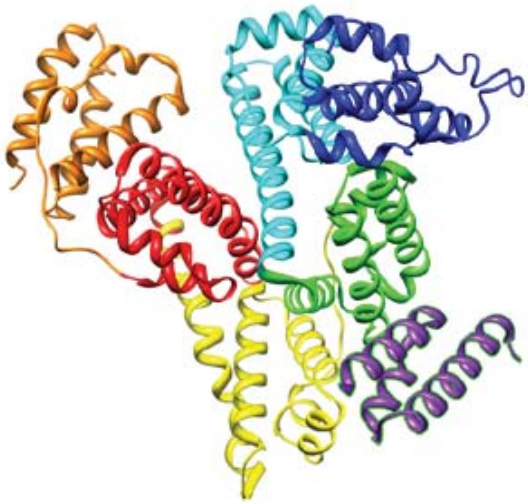

Fig. 6. The HSA-GA complex. HSA is rendered with ribbons colored as in Fig. 1. The GA module is colored in purple. The atomic coordinates have been retrieved from the PDB entry 2VDB [45]. The picture was drawn with UCSF Chimera [86].

4.4. The metal binding sites

HSA displays a wide variety of binding sites for several metal ions, including Mg(II), Al(III), Ca(II), Mn(II), Co(II/III), Ni(II), Cu(I/II), Zn(II), Cd(II), Pt(II), Au(I/II), Hg(II), and Tb(III) [1,46-48]. So far, three major binding sites endowed with appropriate residues matching for the different metal geometries have been extensively investigated. The first site (usually labelled as *N*-terminal binding site, NTS) is located at the *N*-terminus, where Cu(II), Co(II), and Ni(II) are coordinated by nitrogen donor atoms from Asp1, Ala2, and His3 [49]. The second site is represented by the free Cys34 thiol that binds Au(I), Hg(II), and Pt(II) ions [1]. The third metal binding site is the so-called multi-metal binding site or Cadmium site A (MBS-A), which involves His67, Asn99, His247, and Asp249 residues. Due to its pseudo-octahedral geometry, this cleft is able to stably allocate different metal ions. Indeed, MBS-A has been suggested to be the primary site of Zn(II) and Cd(II), and the secondary cleft for Cu(II) and Ni(II) [50]. Despite the current lack of experimental evidence, a secondary site for Cd(II) binding, called Cadmium site B (MBS-B), has been postulated [51]. Eventually, other metal ions bind either unspecifically or to undefined regions [1,3].

4.5. The Cys34 residue

Like other mammalian albumins, HSA contains 17 disulfide bridges and a free thiol at Cys34, which represents the largest fraction of free thiol in blood serum. Cys34 is buried in a 9.5 Å deep crevice on the surface of HSA (Fig. 1) , with the sulfur atom being surrounded by carboxylate group of Asp38, the imidazole ring of His39 and hydroxyl group of Tyr84, together affecting the ionization state of Cys34 thus modulating its reactivity [52,53]. Remarkably, chemical modifications of Cys34 modulate allosterically and competitively HSA reactivity [3,53,54].

In healthy adults, about 70-80% of the Cys34 in HSA contains a free sulfhydryl group, whereas about 25-30% of Cys34

forms a mixed disulfide bound with either cysteine or homocysteine or glutathione, thus affecting its redox potential. Whereas the concentration of free glutathione is in the lower micromolar range, HSA-bound glutathione may represent a significant pool. Whether the glutathione adduct merely serves as a kind of storage and transport of glutathione, or it has a functional role in modulating the redox potential of Cys34 still remains unclear [3,55].

Cys34 serves not only as metal ion binding site (see 4.4), but also as a physiological antioxidant participating in radical scavenging. Moreover, Cys34 binds a number of endogenous and exogenous small molecules, such as NO, as well as certain drugs containing thiol(s) [8,53,55,56].

5. Human serum heme-albumin

HSA is crucial for heme scavenging, providing protection against free heme oxidative damage, limiting the access of pathogens to heme, and contributing to iron homeostasis by recycling the heme iron. The HSA-heme-Fe(III) plasmatic level is about 1×10^{-6} M under physiological condition, which arises to a maximum of about 4×10^{-5} M in patients affected with severe hematologic diseases characterized by excessive intravascular hemolysis [57,58]. Upon increasing heme plasma level, hemopexin (HPX), the primary heme transporter undergoes heme saturation, though it binds heme with extremely high affinity (K_a = 6.8×10^{10} M^{-1}), its plasma concentration (~ 1.8×10^{-5} M) is about two orders of magnitude lower than that of HSA (~ 7.5×10^{-4} M) [1], thus HSA acts as the main heme-Fe(III) plasma depot and largely averts the toxic effect of heme [3,11,58-61].

Besides the trapping function of HSA and HPX, a quantitative model of time-dependent heme distribution among plasma proteins low density lipoproteins (LDL), high density lipoproteins (HDL), HSA and HPX, revealing a remarkable

importance of lipoproteins in the beginning of the scavenging process, has been proposed. HDL and LDL, though the most oxidatively intolerant plasma components, bind heme with the highest affinity, kinetics of heme transfer from HDL and LDL to HSA and HPX is faster than kinetics of heme-induced lipoprotein oxidation. During the first seconds after heme appearance in plasma, more than 80% of this powerful oxidizer binds to HDL and LDL, and only the remaining 20% binds to HSA and HPX, within the 50 s after heme encounter, HDL is the major heme carrier. Then the released heme from lipoproteins moves to HSA and HPX, and soon reaches 44% of heme bind to HSA, and 35% to HPX, which consolidates the depot function of HSA. Afterwards, heme transits from HSA to HPX, then releases to hepatic parenchymal cells after internalization of the HPX-heme complex by CD91 receptor-mediated endocytosis [1,3,11,58,62-70].

Remarkably, heme binding confers to HSA globin-like spectroscopic and reactivity properties, providing a suitable tool to investigate allosteric and competitive modulations. Interestingly, both heme binding to HSA and HSA-heme reactivity are modulated allosterically [3,13,18,20,30-71-84].

6. Human serum albumin: a monomeric allosteric protein

The multidomain structural organization of monomeric HSA is at the root of its allosteric properties, that recall those of multimeric proteins. Indeed, the conformational adaptability of HSA involves more than the immediate vicinity of the binding site(s), affecting both the spectroscopic and the ligand binding properties of the whole molecule [3,20].

HSA conformational transitions are not only associated to pH changes but also to the binding of endogenous and exogenous ligand (*e.g.*, FAs, heme, and drugs). Indeed, the pH-induced N-to-

B transition (occurring in the 6 to 9 pH range) replicates that induced by FAs (Fig. 7) [19,85].

Allosteric regulation of ligand binding to HSA is not only relevant physiologically, but also pharmacokinetically in terms of drug administration. Indeed, drug binding to plasma proteins is an important determinant for their biological efficacy by modulation of drug availability to the intended target [3,15,20].

The multiplicity of ligand binding sites renders very difficult to dissect the allosteric linkages occurring in HSA. As a case it should be noted that ibuprofen binding to its primary site FA3-FA4 (corresponding to Sudlow's site II) does not affect allosterically the reactivity properties of the FA1 site. On the other hand, warfarin binding to its primary site (*i.e.*, FA7) modulates allosterically the FA1 site reactivity. However, a functional link between the secondary ibuprofen binding site FA6 and FA1 occurs. Moreover, FAs (representing, among others, the physiological ligands of HSA) modulate allosterically and competitively not only their binding properties, but also endogenous and exogenous ligand association [3,20].

References

1. Peters, T. Jr. (Ed.) 1996. All about Albumin: Biochemistry, Genetics and Medical Applications. Academic Press, San Diego and London.
2. Fasano, M., Fanali, G., Leboffe, L., et al., 2007. Heme binding to albuminoid proteins is the result of recent evolution. IUBMB Life 59, 436-440.
3. Fanali, G., di Masi, A., Trezza, V., et al., 2012. Human serum albumin: from bench to bed. Mol. Aspects Med., in press.
4. Sudlow, G., Birkett, D.J., and Wade, D.N., 1975. The characterization of two specific drug binding sites on human serum albumin. Mol. Pharmacol. 11, 824-832.

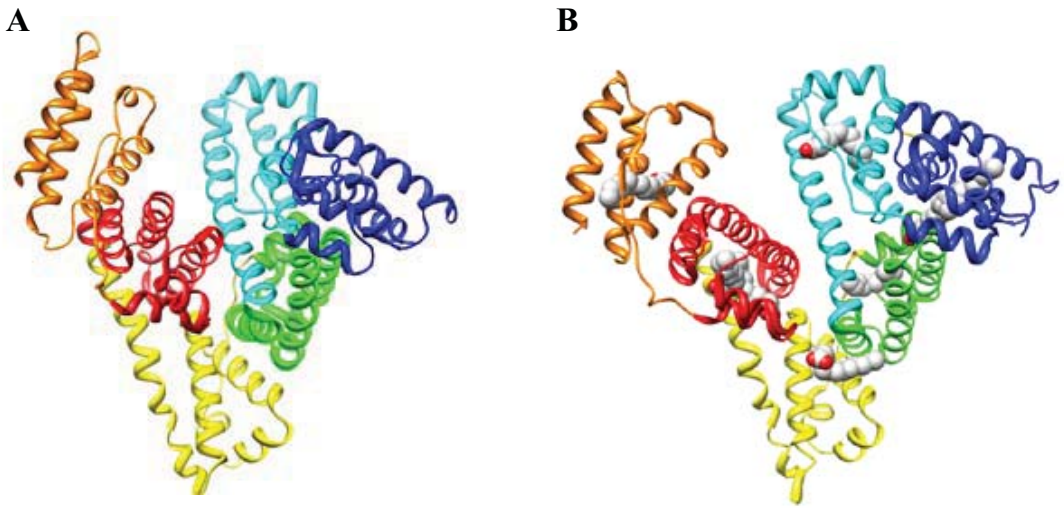

Fig. 7. FA-free (panel A) and FA-bound (panel B) HSA. The structures are colored as in Fig.1. The atomic coordinates have been retrieved from PDB entries 1E78 and 1E7G [22]. The picture was drawn with UCSF Chimera [86].

5. Carter, D.C., and Ho, J.X., 1994. Structure of serum albumin. Adv. Protein Chem. 45, 153-203.
6. Bertucci, C., and Domenici, E., 2002. Reversible and covalent binding of drugs to human serum albumin: methodological approaches and physiological relevance. Curr. Med. Chem. 9, 1463-1481.
7. Curry, S., 2002. Beyond expansion: structural studies on the transport roles of human serum albumin. Vox Sang. 83, Suppl. 1, 315-319.
8. Kragh-Hansen, U., Chuang, V.T., and Otagiri, M., 2002. Practical aspects of the ligand-binding and enzymatic properties of human serum albumin. Biol. Pharm. Bull. 25, 695-704.
9. Sakurai, Y., Ma, S.F., Watanabe, H., et al., 2004. Esterase-like activity of serum albumin: characterization of its structural chemistry using *p*-nitrophenyl esters as substrates. Pharm. Res. 21, 285-292.
10. Sułkowska, A., Bojko, B., Równicka, J., et al., 2006. Competition of cytarabine and aspirin in binding to serum albumin in multidrug therapy. Biopolymers 81, 464-472
11. Ascenzi, P., Bocedi, A., Visca, P., et al., 2005a. Hemoglobin and heme scavenging. IUBMB Life 57, 749-759.
12. Bocedi, A., Notari, S., Menegatti, E., et al., 2005. Allosteric modulation of anti-HIV drug and ferric heme binding to human serum albumin. FEBS J. 272, 6287-6296.
13. Fasano, M., Curry, S., Terreno, E., et al., 2005. The extraordinary ligand binding properties of human serum albumin. IUBMB Life 57, 787-796.
14. Ghuman, J., Zunszain, P.A., Petitpas, I., et al., 2005. Structural basis of the drug-binding specificity of human serum albumin. J. Mol. Biol. 353, 38-52.
15. Ascenzi, P., Bocedi, A., Notari, S., et al., 2006. Allosteric modulation of drug binding to human serum albumin. Mini Rev. Med. Chem. 6, 483-489.
16. Fanali, G., Ascenzi, P., Fasano, M., 2007. Effect of prototypic

drugs ibuprofen and warfarin on global chaotropic unfolding of human serum heme-albumin: a fast-field-cycling ^{1}H-NMR relaxometric study. Biophys. Chem. 129, 29-35.
17. Yang, F., Bian, C., Zhu, L., et al., 2007. Effect of human serum albumin on drug metabolism: structural evidence of esterase activity of human serum albumin. J. Struct. Biol. 157, 348-355.
18. Ascenzi, P., di Masi, A., Coletta, M., et al., 2009. Ibuprofen impairs allosterically peroxynitrite isomerization by ferric human serum heme-albumin. J. Biol. Chem. 284, 31006-31017.
19. Curry, S., 2009. Lessons from the crystallographic analysis of small molecule binding to human serum albumin. Drug. Metab. Pharmacokinet. 24, 342-357.
20. Ascenzi, P., and Fasano, M., 2010. Allostery in a monomeric protein: the case of human serum albumin. Biophys. Chem. 148, 16-22.
21. Varshney, A., Sen, P., Ahmad, E., et al., 2010. Ligand binding strategies of human serum albumin: how can the cargo be utilized? Chirality 22, 77-87.
22. Bhattacharya, A.A., Grüne, T., and Curry, S., 2000. Crystallographic analysis reveals common modes of binding of medium and long-chain fatty acids to human serum albumin. J. Mol. Biol. 303, 721-732.
23. Simard, J.R., Zunszain, P.A., Hamilton, J.A., et al., 2006. Location of high and low affinity fatty acid binding sites on human serum albumin revealed by NMR drug-competition analysis. J. Mol. Biol. 361, 336-351.
24. Wardell, M., Wang, Z., Ho, J.X., et al., 2002. The atomic structure of human methemalbumin at 1.9 Å. Biochem. Biophys. Res. Commun. 291, 813-819.
25. Zunszain, P.A., Ghuman, J., Komatsu, T., et al., 2003. Crystal structural analysis of human serum albumin complexed with hemin and fatty acid. BMC Struct. Biol. 3, 6.
26. Zunszain, P.A., Ghuman, J., McDonagh, A.F., et al., 2008.

Crystallographic analysis of human serum albumin complexed with 4*Z*,15*E*-bilirubin-IXα. J. Mol. Biol. 381, 394-406.
27. Fanali, G., Fesce, R., Agrati, C., et al., 2005. Allosteric modulation of myristate and Mn(III)heme binding to human serum albumin: optical and NMR spectroscopy characterization. FEBS J. 272, 4672-4683.
28. Fanali, G., Bocedi, A., Ascenzi, P., et al., 2007. Modulation of heme and myristate binding to human serum albumin by anti-HIV drugs: an optical and NMR spectroscopic study. FEBS J. 274, 4491-4502.
29. Nicoletti, F.P., Howes, B.D., Fittipaldi, M., et al., 2008. Ibuprofen induces an allosteric conformational transition in the heme complex of human serum albumin with significant effects on heme ligation. J. Am. Chem. Soc. 130, 11677-11688.
30. Ascenzi, P., di Masi, A., De Sanctis, G., et al., 2009. Ibuprofen modulates allosterically NO dissociation from ferrous nitrosylated human serum heme-albumin by binding to three sites. Biochem. Biophys. Res. Commun. 387, 83-86.
31. Sudlow, G., Birkett, D.J., and Wade, D.N., 1976. Further characterization of specific drug binding sites on human serum albumin. Mol. Pharmacol. 12, 1052-1061.
32. Curry, S., Mandelkov, H., Brick, P., et al., 1998. Crystal structure of human serum albumin complexed with fatty acid reveals an asymmetric distribution of binding sites. Nat. Struct. Biol. 5, 827-835.
33. Yamasaki, K., Maruyama, T., Yoshimoto, K., et al., 1999. Interactive binding to the two principal ligand binding sites of human serum albumin: effect of the neutral-to-base transition. Biochim. Biophys. Acta 1432, 313-323.
34. Petitpas, I., Bhattacharya, A.A., Twine. S., et al., 2001. Crystal structure analysis of warfarin binding to human serum albumin: anatomy of drug site I. J. Biol. Chem. 276, 22804-22809.

35. Hamilton, J.A., 2004. Fatty acid interactions with proteins: what X-ray crystal and NMR solution structures tell us. Prog. Lipid .Res. 43, 177-199.
36. Kragh-Hansen, U., 1981. Molecular aspects of ligand binding to serum albumin. Pharmacol. Rev. 33, 17-53.
37. Cheruvallath, V.K., Riley, C.M., Narayanan, S.R., et al., 1997. A quantitative circular dichroic investigation of the binding of the enantiomers of ibuprofen and naproxen to human serum albumin. J. Pharm. Biomed. Anal. 15, 1719-1724.
38. Fitos, I., Visy, J., and Kardos, J., 2002. Stereoselective kinetics of warfarin binding to human serum albumin: effect of an allosteric interaction. Chirality 14, 442-448.
39. Baroni, S., Mattu, M., Vannini, A., et al., 2001. Effect of ibuprofen and warfarin on the allosteric properties of haem-human serum albumin. A spectroscopic study. Eur. J. Biochem. 268, 6214-6220.
40. Fanali, G., De Sanctis, G., Gioia, M., et al., 2009. Reversible two-step unfolding of heme-human serum albumin: a ^{1}H-NMR relaxometric and circular dichroism study. J. Biol. Inorg Chem. 14, 209-217.
41. Fanali, G., Rampoldi, V., di Masi, A., et al., 2010. Binding of anti-Parkinson's disease drugs to human serum albumin is allosterically modulated. IUBMB Life 62, 371-376.
42. Petitpas, I., Petersen, C.E., Ha, C.E., et al., 2003. Structural basis of albumin-thyroxine interactions and familial dysalbuminemic hyperthyroxinemia. Proc. Natl. Acad. Sci. USA 100, 6440-6445.
43. de Château, M., and Björck, L., 1994. Protein PAB, a mosaic albumin-binding bacterial protein representing the first contemporary example of module shuffling. J. Biol. Chem. 269, 12147-12151.
44. Björck, L., and Kronvall, G., 1984. Purification and some properties of streptococcal protein G, a novel IgG-binding reagent. J. Immunol. 133, 969-974.

45. Lejon, S., Frick, I.M., Bjorck, L., et al., 2004. Crystal structure and biological implications of a bacterial albumin binding module in complex with human serum albumin. J. Biol. Chem. 279, 42924-42928.
46. Sokołowska, M., Wszelaka-Rylik, M., Poznański, J., et al., 2009. Spectroscopic and thermodynamic determination of three distinct binding sites for Co(II) ions in human serum albumin. J. Inorg. Biochem. 103, 1005-1013.
47. Sokołowska, M., Pawlas, K., and Bal, W. 2010. Effect of common buffers and heterocyclic ligands on the binding of Cu(II) at the multimetal binding site in human serum albumin. Bioinorg. Chem. Appl. doi: 10.1155/2010/725153.
48. Deng, B., Wang, Y., Zhu, P., et al., 2010. Study of the binding equilibrium between Zn(II) and HSA by capillary electrophoresis-inductively coupled plasma optical emission spectrometry. Anal. Chim. Acta 683, 58-62.
49. Sadler, P.J., Tucker, A., Viles, J.H., 2005. Involvement of a lysine residue in the N-terminal Ni^{2+} and Cu^{2+} binding site of serum albumins. Comparison with Co^{2+}, Cd^{2+} and Al^{3+}. FEBS J. 220, 193-200.
50. Blindauer, C.A., Harvey, I., Bunyan, K.E., et al., 2009. Structure, properties, and engineering of the major zinc binding site on human albumin. J. Biol. Chem. 284, 23116-23124.
51. Mothes, E., and Faller, P., 2007. Evidence that the principal Co^{II}-binding site in human serum albumin is not at the N-terminus: implication on the albumin cobalt binding test for detecting myocardial ischemia. Biochemistry. 46, 2267-2274.
52. Ascenzi, P., Colasanti, M., Persichini, T., et al., 2000. Re-evaluation of amino acid sequence and structural consensus rules for cysteine-nitric oxide reactivity. Biol. Chem. 381, 623-627.
53. Stewart, A.J., Blindauer, C.A., Berezenko, S., et al., 2005. Role of Tyr84 in controlling the reactivity of Cys34 of human albumin. FEBS J. 272, 353-362.

54. Bertucci, C., Nanni, B., and Salvadori, P., 1999. Reversible binding of ethacrynic acid to human serum albumin: difference circular dichroism study. Chirality 11, 33-38.
55. Oettl, K., and Stauber, R.E., 2007. Physiological and pathological changes in the redox state of human serum albumin critically influence its binding properties. Br. J. Pharmacol. 151, 580-590.
56. Christodoulou, J., Sadler, P.J., and Tucker, A., 1995. ^{1}H-NMR of albumin in human blood plasma: drug binding and redox reactions at Cys34. FEBS Lett. 376, 1-5.
57. Muller-Eberhard, U., Javid, J., Liem, H.H., et al. 1968. Plasma concentrations of hemopexin, haptoglobin and heme in patients with various hemolytic diseases. Blood 32, 811-815.
58. Miller, Y.I., and Shaklai, N., 1999. Kinetics of hemin distribution in plasma reveals its role in lipoprotein oxidation. Biochim. Biophys. Acta 1454, 153-164.
59. Morgan, W.T., Liem, H.H., Sutor, R.P., et al., 1976. Transfer of heme from heme-albumin to hemopexin. Biochim. Biophys. Acta 444, 435-445.
60. Pasternack, R.F., Gibbs, E.J., Hoeflin, E., et al., 1983. Hemin binding to serum proteins and the catalysis of interprotein transfer. Biochemistry 22, 1753-1758.
61. Pasternack, R.F., Gibbs, E.J., Mauk, A.G., et al., 1985. Kinetics of hemoprotein reduction and interprotein heme transfer. Biochemistry 24, 5443-5448.
62. Smith, A., and Hunt, R.C., 1990. Hemopexin joins transferrin as representative members of a distinct class of receptor-mediated endocytic transport systems. Eur. J. Cell. Biol. 53, 234-245.
63. Conrad, M.E., Umbreit, J.N., and Moore, E.G., 1999. Iron absorption and transport. Am. J. Med. Sci. 318, 213-229.
64. Conrad, M.E., and Umbreit, J.N., 2000. Iron absorption and transport-an update. Am. J. Hematol. 64, 287-298.
65. Delanghe, J.R., and Langlois, M.R., 2001. Hemopexin: a

review of biological aspects and the role in laboratory medicine. Clin. Chim. Acta 312, 13-23.
66. Conrad, M.E., and Umbreit, J.N., 2002. Pathways of iron absorption. Blood Cells Mol. Dis. 29, 336-355.
67. Goswami, T., Rolfs, A., and Hediger, M.A., 2002. Iron transport: emerging roles in health and disease. Biochem. Cell. Biol. 80, 679-689.
68. Tolosano, E., and Altruda, F., 2002. Hemopexin: structure, function, and regulation. DNA Cell Biol. 21, 297-306.
69. Hvidberg, V., Maniecki, M.B., Jacobsen, C., et al., 2005. Identification of the receptor scavenging hemopexin-heme complexes. Blood 106, 2572-2579.
70. Tolosano, E., Fagoonee, S., Morello, N., et al., 2010. Heme scavenging and the other facets of hemopexin. Antioxid. Redox Signal. 12, Suppl. 2, 305-320.
71. Carter, D.C., Ho, J.X., and Rüker, F., 1999. Oxygen-transporting albumin: albumin-based blood replacement composition and blood volume expander. US Pat. No.5,948,609.
72. Grinberg, L.N., O'Brien, P.J., and Hrkal, Z., 1999. The effects of heme-binding proteins on the peroxidative and catalatic activities of hemin. Free Radic. Biol. Med. 27, 214-219.
73. Komatsu, T., Matsukawa, Y., and Tsuchida, E., 2000. Kinetics of CO and O_2 binding to human serum albumin-heme hybrid. Bioconjug. Chem. 11, 772-776.
74. Mattu, M., Vannini, A., Coletta, M., et al., 2001. Effect of bezafibrate and clofibrate on the heme-iron geometry of ferrous nitrosylated heme-human serum albumin: an EPR study. J. Inorg. Biochem. 84, 293-296.
75. Monzani, E., Bonafè, B., Fallarini, A., et al., 2001. Enzymatic properties of hemalbumin. Biochim. Biophys. Acta 1547, 302-312.
76. Fasano, M., Mattu, M., Coletta, M., et al., 2002. The heme-iron geometry of ferrous nitrosylated heme-serum lipoproteins, hemopexin, and albumin: a comparative EPR

study. J. Inorg. Biochem. 91, 487-490.
77. Kamal, J.K.A., and Behere, D.V., 2002. Spectroscopic studies on human serum albumin and methemalbumin: optical, steady-state, and picosecond time-resolved fluorescence studies, and kinetics of substrate oxidation by methemalbumin. J. Biol. Inorg. Chem. 7, 273-283.
78. Monzani, E., Curto, M., Galliano, M., et al., 2002. Binding and relaxometric properties of heme complexes with cyanogen bromide fragments of human serum albumin. Biophys. J. 83, 2248-2258
79. Komatsu, T., Ohmichi, N., Zunszain, P.A., et al., 2004. Dioxygenation of human serum albumin having a prosthetic heme group in a tailor-made heme pocket. J. Am. Chem. Soc. 126, 14304-14305.
80. Komatsu, T., Oguro, Y., Nakagawa, A., et al., 2005. Albumin clusters: structurally defined protein tetramer and oxygen carrier including thirty-two iron(II) porphyrins. Biomacromolecules 6, 3397-3403.
81. Komatsu, T., Ohmichi, N., Nakagawa, A., et al., 2005. O_2 and CO binding properties of artificial hemoproteins formed by complexing iron protoporphyrin IX with human serum albumin mutants. J. Am. Chem. Soc. 127, 15933-15942.
82. Ascenzi, P., and Fasano, M., 2007. Abacavir modulates peroxynitrite-mediated oxidation of ferrous nitrosylated human serum heme-albumin. Biochem. Biophys. Res. Commun. 353, 469-474.
83. Ascenzi, P., Imperi, F., Coletta, M., et al., 2008. Abacavir and warfarin modulate allosterically kinetics of NO dissociation from ferrous nitrosylated human serum heme-albumin. Biochem. Biophys. Res. Commun. 369, 686-691.
84. Cao, Y., Nicoletti, F.P., De Sanctis, G., et al., 2011. Evidence for pH-dependent multiple conformers in iron(II) heme-human serum albumin: spectroscopic and kinetic investigation of carbon monoxide binding. J. Biol. Inorg. Chem. doi: 10.1007/s00775-011-0837-0.

85. van der Vusse, G.J., 2009. Albumin as fatty acid transporter. Drug Metab. Pharmacokinet. 24, 300-307.
86. Pettersen, E.F., Goddard, T.D., Huang, C.C., et al., 2004. UCSF Chimera - a visualization system for exploratory research and analysis. J. Comput. Chem. 25, 1605-1612.

7. Aims

The multifaceted structural organization of HSA and its versatile ligand binding properties render this monomeric protein functionally similar to allosteric multimeric macromolecules. Remarkably, the modulation of ligand binding to HSA by third components is relevant from both physiological and pathological viewpoints.

To highlight the molecular bases of the HSA allosteric properties, the reductive nitrosylation of ferric human serum heme-albumin (HSA-heme-Fe(III)), the carbonylation of ferrous human serum heme-albumin (HSA-heme-Fe(II)), the modulation of HSA-heme-Fe(II) nitrosylation by ibuprofen and warfarin, and the modulation of Δ9-tetrahydro-cannabinol (THC) and diazepam binding to HSA and HSA-heme-Fe(III) by endogenous and exogenous compounds have been investigated.

The bio-physico-chemical characterization of HSA evidenced the following peculiar binding properties. (*i*) HSA-heme-Fe(II) is a mixture of species that accounts for the multi-exponential carbonylation and nitrosylation kinetics, this reflects the very slow interconversion between the different HSA species. (*ii*) Ibuprofen and warfarin binding to FA2, FA6, and FA7 sites impair allosterically HSA-heme-Fe(II) nitrosylation occurring at the FA1 cleft. (*iii*) Heme binding to the FA1 site and the redox state of the heme-Fe atom affect allosterically drug binding to multiple HSA sites. (*iv*) THC binding to the high-affinity site FA2 accounts for the low free fraction of the drug in plasma; moreover, the HSA conformational transition(s) accompanying THC binding and dissociation may account for drug delivery to the liver through receptor-mediated endocytosis.

These studies gain some insights into the intricate allosteric mechanism(s) of HSA and appear of physiological and pathological relevance, broadening the understanding of the relationship between the functional versatility of HSA and its remarkable structural flexibility.

the FEBS Journal

Reductive nitrosylation of ferric human serum heme-albumin

Paolo Ascenzi[1,2,*], Yu Cao[1,3,*], Alessandra di Masi[1], Francesca Gullotta[1], Giampiero De Sanctis[4], Gabriella Fanali[5], Mauro Fasano[5] and Massimo Coletta[3,6]

1 Department of Biology, University Roma Tre, Italy
2 National Institute for Infectious Diseases I.R.C.C.S. ''Lazzaro Spallanzani'', Roma, Italy
3 Department of Experimental Medicine and Biochemical Sciences, University of Roma 'Tor Vergata', Italy
4 Department of Molecular, Cellular and Animal Biology, University of Camerino, Italy
5 Department of Structural and Functional Biology, and Center of Neuroscience, University of Insubria, Busto Arsizio (VA), Italy
6 Interuniversity Consortium for the Research on the Chemistry of Metals in Biological Systems, Bari, Italy

Keywords
ferric human serum heme-albumin; irreversible reductive nitrosylation; kinetics; reversible nitrosylation; thermodynamics

Correspondence
P. Ascenzi, Department of Biology, University Roma Tre, Viale Guglielmo Marconi 446, I-00146 Roma, Italy
Fax: +39 06 57336321
Tel: +39 06 57333494
E-mail: ascenzi@uniroma3.it

*These authors contributed equally to this study

(Received 22 December 2009, revised 17 February 2010, accepted 25 March 2010)

doi:10.1111/j.1742-4658.2010.07662.x

Heme endows human serum albumin (HSA) with heme-protein-like reactivity and spectroscopic properties. Here, the kinetics and thermodynamics of reductive nitrosylation of ferric human serum heme-albumin [HSA-heme-Fe(III)] are reported. All data were obtained at 20 °C. At pH 5.5, HSA-heme-Fe(III) binds nitrogen monoxide (NO) reversibly, leading to the formation of nitrosylated HSA-heme-Fe(III) [HSA-heme-Fe(III)-NO]. By contrast, at pH ≥ 6.5, the addition of NO to HSA-heme-Fe(III) leads to the transient formation of HSA-heme-Fe(III)-NO in equilibrium with HSA-heme-Fe(II)-NO^+. Then, HSA-heme-Fe(II)-NO^+ undergoes nucleophilic attack by OH^- to yield ferrous human serum heme-albumin [HSA-heme-Fe(II)]. HSA-heme-Fe(II) further reacts with NO to give nitrosylated HSA-heme-Fe(II) [HSA-heme-Fe(II)-NO]. The rate-limiting step for reductive nitrosylation of HSA-heme-Fe(III) is represented by the OH^--mediated reduction of HSA-heme-Fe(II)-NO^+ to HSA-heme-Fe(II). The value of the second-order rate constant for OH^--mediated reduction of HSA-heme-Fe(II)-NO^+ to HSA-heme-Fe(II) is 4.4×10^3 $M^{-1} \cdot s^{-1}$. The present results highlight the role of HSA-heme-Fe in scavenging reactive nitrogen species.

Introduction

Human serum albumin (HSA), the most abundant protein in plasma (reaching a blood concentration of about 7.0×10^{-4} M), is a depot and a carrier for many endogenous and exogenous compounds, affects the pharmacokinetics of many drugs, holds some ligands in a strained orientation which results in their metabolic modification, renders potential toxins harmless by transporting them to disposal sites, accounts for most of the antioxidant capacity of human serum and displays (pseudo-)enzymatic properties [1–13].

HSA is a single, nonglycosylated all-α-chain protein of 585 amino acids, which contains three homologous domains (labeled I, II and III). Each domain is composed of two separate helical subdomains (named A and B) connected by random coils. Terminal regions of sequential domains contribute to the formation of interdomain helices linking domain IB to domain IIA, and domain IIB to domain IIIA, respectively [3,7,11,13–21].

The structural organization of HSA provides a variety of ligand-binding sites. The heme binds physiologically

Abbreviations
CO, carbon monoxide; *G. max* Lb, *Glycine max* leghemoglobin; Hb, hemoglobin; HPX-heme-Fe, hemopexin-heme-Fe; HSA, human serum albumin; HSA-heme-Fe(II), ferrous HSA-heme-Fe; HSA-heme-Fe(II)-NO, nitrosylated HSA-heme-Fe(II); HSA-heme-Fe(III), ferric HSA-heme-Fe; HSA-heme-Fe(III)-NO, nitrosylated HSA-heme-Fe(III); HSA-heme-Fe, human serum heme-albumin; Mb, myoglobin; NO, nitrogen monoxide.

to the fatty acid site 1, located within the IB subdomain, with high affinity ($K_{heme} \sim 1 \times 10^{-8}$ M). The tetrapyrrole ring is arranged in a D-shaped cavity limited by Tyr138 and Tyr161 residues that provide a π–π stacking interaction with the porphyrin and supply a donor oxygen (from Tyr161) for the heme-Fe(III)-atom [11,20–22]. Heme endows HSA with heme-protein-like reactivity [7,20,22–34] and spectroscopic properties [12,23,25,27,32,34–37]. Remarkably, HSA–heme has been reported to bind nitrogen monoxide (NO) [24,25,27,30,33,35] and to act as a NO and peroxynitrite scavenger [29,34].

Here, the kinetics and thermodynamics of the reversible nitrosylation of ferric HSA-heme-Fe [HSA-heme-Fe(III)] at pH 5.5 and of the irreversible reductive nitrosylation of HSA-heme-Fe(III) between pH 6.5 and pH 9.5 are reported. The rate-limiting step of reductive nitrosylation of HSA-heme-Fe(III) is represented by the OH^--mediated reduction of ferric nitrosylated HSA-heme-Fe [HSA-heme-Fe(III)-NO] to ferrous HSA-heme-Fe [HSA-heme-Fe(II)]. In turn, HSA-heme-Fe(II) undergoes fast nitrosylation [to HSA-heme-Fe(II)-NO]. This purely fundamental study highlights the role of HSA-heme-Fe in scavenging reactive nitrogen species.

Results

The kinetics and thermodynamics of reversible nitrosylation of HSA-heme-Fe(III) at pH 5.5, and of irreversible reductive nitrosylation of HSA-heme-Fe(III) between pH 6.5 and pH 9.5, were fitted to the minimum reaction mechanism represented by the following reactions in Scheme 1 [9,38–42]:

$$\text{HSA-heme-Fe(III)} + \text{NO} \underset{k_{off}}{\overset{k_{on}}{\leftrightarrow}} \text{HSA-heme-Fe(III)-NO} \quad (a)$$

$$\text{HSA-heme-Fe(III)-NO} \overset{fast}{\leftrightarrow} \text{HSA-heme-Fe(II)-NO}^+ \quad (b)$$

$$\text{HSA-heme-Fe(II)-NO}^+ + \text{OH}^- \overset{h_{OH-}}{\rightarrow} \text{HSA-heme-Fe(II)} + \text{HNO}_2 \quad (c)$$

$$\text{HSA-heme-Fe(II)} + \text{NO} \underset{l_{off}}{\overset{l_{on}}{\leftrightarrow}} \text{HSA-heme-Fe(II)-NO} \quad (d)$$

Scheme 1. HSA-heme-Fe nitrosylation.

Reversible nitrosylation of HSA-heme-Fe(III) at pH 5.5

The addition of NO to the HSA-heme-Fe(III) solution was accompanied by a shift in the maximum of the optical absorption spectrum in the Soret band from 403 nm [i.e. HSA-heme-Fe(III)] to 368 nm [i.e. HSA-heme-Fe(III)-NO] and a corresponding change of the extinction coefficient from $\varepsilon_{403\ nm} = 1.1 \times 10^5$ $M^{-1} \cdot cm^{-1}$ to $\varepsilon_{368\ nm} = 5.4 \times 10^4$ $M^{-1} \cdot cm^{-1}$. The reaction was completely reversible as the spectrum reverted to the initial absorption spectrum by merely pumping off gaseous NO or bubbling helium through the HSA-heme-Fe(III)-NO solution. The optical absorption spectra of HSA-heme-Fe(III) and HSA-heme-Fe(III)-NO observed here correspond to those reported in the literature [29,35,43].

Under all the experimental conditions, the time course for reversible nitrosylation of HSA-heme-Fe(III) conformed to a single-exponential decay for 94–98% of its course (Fig. 1 and Eqn 1). Values of k^{obs} were wavelength-independent and NO-independent at a fixed concentration of NO. Figure 1 shows the dependence of k^{obs} for HSA-heme-Fe(III) nitrosylation on the NO concentration (i.e. [NO]). The analysis of data according to Eqn (2) allowed the values of k_{on} ($= 1.3 \times 10^4$ $M^{-1} \cdot s^{-1}$) and k_{off} ($= 2.0 \times 10^{-1}$ s^{-1}) to be determined, at pH 5.5 and 20 °C (Table 1).

The dependence of the molar fraction of HSA-heme-Fe(III)-NO (i.e. Y) on the NO concentration (i.e. [NO]) is shown in Fig. 1. The analysis of data according to Eqn (3) allowed the value of K ($= 1.5 \times 10^{-5}$ M), at pH 5.5 and 20 °C (Table 1) to be determined. Consistently with the stoichiometry of reaction (a) in Scheme 1, the Hill coefficient n was 1.01 ± 0.02. As expected for simple systems [44], the experimentally determined value of K ($= 1.5 \times 10^{-5}$ M) corresponded to that calculated from k_{off} and k_{on} values (i.e. $K = k_{off}/k_{on} = 1.5 \times 10^{-5}$ M).

Note that HSA-heme-Fe(III)-NO does not undergo significant reductive nitrosylation at pH 5.5 and 20 °C (< 5% after 30 min).

Irreversible reductive nitrosylation of HSA-heme-Fe(III) between pH 6.5 and pH 9.5

Mixing the HSA-heme-Fe(III) and NO solutions induced a shift of the optical absorption maximum of the Soret band from 403 nm [i.e. HSA-heme-Fe(III)] to 368 nm [i.e. HSA-heme-Fe(III)-NO/HSA-heme-Fe(II)-NO^+] and a corresponding change of the extinction coefficient from $\varepsilon_{403\ nm} = 1.1 \times 10^5$ $M^{-1} \cdot cm^{-1}$ to $\varepsilon_{368\ nm} = 5.4 \times 10^4$ $M^{-1} \cdot cm^{-1}$. Then, the HSA-heme-Fe(III)-NO/HSA-heme-Fe(II)-NO^+ solution underwent a shift of the optical absorption maximum of the Soret band from 368 nm [i.e. HSA-heme-Fe(III)-NO/HSA-heme-Fe(II)-NO^+] to 389 nm [i.e. HSA-heme-Fe(II)-NO] and a change of the corresponding extinction coefficient from $\varepsilon_{368\ nm} = 5.4 \times 10^4$ $M^{-1} \cdot cm^{-1}$ to $\varepsilon_{389\ nm} = 6.3 \times 10^4$ $M^{-1} \cdot cm^{-1}$. The reaction was irreversible

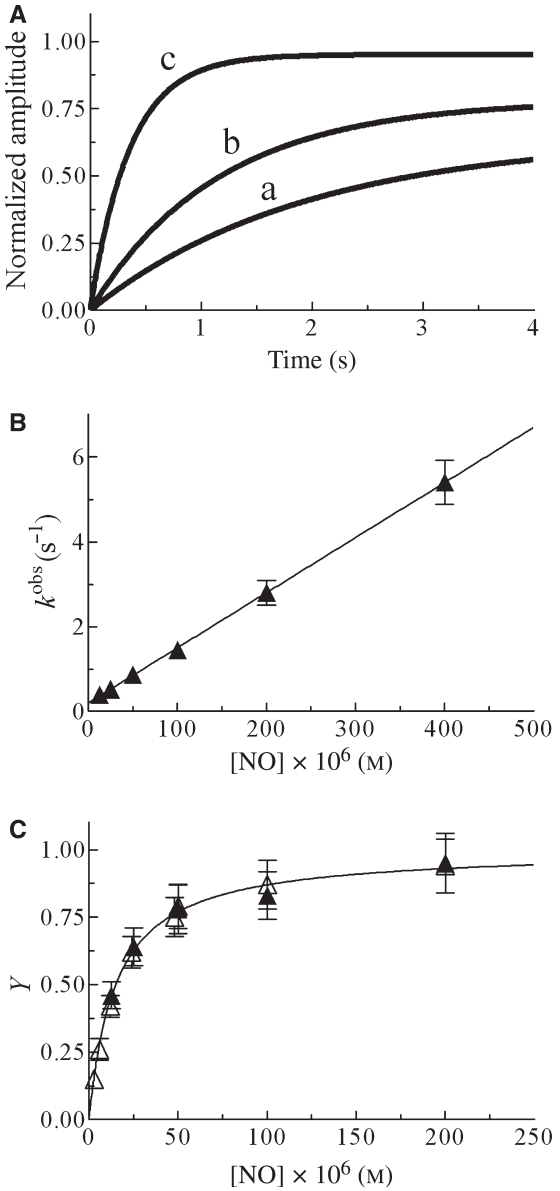

Fig. 1. NO binding to HSA-heme-Fe(III), at pH 5.5 and 20 °C. (A) Normalized averaged time courses of HSA-heme-Fe(III) nitrosylation. The NO concentrations were 2.5×10^{-5} M (trace a), 5.0×10^{-5} M (trace b) and 2.0×10^{-4} M (trace c). The time course analysis according to Eqn (1) allowed the determination of the following values of k^{obs} and Y: trace a, $k^{obs} = 5.2 \times 10^{-1}$ s^{-1} and $Y = 0.64$; trace b, $k^{obs} = 8.7 \times 10^{-1}$ s^{-1} and $Y = 0.78$; and trace c, $k^{obs} = 2.8$ s^{-1} and $Y = 0.95$. (B) Dependence of k^{obs} for HSA-heme-Fe(III) nitrosylation on [NO]. The continuous line was generated from Eqn (2) with $k_{on} = (1.3 \pm 0.2) \times 10^4$ $M^{-1} \cdot s^{-1}$ and $k_{off} = (2.0 \pm 0.2) \times 10^{-1}$ s^{-1}. (C) Dependence of Y for HSA-heme-Fe(III) nitrosylation on free [NO]. Open and filled triangles indicate values of Y obtained from equilibrium and kinetic experiments, respectively. The continuous line was generated from Eqn (3) with $K = (1.5 \pm 0.2) \times 10^{-5}$ M. The HSA-heme-Fe(III) concentration was 3.3×10^{-6} M. The equilibration time was 10 min. For details, see the text.

because the spectrum of HSA-heme-Fe(II)-NO reverted to HSA-heme-Fe(II) instead of to HSA-heme-Fe(III) by merely pumping off gaseous NO or by bubbling helium through the HSA-heme-Fe(II)-NO solution; however, the denitrosylation process needs about 12 h for completion.

The optical absorption spectra of the HSA-heme derivatives observed here correspond to those reported in the literature [29,35,43]. Free HSA-heme-Fe(II) was never detected spectrophotometrically because of the very rapid reaction between HSA-heme-Fe(II) and NO ($l_{on} \geq 1.2 \times 10^7$ $M^{-1} \cdot s^{-1}$; see Table 1).

Over the whole NO concentration range explored, the time course for HSA-heme-Fe(III) reductive nitrosylation corresponded to a biphasic process (Fig. 2 and Eqn 4); values of k^{obs} and h^{obs} were wavelength-independent at a fixed concentration of NO. The first step of kinetics for HSA-heme-Fe(III) reductive nitrosylation (indicated by k_{on} in Scheme 1) was a bimolecular process, as observed under pseudo-first-order conditions (Fig. 2). Plots of k^{obs} versus [NO] were linear (Eqn 2), the slope corresponding to k_{on}. Values of k_{on} ranged between 7.5×10^3 and 2.4×10^4 $M^{-1} \cdot s^{-1}$ over the pH range explored (Table 1). The y intercept of plots of k^{obs} versus [NO] corresponded to k_{off}; the values of k_{off} ranged between 1.9×10^{-1} and 4.8×10^{-1} s^{-1} (Table 1). By contrast, the second step (indicated by h^{obs} in Scheme 1) followed an [NO]-independent monomolecular behavior (Fig. 2) at all pH values investigated. According to Scheme 1, the value of h^{obs} increased linearly on increasing [OH^-] (i.e. from pH 6.5 to 9.5; see Fig. 3, Table 1 and Eqn 5). The slope and the y intercept of the plot of h^{obs} versus [OH^-] corresponded to h_{OH^-} ($= 4.4 \times 10^3$ $M^{-1} \cdot s^{-1}$) and to h_{H_2O} ($= 3.5 \times 10^{-4}$ s^{-1}), respectively (Table 1).

Between pH 6.5 and pH 9.5, the molar fraction of HSA-heme-Fe(III)-NO (i.e. Y) increased on free [NO], tending to level off at [NO] > $10 \times K$, according to Eqn (3). The analysis of data according to Eqn (3) allowed us to determine values of K, ranging between 1.3×10^{-5} and 3.1×10^{-5} M, at 20 °C over the pH range investigated (Table 1). According to the HSA-heme-Fe(III) : NO 1 : 1 stoichiometry of reaction (a) in Scheme 1, the Hill coefficient n was 1.00 ± 0.02. As expected for a simple system [44], values of K corresponded to those of k_{off}/k_{on}, under all the experimental conditions investigated (Table 1).

Determination of nitrite, nitrate and *S*-nitrosothiols

The concentrations of nitrite, nitrate and *S*-nitrosothiols were determined after HSA-heme-Fe(III) reductive

Table 1. Values of thermodynamic and kinetic parameters for reductive nitrosylation of HSA-heme-Fe(III), at 20 °C. ND, not determined.

pH	K (M)	k_{on} ($M^{-1}\cdot s^{-1}$)	k_{off} (s^{-1})	k_{off}/k_{on} (M)	h^{obs} (s^{-1})	L (M)	l_{on} ($M^{-1}\cdot s^{-1}$)	l_{off} (s^{-1})	l_{off}/l_{on} (M)
5.5	1.5×10^{-5}	1.3×10^{4}	2.0×10^{-1}	1.5×10^{-5}	[a] –	$\leq 3.3 \times 10^{-8}$	1.6×10^{7}	1.3×10^{-4}	8.1×10^{-12}
6.5	2.9×10^{-5}	1.5×10^{4}	4.8×10^{-1}	3.2×10^{-5}	2.1×10^{-4}	$\leq 3.3 \times 10^{-8}$	ND	2.4×10^{-4}	ND
7.5	1.8×10^{-5}	2.1×10^{4}	3.1×10^{-1}	1.5×10^{-5}	1.7×10^{-3}	$\leq 3.3 \times 10^{-8}$	2.1×10^{7}	1.4×10^{-4}	6.7×10^{-12}
8.1	3.1×10^{-5}	8.5×10^{3}	2.5×10^{-1}	2.9×10^{-5}	6.3×10^{-3}	$\leq 3.3 \times 10^{-8}$	ND	2.1×10^{-4}	ND
8.5	1.3×10^{-5}	1.6×10^{4}	1.9×10^{-1}	1.2×10^{-5}	1.4×10^{-2}	$\leq 3.3 \times 10^{-8}$	1.2×10^{7}	1.7×10^{-4}	1.4×10^{-11}
9.0	1.9×10^{-5}	2.4×10^{4}	3.6×10^{-1}	1.5×10^{-5}	3.5×10^{-2}	$\leq 3.3 \times 10^{-8}$	ND	1.9×10^{-4}	ND
9.5	2.6×10^{-5}	7.5×10^{3}	2.1×10^{-1}	2.8×10^{-5}	1.4×10^{-1}	$\leq 3.3 \times 10^{-8}$	1.8×10^{7}	2.6×10^{-4}	1.4×10^{-11}

[a] HSA-heme-Fe(III)-NO does not undergo significant reductive nitrosylation at pH 5.5 (< 5% in 30 min).

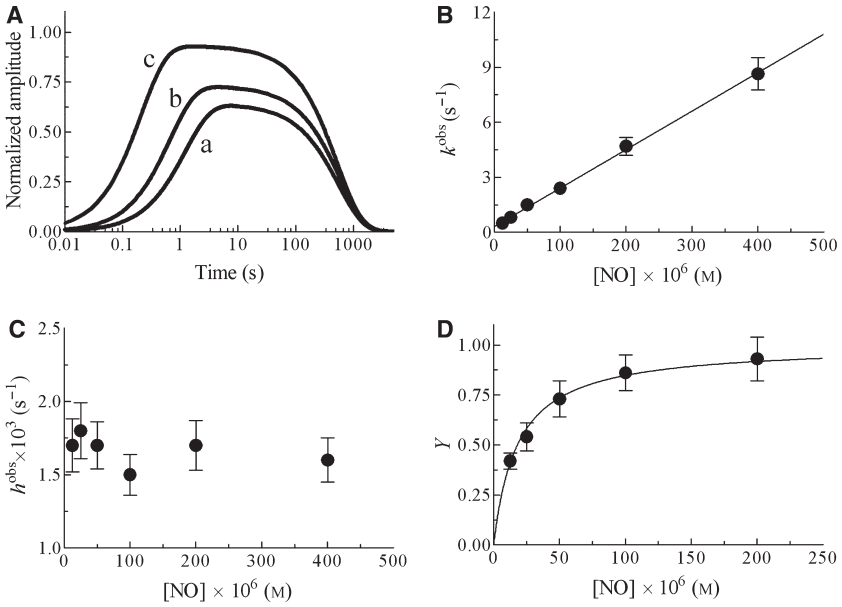

Fig. 2. HSA-heme-Fe(III) reductive nitrosylation, at pH 7.5 and 20 °C. (A) Normalized averaged time courses of HSA-heme-Fe(III) reductive nitrosylation. The NO concentrations were 2.5×10^{-5} M (trace a), 5.0×10^{-5} M (trace b) and 2.0×10^{-4} M (trace c). The time course analysis according to Eqn (4a–c) allowed the determination of the following values of k^{obs}, h^{obs} and Y: trace a, $k^{obs} = 8.1 \times 10^{-1}$ s^{-1}, $h^{obs} = 1.8 \times 10^{-3}$ s^{-1} and $Y = 0.64$; trace b, $k^{obs} = 1.5$ s^{-1}, $h^{obs} = 1.7 \times 10^{-3}$ s^{-1} and $Y = 0.73$; and trace c, $k^{obs} = 4.7$ s^{-1}, $h^{obs} = 1.9 \times 10^{-3}$ s^{-1} and $Y = 0.93$. (B) Dependence of k^{obs} for HSA-heme-Fe(III) reductive nitrosylation on [NO]. The continuous line was generated from Eqn (2) with $k_{on} = (2.1 \pm 0.2) \times 10^4$ $M^{-1}\cdot s^{-1}$ and $k_{off} = (3.1 \pm 0.3) \times 10^{-1}$ s^{-1}. (C) Dependence of h^{obs} for HSA-heme-Fe(III) reductive nitrosylation on [NO]. The average h^{obs} value is 1.7×10^{-3} s^{-1}. (D) Dependence of Y for HSA-heme-Fe(III) reductive nitrosylation on free [NO]. The continuous line was generated from Eqn (3) with $K = (1.8 \pm 0.2) \times 10^{-5}$ M. The HSA-heme-Fe(III) concentration was 3.3×10^{-6} M. For details, see the text.

nitrosylation, at pH 7.5 and 20 °C. As shown in Table 2, reductive nitrosylation of HSA-heme-Fe(III) yielded essentially NO_2^- (NO_3^- < 10%). Under conditions where [NO] ≤ [HSA-heme-Fe(III)], $[NO_2^-] + [NO_3^-] = ½[NO]$. However, where [NO] = 2 × [HSA-heme-Fe(III)], $[NO_2^-] + [NO_3^-] = [$HSA-heme-Fe(III)$]$. Moreover, the [HSA-heme-Fe(III)] : NO : [HSA-heme-Fe(II)-NO] : NO_2^- stoichiometry is 1 : 2 : 1 : 1. Lastly, *S*-nitrosylation of the single thiol present in HSA (i.e. Cys34) does not significantly occur during reductive nitrosylation of HSA-heme-Fe(III) (< 10%; data not shown).

Reversible nitrosylation of HSA-heme-Fe(II) between pH 5.5 and pH 9.5

The addition of NO (either gaseous or dissolved in the buffer solution) to the HSA-heme-Fe(II) solution brings about a shift in the maximum of the optical absorption spectrum in the Soret band from 418 nm [i.e. HSA-heme-Fe(II)] to 389 nm [i.e. HSA-heme-Fe(II)-NO] and a corresponding change of the extinction coefficient from $\varepsilon_{418\ nm} = 8.7 \times 10^4$ $M^{-1}\cdot cm^{-1}$ to $\varepsilon_{389\ nm} = 6.4 \times 10^4$ $M^{-1}\cdot cm^{-1}$. The optical absorption spectra of HSA-heme-Fe(II) and HSA-heme-Fe(II)-NO

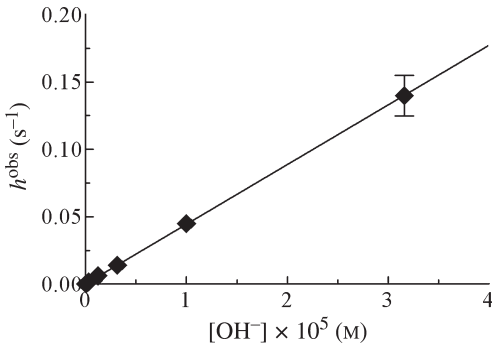

Fig. 3. Dependence of h^{obs} on [OH$^-$] for HSA-heme-Fe(III) reductive nitrosylation, at 20 °C. The continuous line was generated from Eqn (5) with $h_{OH^-} = (4.4 \pm 0.3) \times 10^3$ M^{-1}·s^{-1} and $h_{H_2O} = (3.5 \pm 0.4) \times 10^{-4}$ s^{-1} For details, see the text.

Table 2. NO_2^- and NO_3^- concentration obtained by reductive nitrosylation of HSA-heme-Fe(III), at pH 7.5 and 20 °C. The HSA-heme-Fe(III) concentration was 1.0×10^{-4} M.

[NO] (M)	[NO_2^-] (M)	[NO_3^-] (M)	[NO_2^-] + [NO_3^-] (M)
5.0×10^{-5}	$(2.4 \pm 0.3) \times 10^{-5}$	$(1.2 \pm 0.2) \times 10^{-6}$	2.5×10^{-5}
1.0×10^{-4}	$(4.7 \pm 0.5) \times 10^{-5}$	$(3.1 \pm 0.4) \times 10^{-6}$	5.0×10^{-5}
2.0×10^{-4}	$(9.2 \pm 0.9) \times 10^{-5}$	$(7.1 \pm 0.8) \times 10^{-6}$	9.9×10^{-5}

determined here correspond to those reported in the literature [25,27,28,32,34,35,43]. The reaction is completely reversible because the spectrum reverts to the initial absorption spectrum by merely pumping off gaseous NO or bubbling helium through the solution; however, the denitrosylation process needs about 12 h to be completed.

Under all the experimental conditions investigated, the time course for reversible nitrosylation of HSA-heme-Fe(II) conformed to a single-exponential decay for 90–94% of its course (Fig. 4 and Eqn 6). Values of l^{obs} were wavelength- and NO-independent at fixed NO concentrations. Figure 4 shows the linear dependence of l^{obs} for HSA-heme-Fe(II) nitrosylation on the NO concentration (i.e. [NO]). The analysis of data according to Eqn (7) allowed us to determine values of k_{on} ranging between 1.2×10^7 and 2.1×10^7 M^{-1}·s^{-1} (Table 1).

Under all the experimental conditions, the time-course for HSA-heme-Fe(II)-NO denitrosylation [i.e. NO replacement by carbon monoxide (CO)] conforms to a single-exponential decay (from 97% to 102%) of its course (Fig. 4). The analysis of data according to Eqn (8) allowed us to determine l_{off} values ranging between 1.3×10^{-4} and 2.6×10^{-4} s^{-1}, at 20 °C over the pH range explored (Table 1). Values of l_{off} are pH-, wavelength- and CO-independent in the presence of an excess of sodium dithionite. The l_{off} values reported here correspond to those determined previously in the absence of allosteric effectors [24,30,33].

Figure 4 shows the dependence of the molar fraction of HSA-heme-Fe(II)-NO (i.e. Y) on the NO concentration (i.e. [NO]). The value of Y increased linearly with the NO concentration, reaching the maximum ($= 1.0 \pm 0.05$) at the 1 : 1 HSA-heme-Fe(II):NO molar ratio, even at the minimum HSA-heme-Fe(II) concentration investigated ($= 3.3 \times 10^{-6}$ M). According to the literature [45], this behavior reflects a very high affinity of NO for HSA-heme-Fe(II), the value of the dissociation equilibrium constant L being lower than that of the HSA-heme-Fe(II) concentration by at least two orders of magnitude; thus, $L \leq 3 \times 10^{-8}$ M over the whole pH range explored, at 20 °C (Table 1). As expected for a simple reversible ligand-binding system [44], the values of L agree with those calculated from l_{on} and l_{off} (i.e. $L = l_{off}/l_{on}$), under all the experimental conditions investigated (Table 1).

Discussion

HSA-heme-Fe(III) undergoes irreversible reductive nitrosylation between pH 6.5 and pH 9.5, under anaerobic conditions. In fact, the addition of NO to HSA-heme-Fe(III) leads to the transient formation of HSA-heme-Fe(III)-NO in equilibrium with HSA-heme-Fe(II)-NO^+. Then, HSA-heme-Fe(II)-NO^+ undergoes nucleophilic attack by OH^- to yield HSA-heme-Fe(II). HSA-heme-Fe(II) thus produced reacts further with NO to give HSA-heme-Fe(II)-NO. By contrast, at pH 5.5, HSA-heme-Fe(III) undergoes fully reversible NO binding. In fact, the HSA-heme-Fe(III)-NO derivative does not convert significantly to HSA-heme-Fe(II)-NO (Fig. 1 and Table 1). The data reported here match well with Scheme 1, the NO : NO_2^- stoichiometry being 2 : 1. Moreover, no significant formation of *S*-nitrosothiol occurs during the reductive nitrosylation of HSA-heme-Fe(III).

The analysis of kinetic and thermodynamic parameters reported in Table 3 allows the following considerations.

(a) The values of k_{on} and l_{on} for the reductive nitrosylation of ferric rabbit hemopexin-heme-Fe (HPX-heme-Fe) [46] and horse cytochrome *c* [38,39] are lower than those reported for HSA-heme-Fe (the present study), *Glycine max* leghemoglobin (*G. max* Lb) [42], sperm whale myoglobin (Mb) [38,39] and tetrameric human hemoglobin (Hb) [39]. This reflects the hexa-coordination of the heme-Fe atom of rabbit HPX-heme-Fe and horse

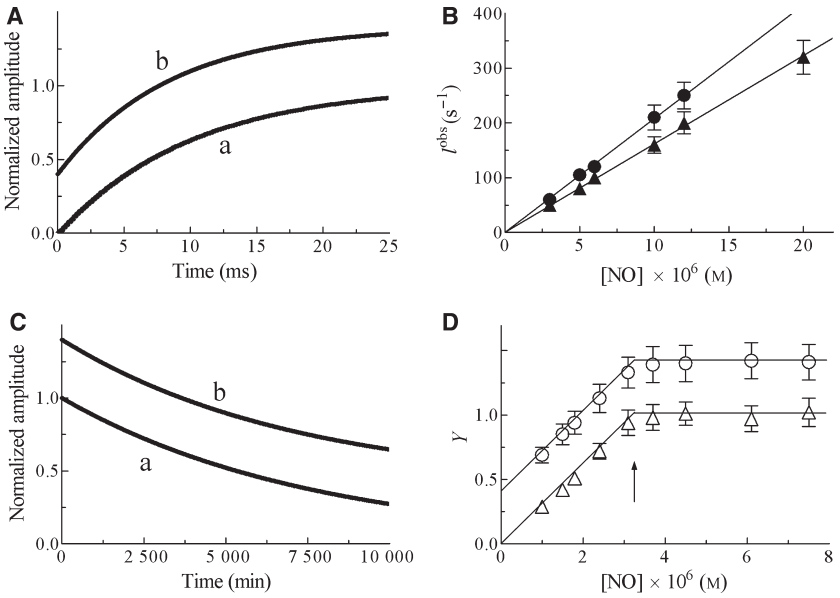

Fig. 4. HSA-heme-Fe(II) nitrosylation at pH 5.5 and 7.5, and at 20 °C. (A) Normalized averaged time course of HSA-heme-Fe(II) nitrosylation at pH 5.5 (trace a) and 7.5 (trace b), and at 20 °C. The time course analysis according to Eqn (6) allowed the determination of the following values of k^{obs}: 1.0×10^2 s^{-1} (trace a) and 1.2×10^2 s^{-1} (trace b). For clarity, the time course obtained at pH 7.5 was up-shifted by 0.4. The HSA-heme-Fe(II) and NO concentrations were 1.2×10^{-6} and 6.0×10^{-6} M, respectively. (B) Dependence of k^{obs} for HSA-heme-Fe(II) nitrosylation on [NO] at pH 5.5 (triangles) and 7.5 (circles), and at 20 °C. The continuous lines were generated from Eqn (7) using the following values of k_{on}: $(1.6 \pm 0.2) \times 10^7$ $M^{-1} \cdot s^{-1}$ (pH 5.5) and $(2.1 \pm 0.2) \times 10^7$ $M^{-1} \cdot s^{-1}$ (pH 7.5). (C) Normalized averaged time courses of HSA-heme-Fe(II)-NO denitrosylation, at pH 5.5 (trace a) and 7.5 (trace b), and at 20 °C. The time course analysis according to Eqn (8) allowed the determination of the following values of k_{off}: 1.3×10^{-4} s^{-1} (trace a) and 1.4×10^{-4} (trace b). For clarity, the time course obtained at pH 7.5 was up-shifted by 0.4. The HSA-heme-Fe(II)-NO, CO and sodium dithionite concentrations were 3.3×10^{-6}, 2.0×10^{-4} and 1.0×10^{-2} M, respectively. (D) Dependence of Y on [NO] for HSA-heme-Fe(II) nitrosylation at pH 5.5 (triangles) and 7.5 (circles), and at 20 °C. The arrow indicates the 1 : 1 molar ratio of HSA-heme-Fe(II) : NO. For clarity, the values of Y obtained at pH 7.5 were up-shifted by 0.4. The HSA-heme-Fe(II) concentration was 3.3×10^{-6} M. For details, see the text.

cytochrome *c*, which must undergo transient penta-coordination to allow exogenous ligand (i.e. NO) binding [47,48].

(b) Values of k_{off} for NO dissociation from heme-Fe(III)-NO complexes range between $\leq 10^{-4}$ and 1.4×10^1 s^{-1}, while values of l_{off} for NO dissociation from heme-Fe(II)-NO complexes are always $\leq 10^{-3}$ s^{-1}. This may reflect the different stabilization mode of the heme-Fe bound (e.g. NO) by heme distal residues [32,47–53].

(c) Although values of k_{on} and k_{off} for NO binding to heme-Fe(III) proteins are very different, values of K ($= k_{off}/k_{on}$) are closely similar, indicating the occurrence of kinetic compensation phenomena. By contrast, values of L ($= l_{off}/l_{on}$) are markedly different, primarily as a result of l_{on} values. As a whole, this may reflect the interplay between the redox state of the heme-Fe atom and the nitrosylation process.

(d) The h_{OH^-} value for reductive nitrosylation of rabbit HPX-heme-Fe(III) ($\geq 7 \times 10^5$ $M^{-1} \cdot s^{-1}$) [46] is larger than those reported for HSA-heme-Fe(III) (the present study), horse cytochrome *c*(III) [38,39], *G. max* Lb(III) [42], sperm whale Mb(III) [38,39] and human Hb(III) [39], ranging between 3.2×10^2 and 4.4×10^3 $M^{-1} \cdot s^{-1}$. This may reflect different anion accessibility to the heme pocket [44,54] and heme-protein reduction potentials [39,42].

(e) Although the values of h_{OH^-} and h_{H_2O} cannot be compared directly, OH^- ions catalyze reductive nitrosylation of HSA-heme-Fe(II)-NO^+ much more efficiently than H_2O (the present study), as previously reported for *G. max* Lb(III) [42] and human Hb(III) [39], reflecting the role of OH^- in heme-Fe(II) formation [39]. According to the literature [39,42], the pH dependence of h^{obs} has been attributed to changes of the OH^- concentration. The linear dependence of h^{obs} on [OH^-] indicates that no additional elements appear to be involved in irreversible reductive nitrosylation of HSA-heme-Fe(III) (see Scheme 1, Eqn 5 and Fig. 3).

Table 3. Values of thermodynamic and kinetic parameters for reductive nitrosylation of heme proteins. ND, not determined.

Heme protein	K (M)	k_{on} (M^{-1}·s^{-1})	k_{off} (s^{-1})	k_{off}/k_{on} (M)	h_{OH^-} (M^{-1}·s^{-1})	h_{H_2O} (s^{-1})	L (M)	l_{on} (M^{-1}·s^{-1})	l_{off} (s^{-1})	l_{off}/l_{on} (M)
HSA-heme-Fe	[a]1.8×10^{-5}	[a]2.1×10^{4}	[a]3.1×10^{-1}	[a]1.5×10^{-5}	[b]4.4×10^{3}	[b]3.5×10^{-4}	[a]$\leq 2 \times 10^{-8}$	[a]2.1×10^{7}	[a]1.4×10^{-4}	[a]6.7×10^{-12}
Rabbit HPX-heme-Fe	ND	[c]1.3×10^{1}	[c]$\leq 10^{-4}$	[c]$\leq 8 \times 10^{-6}$	[d]$\geq 7 \times 10^{5}$	ND	[e]1.4×10^{-7}	[f]6.3×10^{3}	[f]9.1×10^{-4}	[f]1.4×10^{-7}
Horse cytochrome *c*	[g]6.1×10^{-5}	[g]7.2×10^{2}	[g]4.4×10^{-2}	[g]6.1×10^{-5}	[h]1.5×10^{3}	ND	[g]3.4×10^{-6}	[g]8.3	[g]2.9×10^{-5}	[g]3.5×10^{-6}
G. max Lb	[i]2.1×10^{-5}	[i]1.4×10^{5}	[i]3.0	[i]2.1×10^{-5}	[i]3.3×10^{3}	[i]3.0×10^{-4}	ND	[k]1.2×10^{8}	[k]2.4×10^{-5}	[k]2.0×10^{-13}
Sperm whale Mb	[g]7.7×10^{-5}	[g]1.9×10^{6}	[g]1.4×10^{1}	[g]7.5×10^{-5}	[h]3.2×10^{2}	ND	ND	[l]1.7×10^{7}	[l]1.2×10^{-4}	[l]7.1×10^{-12}
Tetrameric human Hb										
α subunits	[m]8.3×10^{-5}	[n]1.7×10^{3}	[n]6.5×10^{-1}	[n]3.8×10^{-4}	[h]3.2×10^{3}	[h]1.1×10^{-3}	[l]$\leq 10^{-11}$	[o]2.6×10^{7}	[l]$\leq 10^{-3}$	ND
β subunits	[m]8.3×10^{-5}	[n]6.4×10^{3}	[n]1.5	[n]2.3×10^{-4}	[h]3.2×10^{3}	[h]1.1×10^{-3}	[l]$\leq 10^{-11}$	[o]2.6×10^{7}	[l]$\leq 10^{-3}$	ND

[a] 1.0×10^{-1} M Bis-Tris propane buffer, pH 7.5 and 20 °C. Present study. [b] 1.0×10^{-1} M Bis-Tris propane buffer and 20 °C. Present study. [c] 1.0×10^{-1} M phosphate buffer, pH 7.0 and 10 °C [46]. [d] 1.0×10^{-1} M phosphate buffer and 10 °C [46]; $h_{OH^-} = h^{obs}/[OH^-]$, $[OH^-] = 1.0 \times 10^{-7}$ M. [e] 1.0×10^{-1} M phosphate buffer, pH 7.0 and 10 °C [43]. [f] 1.0×10^{-1} M phosphate buffer, pH 7.0 and 10 °C [59]. [g] Distilled water, pH 6.5 and 20 °C [38]. [h] 1.0×10^{-1} M phosphate buffer, 20 °C [39]. [i] 1.0×10^{-1} M phosphate buffer, pH 7.0 and 20 °C [42]. [j] 1.0×10^{-1} M phosphate buffer and 20 °C [42]. [k] 1.0×10^{-1} M phosphate buffer, pH 7.0 and 20 °C [60]. [l] 5.0×10^{-2} M phosphate buffer, pH 7.0 and 20 °C [61]. [m] 1.0×10^{-1} M phosphate buffer, pH 7.1 and 20 °C [39]. [n] 1.0×10^{-1} M Bis-Tris propane buffer, pH 7.0 and 20 °C [62]. [o] 5.0×10^{-2} M Bis-Tris propane buffer, pH 7.0 and 20.0 °C [63].

However, we cannot exclude that the observed pH effects could also reflect reversible pH-dependent conformational transitions of HSA. In fact, between pH 4.3 and pH 8.0, HSA displays the neutral form, while at pH > 8.0, HSA exhibits the basic form [3,9,36,37].

(f) Different rate-limiting steps affect the reductive nitrosylation of heme-Fe(III) proteins. Indeed, reductive nitrosylation of HSA-heme-Fe(III) (the present study), *G. max* Lb(III) [42], sperm whale Mb(III) [39] and human Hb(III) [39] is limited by the OH^--mediated reduction of HSA-heme-Fe(II)-NO^+ to HSA-heme-Fe(II) (reaction (c) in Scheme 1). By contrast, NO binding to hexa-coordinated rabbit HPX-heme(III) and horse cytochrome *c*(III) (reaction (a) in Scheme 1) represents the rate-limiting step [39,46].

The present results highlight the role of HSA-heme-Fe in the scavenging of reactive nitrogen species. In fact, HSA-heme-Fe(III) facilitates the conversion of NO to NO_2^- (reaction (c) in Scheme 1, and Table 2; the present study) and peroxynitrite isomerization to NO_3^- [34]. Moreover, HSA-heme-Fe(II)-NO catalyzes peroxynitrite detoxification [29]. NO and peroxynitrite scavenging by HSA-heme-Fe (the present study and [29,34]) could occur in patients displaying a variety of severe hemolytic diseases characterized by excessive intravascular hemolysis [29,34]. In fact, under these pathological conditions, the HSA-heme-Fe plasmatic level increases from the low physiological concentration (approximately 1×10^{-6} M), which appears to be irrelevant for catalysis, to high concentrations ($> 1 \times 10^{-5}$ M), which appear to be enzymatically relevant [34].

Lastly, HSA, acting not only as a heme carrier but also displaying transient heme-based properties, represents a case for 'chronosteric effects' [31], which opens the scenario towards the possibility of a time- and metabolite-dependent multiplicity of roles for HSA.

Materials and methods

Materials

HSA (essentially fatty-acid free, ≥ 96%), hemin [iron(III)–protoporphyrin(IX)], Bis-Tris propane and Mes were obtained from Sigma-Aldrich (St Louis, MO, USA). Gaseous NO was purchased from Aldrich Chemical Co. (Milwaukee, WI, USA) and purified by flowing through a NaOH column in order to remove acidic nitrogen oxides. CO was purchased from Linde AG (Höllriegelskreuth, Germany). All other chemicals were obtained from Sigma-Aldrich and Merck AG (Darmstadt, Germany). All

products were of analytical or reagent grade and used without purification unless stated otherwise.

The HSA-heme-Fe(III) solution (1.2×10^{-6}, 3.3×10^{-6} and 2.0×10^{-4} M) was prepared by adding a 0.7 M defect of the heme-Fe(III) stock solution (1.0×10^{-2} M NaOH) to the HSA solution (1.0×10^{-1} M Mes, pH 5.5, or 1.0×10^{-1} M Bis-Tris propane, pH 6.5 to 9.5) at 20 °C [35]. Then, the HSA-heme-Fe(III) solution was degassed and kept under helium.

HSA-heme-Fe(II) was prepared by adding very few grains of sodium dithionite to the HSA-heme-Fe(III) solution (1.2×10^{-6} and 3.3×10^{-6} M) either at pH 5.5 (1.0×10^{-1} M Mes) or between pH 6.5 and pH 9.5 (1.0×10^{-1} M Bis-Tris propane) and 20 °C, under anaerobic conditions [44].

The NO and CO stock solutions were prepared anaerobically by keeping distilled water in a closed vessel under purified NO or CO, at 760.0 mmHg and 20 °C. The solubility of NO and CO in the water is 2.05×10^{-3} and 1.03×10^{-3} M, respectively, at 760.0 mmHg and 20 °C [44]. The NO and CO stock solutions were diluted with degassed 1.0×10^{-1} M Mes buffer (pH 5.5) or Bis-Tris propane buffer (pH 6.5–9.5) to reach the desired concentration (3.0×10^{-6} M $\leq$ [NO] $\leq 4.0 \times 10^{-4}$ M, and 1.0×10^{-4} M $\leq$ [CO] $\leq 5.0 \times 10^{-4}$ M).

Methods

Reversible nitrosylation of HSA-heme-Fe(III) at pH 5.5

Values of the pseudo-first-order rate constant (i.e. k^{obs}; reaction (a) in Scheme 1) and of the dissociation equilibrium constant (i.e. $K = k_{off}/k_{on}$; reaction (a) in Scheme 1) for HSA-heme-Fe(III) nitrosylation were obtained by mixing the HSA-heme-Fe(III) solution (final concentration 3.3×10^{-6} M) with the NO solution (final concentration, 3.0×10^{-6} to 4.0×10^{-4} M) under anaerobic conditions. No gaseous phase was present. HSA-heme-Fe(III) nitrosylation was monitored between 350 and 470 nm.

Values of k^{obs} were obtained according to Eqn (1) [44]:

$$[\text{HSA} - \text{heme} - \text{Fe(III)}]_t = [\text{HSA} - \text{heme} - \text{Fe(III)}]_i \times e^{-k^{obs} \times t} \quad (1)$$

Values of the second-order rate constant for HSA-heme-Fe(III) nitrosylation (i.e. k_{on}; reaction (a) in Scheme 1) and of the first-order rate constant for the dissociation of the HSA-heme-Fe(III)-NO adduct (i.e. k_{off}; reaction (a) in Scheme 1) were determined from the dependence of k^{obs} on [NO], according to Eqn (2) [44]:

$$k^{obs} = k_{on} \times [NO] + k_{off} \quad (2)$$

The value of K ($= k_{off}/k_{on}$; reaction (a) in Scheme 1) was determined from the dependence of the molar fraction of HSA-heme-Fe(III)-NO (i.e. Y) on the free NO concentration (i.e. [NO]), according to Eqn (3) [44]:

$$Y = \frac{[NO]}{K + [NO]} \quad (3)$$

Values of K, k_{on} and k_{off} for HSA-heme-Fe(III) nitrosylation (reaction (a) in Scheme 1) were obtained at pH 5.5 (Mes buffer) and 20 °C.

HSA-heme-Fe(III)-NO was also obtained anaerobically by keeping the HSA-heme-Fe(III) solution under purified gaseous NO (760 mmHg), at pH 5.5 (1.0×10^{-1} M Mes buffer) [38,39].

Irreversible reductive nitrosylation of HSA-heme-Fe(III) between pH 6.5 and pH 9.5

Values of the pseudo-first-order rate constants (i.e. k^{obs} and h^{obs}; reactions (a, c) in Scheme 1, respectively) and of the dissociation equilibrium constant [i.e. K ($= k_{off}/k_{on}$); reaction (a) in Scheme 1] for HSA-heme-Fe(III) reductive nitrosylation were obtained by mixing the HSA-heme-Fe(III) solution (final concentration 3.3×10^{-6} M) with the NO solution (final concentration, 1.2×10^{-5} to 4.0×10^{-4} M) under anaerobic conditions. No gaseous phase was present. HSA-heme-Fe(III) reductive nitrosylation was monitored between 350 and 470 nm.

Values of the pseudo-first-order rate constants k^{obs} and h^{obs} were obtained according to Eqn (4a–c) [38–42,46,55]:

$$[\text{Fe(III)}]_t = [\text{Fe(III)}]_i \times e^{-k^{obs} \times t} \quad (4a)$$

$$[\text{Fe(III)} - \text{NO}]_t = [\text{Fe(III)}]_i \times k^{obs} \times \left(\frac{e^{-k^{obs} \times t}}{h^{obs} - k^{obs}} + \frac{e^{-h^{obs} \times t}}{k^{obs} - h^{obs}} \right) \quad (4b)$$

$$[\text{Fe(II)} - \text{NO}]_t = [\text{Fe(III)}]_i - [\text{Fe(III)}]_t + [\text{Fe(III)} - \text{NO}]_t \quad (4c)$$

Values of k_{on} and k_{off} (reaction (a) in Scheme 1) were determined from the dependence of k^{obs} on [NO], according to Eqn (2) [44].

Values of K ($= k_{off}/k_{on}$; reaction (a) in Scheme 1) were determined from the dependence of Y on [NO], according to Eqn (3) [44].

The value of the second-order rate constant for OH^--catalyzed conversion of HSA-heme-Fe(II)-NO^+ to HSA-heme-Fe(II) (i.e. h_{OH^-}; reaction (c) in Scheme 1) was determined from the dependence of h^{obs} on [OH^-] according to Eqn (5) [38,39]:

$$h^{obs} = h_{OH^-} \times [OH^-] + h_{H_2O} \quad (5)$$

where $h_{H_2O}$is the first-order rate constant for the H_2O-catalyzed conversion of HSA-heme-Fe(II)-NO^+ to HSA-heme-Fe(II).

Values of K, k_{on}, k_{off} and h^{obs} for HSA-heme-Fe(III) reductive nitrosylation [reactions (a, c) in Scheme 1] were obtained between pH 6.5 and pH 9.5 (1.0×10^{-1} M Bis-Tris propane buffer) and at 20 °C.

HSA-heme-Fe(III) reductive nitrosylation was also obtained anaerobically by keeping the HSA-heme-Fe(III) solution under purified gaseous NO (760 mmHg), between pH 6.5 and pH 9.5 (1.0×10^{-1} M Bis-Tris propane buffer) and at 20 °C [38,39].

Determination of nitrite, nitrate and *S*-nitrosothiols

The concentrations of nitrite, nitrate and *S*-nitrosothiols were determined after HSA-heme-Fe(III) reductive nitrosylation at pH 7.5 (1.0×10^{-1} M Bis-Tris propane buffer) and at 20 °C. The HSA-heme-Fe(III) concentration was 1.0×10^{-4} M. The NO concentration ranged between 5.0×10^{-5} and 2.0×10^{-4} M. Analysis for nitrite, nitrate and *S*-nitrosothiols was carried out using the Griess and Saville assays, as described previously [34,56–58].

Reversible nitrosylation of HSA-heme-Fe(II) between pH 5.5 and pH 9.5

Values of the pseudo-first-order rate constant [i.e. l^{obs}; see Scheme 1, reaction (d)] for HSA-heme-Fe(II) nitrosylation were obtained by mixing the HSA-heme-Fe(II) (final concentration, 1.2×10^{-6} M) solution with the NO (final concentration, 3.0×10^{-6} to 2.0×10^{-5} M) solution, under anaerobic conditions [44]. No gaseous phase was present. HSA-heme-Fe(II) nitrosylation was monitored between 360 and 460 nm.

Values of l^{obs} were obtained according to Eqn (6) [44]:

$$[\text{HSA} - \text{heme} - \text{Fe(II)}]_t = [\text{HSA} - \text{heme} - \text{Fe(II)}]_i \times e^{-l^{obs} \times t} \quad (6)$$

Values of the second-order rate constant for HSA-heme-Fe(II) nitrosylation [i.e. l_{on}; see Scheme 1, reaction (a)] were determined from the dependence of l^{obs} on [NO], according to Eqn (7) [44]:

$$l^{obs} = l_{on} \times [\text{NO}] \quad (7)$$

Values of the first-order rate constant for NO dissociation from HSA-heme-Fe(II)-NO (i.e. for NO replacement with CO; l_{off}; reaction (d) in Scheme 1) were obtained by mixing the HSA-heme-Fe(II)-NO (final concentration, 3.3×10^{-6} M) solution with the CO (final concentration, 1.0×10^{-4} to 5.0×10^{-4} M) sodium dithionite (final concentration, 1.0×10^{-2} M) solution, under anaerobic conditions [30,33]. No gaseous phase was present. Kinetics was monitored between 360 and 460 nm.

The time course for HSA-heme-Fe(II)-NO denitrosylation [i.e. for HSA-heme-Fe(II) carbonylation] was fitted to a single-exponential process according to the minimum reaction mechanism represented by the following reaction in Scheme 2 [30,34]:

$$\text{HSA-heme-Fe(II)-NO} + \text{CO} \xrightarrow{l_{off}} \text{HSA-heme-Fe(II)}$$
$$+ \text{NO} + \text{CO} \xrightarrow{fast} \text{HSA-heme-Fe(II)-CO} + \text{NO}.$$

Scheme 2. HSA-heme-Fe(II)-NO denitrosylation.

Values of l_{off} were determined from data analysis according to Eqn (8) [30,34]:

$$[\text{HSA} - \text{heme} - \text{Fe(II)} - \text{NO}]_t = [\text{HSA} - \text{heme} - \text{Fe(II)} - \text{NO}]_i \times e^{-l_{off} \times t} \quad (8)$$

Minimum values of the dissociation equilibrium constant for HSA-heme-Fe(II) nitrosylation (i.e., $L = l_{off}/l_{on}$; reaction (d) in Scheme 1) were estimated by titrating the HSA-heme-Fe(II) (final concentration 3.3×10^{-6} M) solution with the NO (final concentration, 1.0×10^{-6} to 2.0×10^{-5} M) solution, under anaerobic conditions. The equilibration time was 5 min. No gaseous phase was present. Thermodynamics was monitored between 360 and 460 nm.

The molar fraction of HSA-heme-Fe(II)-NO (i.e. Y) increases linearly with the NO concentration, reaching the maximum (= 1.0) at the 1 : 1 HSA-heme-Fe(II):NO molar ratio. According to the literature [45], values of L must be lower than the HSA-heme-Fe(II) concentration by at least two orders of magnitude (i.e. $\leq 3.3 \times 10^{-8}$ M) [44].

Values of L, l_{on} and l_{off} for HSA-heme-Fe(II) nitrosylation [reaction (d) in Scheme 1, and Scheme 2] were obtained either at pH 5.5 (1.0×10^{-1} M Mes buffer) or between pH 6.5 and pH 9.5 (1.0×10^{-1} M Bis-Tris propane buffer) and 20 °C.

HSA-heme-Fe(II)-NO was also obtained anaerobically by keeping the HSA-heme-Fe(II) (3.3×10^{-6} M) solution under purified gaseous NO (760 mmHg), either at pH 5.5 (1.0×10^{-1} M Mes buffer) or between pH 6.5 and pH 9.5 (1.0×10^{-1} M Bis-Tris propane buffer) and at 20 °C [24,25,27,30,33,35].

Acknowledgements

This work was partially supported by grants from the Ministero dell'Istruzione, dell'Università e della Ricerca of Italy (PRIN 2007ECX29E_002 and University Roma Tre, CLAR 2009 to P.A.) and from the Ministe-

ro della Salute of Italy (Istituto Nazionale per le Malattie Infettive I.R.C.C.S. 'Lazzaro Spallanzani', Ricerca Corrente 2009 to P.A.).

References

1 Sudlow G, Birkett DJ & Wade DN (1975) The characterization of two specific drug binding sites on human serum albumin. *Mol Pharmacol*, **11**, 824–832.

2 Carter DC & Ho JX (1994) Structure of serum albumin. *Adv Protein Chem*, **45**, 153–203.

3 Peters T (1996) *All about Albumin: Biochemistry, Genetics and Medical Applications*. Academic Press, San Diego and London.

4 Bertucci C & Domenici E (2002) Reversible and covalent binding of drugs to human serum albumin: methodological approaches and physiological relevance. *Curr Med Chem*, **9**, 1463–1481.

5 Kragh-Hansen U, Chuang VT & Otagiri M (2002) Practical aspects of the ligand-binding and enzymatic properties of human serum albumin. *Biol Pharm Bull*, **25**, 695–704.

6 Ascenzi P, Bocedi A, Visca P, Altruda F, Tolosano E, Beringhelli T & Fasano M (2005) Hemoglobin and heme scavenging. *IUBMB Life*, **57**, 749–759.

7 Fasano M, Curry S, Terreno E, Galliano M, Fanali G, Narciso P, Notari S & Ascenzi P (2005) The extraordinary ligand binding properties of human serum albumin. *IUBMB Life*, **57**, 787–796.

8 Ghuman J, Zunszain PA, Petitpas I, Bhattacharya AA, Otagiri M & Curry S (2005) Structural basis of the drug-binding specificity of human serum albumin. *J Mol Biol*, **353**, 38–52.

9 Ascenzi P, Bocedi A, Notari S, Fanali G, Fesce R & Fasano M (2006) Allosteric modulation of drug binding to human serum albumin. *Mini Rev Med Chem*, **6**, 483–489.

10 Yang F, Bian C, Zhu L, Zhao G, Huanga Z & Huang M (2007) Effect of human serum albumin on drug metabolism: structural evidence of esterase activity of human serum albumin. *J Struct Biol* **157**, 348–355.

11 Zunszain PA, Ghuman J, McDonagh AF & Curry S (2008) Crystallographic analysis of human serum albumin complexed with 4*Z*,15*E*-bilirubin-IXalpha. *J Mol Biol*, **381**, 394–406.

12 Ascenzi P & Fasano M (2009) Serum heme-albumin: an allosteric protein. *IUBMB Life*, **61**, 1118–1122.

13 Curry S (2009) Lessons from the crystallographic analysis of small molecule binding to human serum albumin. *Drug Metab Pharmacokinet*, **24**, 342–357.

14 Curry S, Mandelkow H, Brick P & Franks N (1998) Crystal structure of human serum albumin complexed with fatty acid reveals an asymmetric distribution of binding sites. *Nat Struct Biol*, **5**, 827–835.

15 Sugio S, Kashima A, Mochizuki S, Noda M & Kobayashi K (1999) Crystal structure of human serum albumin at 2.5 Å resolution. *Protein Eng*, **12**, 439–446.

16 Bhattacharya AA, Curry S & Franks NP (2000) Binding of the general anesthetics propofol and halothane to human serum albumin. High resolution crystal structures. *J Biol Chem*, **275**, 38731–38738.

17 Bhattacharya AA, Grune T & Curry S (2000) Crystallographic analysis reveals common modes of binding of medium and long-chain fatty acids to human serum albumin. *J Mol Biol*, **303**, 721–732.

18 Petitpas I, Bhattacharya AA, Twine S, East M & Curry S (2001) Crystal structure analysis of warfarin binding to human serum albumin: anatomy of drug site I. *J Biol Chem*, **276**, 22804–22809.

19 Petitpas I, Petersen CE, Ha CE, Bhattacharya AA, Zunszain PA, Ghuman J, Bhagavan NV & Curry S (2003) Structural basis of albumin-thyroxine interactions and familial dysalbuminemic hyperthyroxinemia. *Proc Natl Acad Sci USA*, **100**, 6440–6445.

20 Zunszain PA, Ghuman J, Komatsu T, Tsuchida E & Curry S (2003) Crystal structural analysis of human serum albumin complexed with hemin and fatty acid. *BMC Struct Biol*, **3**, 6.

21 Fasano M, Fanali G, Leboffe L & Ascenzi P (2007) Heme binding to albuminoid proteins is the result of recent evolution. *IUBMB Life*, **59**, 436–440.

22 Fasano M, Baroni S, Vannini A, Ascenzi P & Aime S (2001) Relaxometric characterization of human hemalbumin. *J Biol Inorg Chem*, **6**, 650–658.

23 Marden MC, Hazard ES, Leclerc L & Gibson QH (1989) Flash photolysis of the serum albumin-heme-CO complex. *Biochemistry*, **28**, 4422–4426.

24 Kharitonov VG, Sharma VS, Magde D & Koesling D (1997) Kinetics of nitric oxide dissociation from five- and six-coordinate nitrosyl hemes and heme proteins, including soluble guanylate cyclase. *Biochemistry*, **36**, 6814–6818.

25 Mattu M, Vannin A, Coletta M, Fasano M & Ascenzi P (2001) Effect of bezafibrate and clofibrate on the heme-iron geometry of ferrous nitrosylated heme-human serum albumin: an EPR study. *J Inorg Biochem*, **84**, 293–296.

26 Monzani E, Bonafe B, Fallarini A, Redaelli C, Casella L, Minchiotti L & Galliano M (2001) Enzymatic properties of human hemalbumin. *Biochim Biophys Acta*, **1547**, 302–312.

27 Fasano M, Mattu M, Coletta M & Ascenzi P (2002) The heme-iron geometry of ferrous nitrosylated heme-serum lipoproteins, hemopexin, and albumin: a comparative EPR study. *J Inorg Biochem*, **91**, 487–490.

28 Komatsu T, Ohmichi N, Nakagawa A, Zunszain PA, Curry S & Tsuchida E (2005) O_2 and CO binding properties of artificial hemoproteins formed by complexing

iron protoporphyrin IX with human serum albumin mutants. *J Am Chem Soc*, **127**, 15933–15942.
29 Ascenzi P & Fasano M (2007) Abacavir modulates peroxynitrite-mediated oxidation of ferrous nitrosylated human serum heme-albumin. *Biochem Biophys Res Commun*, **353**, 469–474.
30 Ascenzi P, Imperi F, Coletta M & Fasano M (2008) Abacavir and warfarin modulate allosterically kinetics of NO dissociation from ferrous nitrosylated human serum heme-albumin. *Biochem Biophys Res Commun*, **369**, 686–691.
31 Fasano M, Fanali G, Fesce R & Ascenzi P (2008) Human serum haeme-albumin: an allosteric 'chronosteric' protein. In *Dioxygen Binding and Sensing Proteins*. M. Bolognesi, G. di Prisco and C. Verde (eds.) pp. 121–131. Springer, Heidelberg.
32 Nicoletti FP, Howes BD, Fittipaldi M, Fanali G, Fasano M, Ascenzi P & Smulevich G (2008) Ibuprofen induces an allosteric conformational transition in the heme complex of human serum albumin with significant effects on heme ligation. *J Am Chem Soc*, **130**, 11677–11688.
33 Ascenzi P, di Masi A, De Sanctis G, Coletta M & Fasano M (2009) Ibuprofen modulates allosterically NO dissociation from ferrous nitrosylated human serum heme-albumin by binding to three sites. *Biochem Biophys Res Commun*, **387**, 83–86.
34 Ascenzi P, di Masi A, Coletta M, Ciaccio C, Fanali G, Nicoletti FP, Smulevich G & Fasano M (2009) Ibuprofen impairs allosterically peroxynitrite isomerization by ferric human serum heme-albumin. *J Biol Chem*, **284**, 31006–31017.
35 Baroni S, Mattu M, Vannini A, Cipollone R, Aime S, Ascenzi P & Fasano M (2001) Effect of ibuprofen and warfarin on the allosteric properties of haem-human serum albumin. A spectroscopic study. *Eur J Biochem*, **268**, 6214–6220.
36 Fanali G, Pariani G, Ascenzi P & Fasano M (2009) Allosteric and binding properties of Asp1-Glu382 truncated recombinant human serum albumin – an optical and NMR spectroscopic investigation. *FEBS J*, **276**, 2241–2250.
37 Fanali G, De Sanctis G, Gioia M, Coletta M, Ascenzi P & Fasano M (2009) Reversible two-step unfolding of heme-human serum albumin: a ^{1}H-NMR relaxometric and circular dichroism study. *J Biol Inorg Chem*, **14**, 209–217.
38 Hoshino M, Ozawa K, Seki H & Ford PC (1993) Photochemistry of nitric oxide adducts of water-soluble iron(III) porphyrin and ferrihemoproteins studied by nanosecond laser photolysis. *J Am Chem Soc*, **115**, 9568–9575.
39 Hoshino M, Maeda M, Konishi R, Seki H & Ford PC (1996) Studies on the reaction mechanism for reductive nitrosylation of ferrihemoproteins in buffer solutions. *J Am Chem Soc*, **118**, 5702–5707.
40 Boffi A, Sarti P, Amiconi G & Chiancone E (2002) The interplay between heme iron and protein sulfhydryls in the reaction of dimeric *Scapharca inaequivalvis* hemoglobin with nitric oxide. *Biophys Chem*, **98**, 209–216.
41 Herold S, Fago A, Weber RE, Dewilde S & Moens L (2004) Reactivity studies of the Fe(III) and Fe(II)NO forms of human neuroglobin reveal a potential role against oxidative stress. *J Biol Chem*, **279**, 22841–22847.
42 Herold S & Puppo A (2005) Kinetics and mechanistic studies of the reactions of metleghemoglobin, ferrylleghemoglobin, and nitrosylleghemoglobin with reactive nitrogen species. *J Biol Inorg Chem*, **10**, 946–957.
43 Fasano M, Bocedi A, Mattu M, Coletta M & Ascenzi P (2004) Nitrosylation of rabbit ferrous heme-hemopexin. *J Biol Inorg Chem*, **9**, 800–806.
44 Antonini E & Brunori M (1971) *Hemoglobin and Myoglobin in their Reactions with Ligands*. North-Holland Publishing Co, Amsterdam.
45 Anderson SR & Antonini E (1968) The binding of carbon monoxide by human hemoglobin. Proof of validity of the spectrophotometric method and direct determination of the equilibrium. *J Biol Chem*, **243**, 2918–2920.
46 Ascenzi P, Bocedi A, Antonini G, Bolognesi M & Fasano M (2007) Reductive nitrosylation and peroxynitrite-mediated oxidation of heme-hemopexin. *FEBS J*, **274**, 551–562.
47 Banci L, Bertini I, Huber JG, Spyroulias GA & Turano P (1999) Solution structure of reduced horse heart cytochrome c. *J Biol Inorg Chem*, **4**, 21–31.
48 Paoli M, Anderson BF, Baker HM, Morgan WT, Smith A & Baker EN (1999) Crystal structure of hemopexin reveals a novel high-affinity heme site formed between two beta-propeller domains. *Nat Struct Biol*, **6**, 926–931.
49 Perutz MF (1989) Myoglobin and haemoglobin: role of distal residues in reactions with haem ligands. *Trends Biochem Sci*, **14**, 42–44.
50 Harutyunyan EH, Safonova TN, Kuranova IP, Popov AN, Teplyakov AV, Obmolova GV, Valnshtein BK, Dodson GG & Wilson JC (1996) The binding of carbon monoxide and nitric oxide to leghaemoglobin in comparison with other haemoglobins. *J Mol Biol*, **264**, 152–161.
51 Brucker EA, Olson JS, Ikeda-Saito M & Phillips GN Jr (1998) Nitric oxide myoglobin: crystal structure and analysis of ligand geometry. *Proteins*, **30**, 352–356.
52 Miele AE, Santanché S, Travaglini-Allocatelli C, Vallone B, Brunori M & Bellelli A (1999) Modulation of ligand binding in engineered human hemoglobin distal pocket. *J Mol Biol*, **290**, 515–524.
53 Chan NL, Kavanaugh JS, Rogers PH & Arnone A (2004) Crystallographic analysis of the interaction of nitric oxide with quaternary-T human hemoglobin. *Biochemistry*, **43**, 118–132.
54 Beetlestone JG, Adeosun OS, Goddard JE, Kushimo JB, Ogunlesi MM, Ogunmola GB, Okonjo KO & Seamonds B (1976) Reactivity difference between

haemoglobins. Part XIX. *J Chem Soc Dalton Trans*, 1251–1278.
55 Bateman H (1910) Solution of a system of differential equations occurring in the theory of radioactive transformations. *Proc Cambridge Phil Soc*, **15**, 423–427.
56 Miranda KM, Espey MG & Wink DA (2001) A rapid, simple spectrophotometric method for simultaneous detection of nitrate and nitrite. *Nitric Oxide*, **5**, 62–71.
57 Herold S & Kalinga S (2003) Metmyoglobin and methemoglobin catalyze the isomerization of peroxynitrite to nitrate. *Biochemistry*, **42**, 14036–14046.
58 Ascenzi P, Bocedi A, Bolognesi M, Fabozzi G, Milani M & Visca P (2006) Nitric oxide scavenging by *Mycobacterium leprae* GlbO involves the formation of the ferric heme-bound peroxynitrite intermediate. *Biochem Biophys Res Commun*, **339**, 450–456.
59 Fasano M, Antonini G & Ascenzi P (2006) O_2-mediated oxidation of hemopexin-heme(II)-NO. *Biochem Biophys Res Commun*, **345**, 704–712.
60 Rohlfs RJ, Olson JS & Gibson QH (1988) A comparison of the geminate recombination kinetics of several monomeric heme proteins. *J Biol Chem*, **263**, 1803–1813.
61 Moore EG & Gibson QH (1976) Cooperativity in the dissociation of nitric oxide from hemoglobin. *J Biol Chem*, **251**, 2788–2794.
62 Sharma VS, Traylor TG, Gardiner R & Mizukami H (1987) Reaction of nitric oxide with heme proteins and model compounds of hemoglobin. *Biochemistry*, **26**, 3837–3843.
63 Cassoly R & Gibson Q (1975) Conformation, co-operativity and ligand binding in human hemoglobin. *J Mol Biol*, **91**, 301–313.

IUBMB *Life*, 63(6): 446–451, June 2011

Research Communication

Binding of Δ9-tetrahydrocannabinol and Diazepam to Human Serum Albumin

Gabriella Fanali[1], Yu Cao[1,2], Paolo Ascenzi[2], Viviana Trezza[2], Tiziana Rubino[1], Daniela Parolaro[1] and Mauro Fasano[1]

[1]*Department of Structural and Functional Biology, and Center of Neuroscience, University of Insubria, Via Alberto da Giussano 12, Busto Arsizio (VA), Italy*

[2]*Department of Biology and Interdepartmental Laboratory for Electron Microscopy, University Roma Tre, Viale Guglielmo Marconi 446, Roma, Italy*

Summary

Cannabis is the most commonly used illicit drug worldwide. Cannabis users also appear to use other psychoactive drugs more frequently than noncannabis users. Here, Δ9-tetrahydrocannabinol (THC) and diazepam binding to human serum albumin (HSA) and HSA-heme is reported. THC binds to two different binding sites of HSA ($K_{d1} \leq 10^{-7}$ M and $K_{d2} = 10^{-3}$ M) without affecting diazepam binding ($K_d = 1.2 \times 10^{-5}$ M). THC binding to the high-affinity site accounts for the low free fraction of the drug in plasma. Moreover, THC increases the affinity of heme for HSA. Accordingly, the affinity of THC for HSA-heme is higher than that for HSA. THC could bind to FA2 and FA7 sites, as substantiated by docking simulations; nevertheless, the observed allosteric effect(s) suggests that the primary binding site of THC is the FA2 cleft that positively modulates heme affinity. Possibly, the HSA conformational transition(s) induced by THC binding could account for drug delivery to the liver through receptor-mediated endocytosis.

IUBMB *Life*, 63(6): 446–451, 2011

Keywords human serum albumin; Δ9-tetrahydrocannabinol binding; diazepam binding; pharmacokinetics; conformational transition(s); poly-drug use.

Abbreviations DMSO, dimethyl sulfoxide; FA, fatty acid; GABA, γ-aminobutyric acid; HSA, human serum albumin; THC, Δ9-tetrahydrocannabinol

Additional Supporting Information may be found in the online version of this article.

Received 11 January 2011; accepted 10 March 2011

Address correspondence to: Gabriella Fanali, Department of Structural and Functional Biology, Via Alberto da Giussano 12, I-21052 Busto Arsizio, Italy. Tel: +39-0331-339414. Fax: +39-0331-339459. E-mail: gabriella.fanali@uninsubria.it

ISSN 1521-6543 print/ISSN 1521-6551 online
DOI: 10.1002/iub.466

INTRODUCTION

Cannabis is the most commonly used illicit drug worldwide. Survey data indicate that the percentage of past-month cannabis users who report past-month use of benzodiazepines (5.6%) is greater than the number of nonusers reporting past-month prescription benzodiazepine use (0.4%) (*1*). Recently, it has been reported that the coadministration of exogenous cannabinoid receptor agonists and diazepam produces additive or synergistic anxiolytic effects in rodents (*2*). However, the mechanism(s) underlying the interaction between cannabinoid and γ-aminobutyric acid (GABA)-ergic systems in the control of anxiety-like behaviors remains to be elucidated. The administration of triazolam in cannabis users increases dose-dependently ratings on "positive" drug-effect questionnaire items, as well as some items consistent with its well-documented sedative effects. Moreover, triazolam also induced significant and robust impairment in psychomotor performance (*3*).

Among plasma carrier proteins, human serum albumin (HSA) plays a relevant role as it carries several endogenous and exogenous ligands including many drugs and in turn alters their pharmacokinetic properties. Drugs may bind to the same site or to different functionally linked clefts following competitive and allosteric mechanisms (*4–10*).

HSA is a globular monomeric protein composed of three structurally similar domains (I, II, and III), each containing two subdomains (A and B) (*5, 7, 9, 11*). HSA shows seven binding clefts hosting different ligands such as fatty acids (FAs), and, therefore, labeled FA1 to FA7 (Fig. 1). In particular, FA3 and FA4 compose the so-called Sudlow's site II (located in subdomain IIIA) and FA7 corresponds to the Sudlow's site I (located in subdomain IIA). Remarkably, ibuprofen and diazepam are representative ligands of Sudlow's site II, whereas warfarin is considered as the stereotypical ligand of Sudlow's site I (*6, 14*). HSA specifically binds the heme at the FA1 site (in subdomain

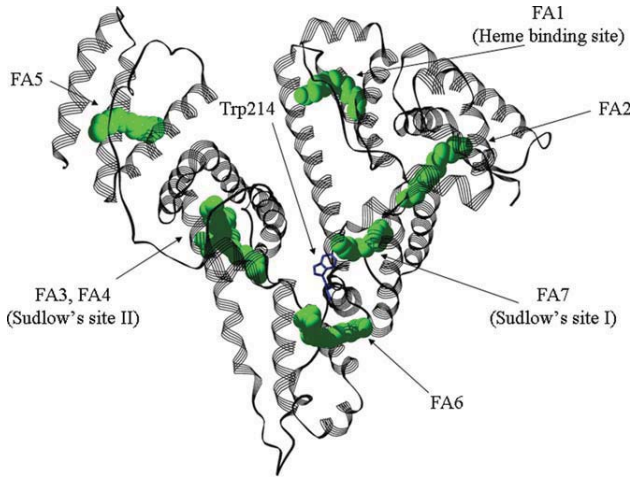

Figure 1. HSA structure. Ribbon representation of the heart-shaped structure of HSA complexed with myristate in fatty acid binding sites (*i.e.*, FAs). Myristate and Trp214 residue are rendered as space-fill (green) and sticks (blue), respectively. Atomic coordinates were taken from PDB entry 1E7G (*12*). The HSA-ligand complex was drawn using UCSF Chimera (*13*). [Color figure can be viewed in the online issue, which is available at wileyonlinelibrary.com.]

IB), contributing to heme homeostasis and possibly to receptor-mediated endocytosis of the heme by hepatocytes (*4, 6, 8, 9, 15–18*). Note that heme binding to HSA is allosterically modulated by ligands that bind to domains I and II and vice versa (*9*).

Here, THC and diazepam binding to HSA and HSA-heme is reported to check the possibility that drug and heme association to HSA could be reciprocally modulated. THC binds to HSA without affecting diazepam binding, thus indicating that these drugs bind to different sites independently. The tight binding of THC to the FA2 site of HSA accounts for the low free fraction of the drug in plasma. Moreover, the HSA conformational transition/s induced by THC binding to the allosteric FA2 site could be at the root of THC delivery to the liver through receptor-mediated endocytosis.

EXPERIMENTAL PROCEDURES

Materials

THC was a generous gifts from GW Pharmaceuticals (Salisbury, UK). All the other reagents (from Sigma-Aldrich, St. Louis, MO) were of the highest purity available. HSA was essentially FA-free (*19–21*). Stock solutions of THC (4.8×10^{-1} M) and diazepam (6.5×10^{-2} M) were prepared by dissolving the drugs in DMSO ($\leq$10%). The heme stock solution was prepared as previously reported (*22*).

Binding of THC to HSA

All experiments have been performed at pH 7.2 (1.0×10^{-1} M phosphate buffer, DMSO $\leq$10%) and 25.0°C. Spectrophotometric experiments have been performed by using an optical cell with 1.0-cm path length on a Cary 50 Bio spectrophotometer (Varian, Palo Alto, CA).

Values of the dissociation equilibrium constants for THC binding to HSA (*i.e.*, K_{d1} and K_{d2}) have been determined spectrophotometrically by adding increasing THC amounts (from 5.0×10^{-7} to 4.0×10^{-5} M) to a fixed HSA concentration (5.0×10^{-6} M). The ligand binding isotherm has been analyzed by plotting the spectral change at 280 nm (*i.e.*, ΔA_{280}) *versus* the THC concentration. Data have been analyzed according to Eq. (1):

$$\Delta A = \Delta A_{\max} - \sum_{i=1}^{2} \frac{\Delta A_i\left([\mathrm{THC}]_t/K_{di} + [\mathrm{HSA}]_t/K_{di} + 1\right) - \sqrt{\left([\mathrm{THC}]_t/K_{di} + [\mathrm{HSA}]_t/K_{di} + 1\right)^2 - 4K_{di}^{-2}[\mathrm{THC}]_t[\mathrm{HSA}]_t}}{2[\mathrm{THC}]_t/K_{di}} \quad (1)$$

where ΔA is the absorbance change at the maximum absorbance wavelength (*i.e.*, at 280 nm), $\Delta A_{\max}$ is the absorbance difference at the saturating THC concentration, ΔA_1 and ΔA_2 are the absorbance differences for drug binding to the high and the low affinity site, respectively, $[THC]_t$ and $[HSA]_t$ are total concentrations.

Values of K_{d1} and K_{d2} for THC binding to HSA have also been obtained spectrofluorimetrically (*23*), using a Cary Eclipse fluorescent spectrophotometer (Varian, Palo Alto, CA). The intrinsic fluorescence of THC and solvents has been subtracted from the THC-induced quenching of HSA intrinsic fluorescence. THC binding to HSA has been analyzed by plotting the difference fluorescence changes with respect to HSA (5.0×10^{-6} M) as a function of the THC concentration (from 5.0×10^{-7} to 4.0×10^{-5} M). Data have been analyzed according to Eq. (2):

$$\Delta I_{336} = \sum_{i=1}^{2} \frac{\Delta I_i\left([\mathrm{THC}]_t/K_{di} + [\mathrm{HSA}]_t/K_{di} + 1\right) - \sqrt{\left([\mathrm{THC}]_t/K_{di} + [\mathrm{HSA}]_t/K_{di} + 1\right)^2 - 4K_{di}^{-2}[\mathrm{THC}]_t[\mathrm{HSA}]_t}}{2[\mathrm{THC}]_t/K_{di}} \quad (2)$$

where ΔI_{336} is the difference of the fluorescence intensity at the maximum emission wavelength (336 nm), ΔI_1 and ΔI_2 are the differences of the fluorescence intensity for drug binding to the high- and low-affinity site, respectively.

Binding of Diazepam to HSA

The value of the dissociation equilibrium constant for diazepam binding to HSA (*i.e.*, K_d) has been determined spectrophotometrically by adding increasing drug amounts (from 2.0×10^{-6} to 1.0×10^{-4} M) to a fixed HSA concentration (5.0×10^{-6} M), in the absence and presence of THC (5.0×10^{-5} M). Data have been analyzed according to Eq. (3):

$$Y = \frac{\Delta A}{\Delta A_{max}} = \frac{\left[\left(K_d^{-1} \cdot [dzp]_t + [\mathrm{HSA}]_t \cdot K_d^{-1} + 1\right) - \sqrt{\left(K_d^{-1} \cdot [dzp]_t + [\mathrm{HSA}]_t \cdot K_d^{-1} + 1\right)^2 - 4K_d^{-2} \cdot [dzp]_t \cdot [\mathrm{HSA}]_t}\right)\right]}{2K_d^{-1} \cdot [dzp]_t} \quad (3)$$

where ΔA is the absorbance difference at the maximum absorbance wavelength (280 nm), ΔA_{max} is the absorbance difference at the saturating diazepam concentration, $[dzp]_t$ is the total diazepam concentration.

Heme Binding to HSA

The value of the dissociation equilibrium constant for heme binding to HSA (*i.e.*, K_d) has been determined spectrophotometrically by adding increasing amounts of HSA to a fixed heme concentration (1.0×10^{-5} M), in the absence and in the presence of 1.0×10^{-4} M THC. Ligand binding isotherms have been analyzed by plotting the absorbance difference at 410 nm *versus* the HSA concentration. Data have been analyzed according to Eq. (4):

$$\Delta A = \frac{\Delta A_{max}\left[\left(K_d^{-1} \cdot [\mathrm{HSA}]_t + [heme]_t \cdot K_d^{-1} + 1\right) - \sqrt{\left(K_d^{-1} \cdot [\mathrm{HSA}]_t + [heme]_t \cdot K_d^{-1} + 1\right)^2 - 4K_d^{-2} \cdot [\mathrm{HSA}]_t \cdot [heme]_t}\right)\right]}{2K_d^{-1} \cdot [\mathrm{HSA}]_t} \quad (4)$$

where ΔA is the absorbance difference at the maximum absorbance wavelength, ΔA_{max} is the absorbance difference at saturating HSA concentration, $[heme]_t$ is the total heme concentration.

Docking Analysis

Automatic flexible ligand docking simulation for THC binding to HSA has been performed by using Autodock 4.0 and the graphical user interface AutoDockTools (*24–26*). The structures of HSA have been downloaded from the Protein Data Bank (PDB entries: 2BXD, 1O9X) (*6, 14*). THC structure has been calculated using the Dundee PRODRG server (*27*). Single bonds have been allowed to rotate freely during the Monte Carlo simulated annealing procedure. The analysis of the conformational space has been restricted to a cubic box of 80-Å edge centered on the coordinates of heme (for FA1), myristate (for FA2 and FA6) and warfarin (for FA7). Monte Carlo simulated annealing has been performed by starting from a temperature of 900 K with a relative cooling factor of 0.95/cycle, to reach the temperature of 5 K in 100 cycles (*24–26*).

RESULTS AND DISCUSSION

THC binding to HSA affects its distribution and metabolism. THC binds to HSA with two independent binding equilibria ($K_{d1} \leq 10^{-7}$ M and $K_{d2} \approx 10^{-3}$ M; Fig. 2A and Supporting Information Fig. S1A). K_d values obtained spectrophotometrically are in agreement with those obtained by analyzing the perturbation of the intrinsic HSA fluorescence (Fig. 2B and Supporting Information Fig. S1B) due to the proximity of the Trp214 residue to the FA7 cleft. Thus, accounting for the physiological concentration of HSA (7.0×10^{-4} M) (*5*), the THC concentration in plasma (3.2×10^{-7} M, after smoking a 3.6% THC cigarette) (*28*), and the K_{d1} value for THC binding to HSA ($\leq 10^{-7}$ M) (present study), the HSA-bound fraction of THC (W) is >99% (for W calculation, *29*).

However, THC does not affect diazepam binding to HSA (Fig. 3), neither by direct competition nor by allosteric effects ($K_d = 1.1 \times 10^{-5}$ and 1.3×10^{-5} M in the absence and presence of THC, respectively). Considering the highest diazepam plasma concentration reported in patients admitted to acute psychiatric treatment (about 5×10^{-6} M) (*30*) and the K_d value for diazepam binding to HSA ($K_d = 1.1 \times 10^{-5}$ M, present study), the HSA-bound fraction of diazepam (W) is >98% (*29*). On this basis, both drugs bind to HSA without affecting their binding properties reciprocally, indicating that the additive and synergistic anxiolytic effects observed during the coadministration of the two drugs (*2*) are not modulated by concomitant binding to HSA. A possible explanation of the drug interaction might rely on the ability of cannabinoid compounds to inhibit glutamate neurotransmission or to amplify GABA(B) signaling, since these receptors share with the CB1 ones the intracellular pathways (Gi/o proteins and modulation of ion channel and

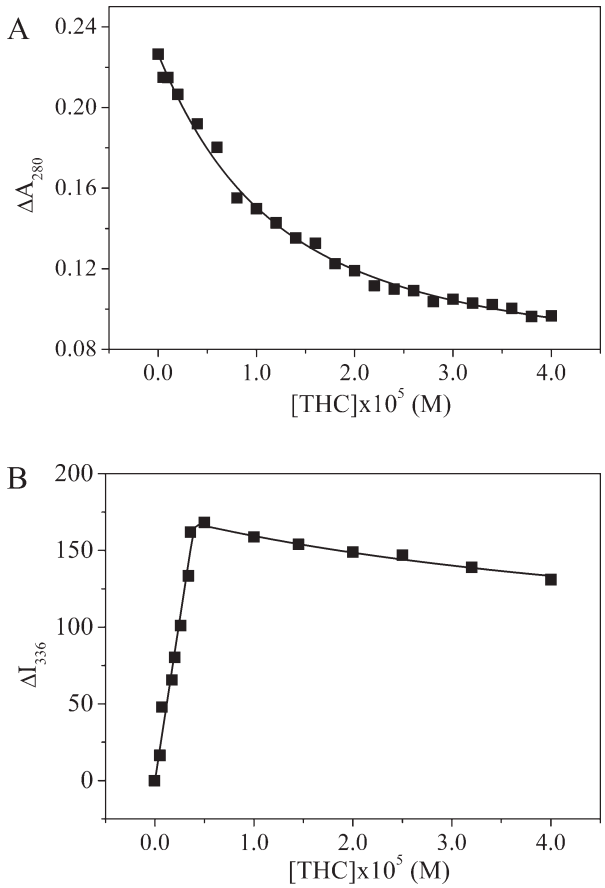

Figure 2. (A) Binding isotherms for THC binding to HSA (5.0×10^{-6} M). The continuous line was calculated according to Eq. (1) with $K_{d1} \leq 10^{-7}$ M and $K_{d2} \approx 10^{-3}$ M. (B) Spectrofluorimetric binding isotherms for THC binding to HSA (5.0×10^{-6} M). The continuous lines were calculated according to Eq. (2) with $K_{d1} \leq 10^{-7}$ M and $K_{d2} \approx 10^{-3}$ M. All data were obtained at pH 7.2 and 25°C.

adenylyl cyclase), but the mechanisms underlying the interaction between cannabinoids and GABAergic systems in the control of anxiety-like behaviors remain to be elucidated (*31*). However, it cannot be ruled out also that the drug interaction may be generated by the metabolite pathways and/or transport.

To better characterize the THC-HSA interaction, heme binding to HSA has been investigated in the presence and in the absence of THC. THC binding to HSA increases the heme affinity for HSA by a factor of 4 ($K_d = 5.0 \times 10^{-7}$ and 1.3×10^{-7} M in the absence and in the presence of THC, respectively; Fig. 4 and Supporting Information Fig. S2), stabilizing heme binding to the protein. The same behavior was observed for myristate binding to HSA-Mn(III)heme and HSA-Fe(III)heme adducts (*32, 33*). The higher affinity of heme for HSA indicates that THC drives a protein conformational change as observed for myristate. In fact, myristate stabilizes the HSA B-conformation

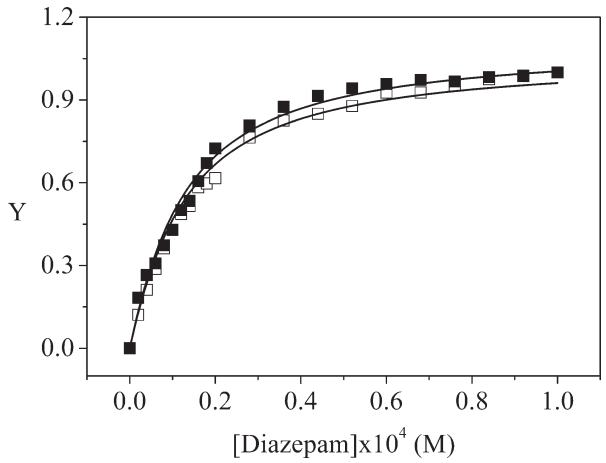

Figure 3. Binding isotherms for diazepam binding to HSA (5.0×10^{-6} M) in the absence (full squares) and in the presence (open squares) of THC (5.0×10^{-5} M). The continuous lines were calculated according to Eq. (3) with $K_d = 1.1 \times 10^{-5}$ and 1.3×10^{-5} M in the absence and presence of THC, respectively. All data were obtained at pH 7.2 and 25°C.

by binding to the FA2 modulatory site responsible for the ligand-induced conformational transition (*9, 32, 33*). Accordingly, THC binding to FA2 shifts HSA toward a compact conformation, where Trp214 is less exposed to the solvent, as witnessed by the enhanced intrinsic fluorescence of HSA upon THC binding. On the other hand, a slight quenching of the Trp214 emission is observed at higher THC concentration, thus suggesting that this drug has a secondary binding site in HSA located in proximity of Trp214. As the observed quenching has been

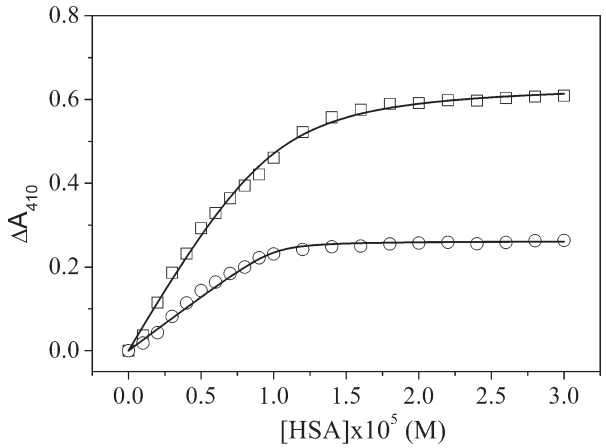

Figure 4. Binding isotherms for heme (1.0×10^{-5} M) binding to HSA in the absence (open squares) and presence of THC (1.0×10^{-4} M; open circles). The continuous lines were calculated according to Eq. (4) with a $K_d = 5.0 \times 10^{-7}$ and 1.3×10^{-7} M in the absence and presence of THC, respectively.

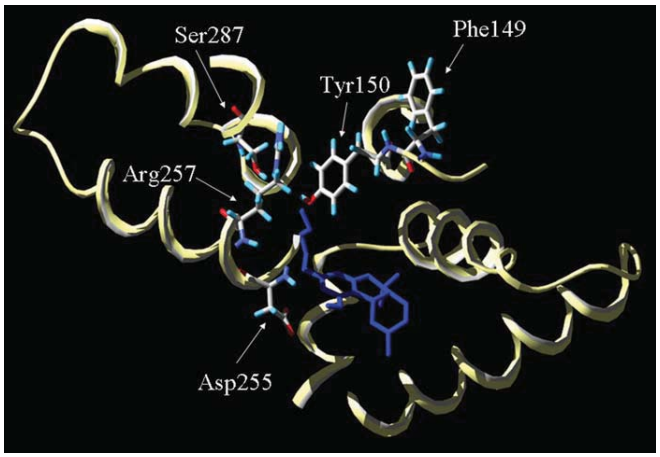

Figure 5. Simulated docking of THC to the FA2 site of HSA. THC is rendered in blue sticks. Phe149, Tyr150, Asp255, Arg257, and Ser287 residues are rendered as sticks. HSA coordinates have been taken from PDB entry 1O9X (*14*). THC coordinates has been calculated by using Autodock 4.0 and the graphical user interface AutoDockTools (*24–26*). [Color figure can be viewed in the online issue, which is available at wileyonlinelibrary.com.]

extensively characterized for several different drugs bound to FA7 (*9, 10, 34*), a second THC molecule could bind with lower affinity to the warfarin site.

Docking simulations (Fig. 5 and Supporting Information Fig. S3) indicate a preferential affinity of THC for FA2 (–36.6 kJ/mol) with respect to FA7 (−32.3 kJ/mol). Although the docking approach did not take into account ligand-induced fit of the binding cavity, the energies reported above are consistent with two orders of magnitude different affinities. Noticeably, THC partially enters the FA2 cavity with the aliphatic tail protruding into the cleft where the FA usually binds. Although the myristate interaction is stabilized by polar contacts of the carboxylate moiety with Tyr150, Arg257, and Ser287 residues, THC appears to establish stabilizing contacts between the phenolic group and Asp255 (Fig. 5 and Supporting Information Fig. S4). This contact could induce the reorientation of Arg257 and of the Phe149-Tyr150 dyad that in turn alters the FA7 conformation (*9*). Indeed, ligand binding to FA2 has a pivotal role in determining the ligand-induced conformational transition(s) in HSA (*9, 10, 29*). The FA2 site is only accessible in the B form; after ligand binding to FA2, the reorientation of domains I and II lines up the two half-cavities and reconstitutes the ligand binding site (*i.e.*, the ligand-dependent induced-fit mechanism is occurring). Accordingly, THC binding to FA2 should be associated with a dramatic conformational change(s). This structural rearrangement has been postulated to be at the root of HSA depletion of FAs (*i.e.*, FA delivery) to the liver by receptor-mediated endocytosis (*9*). Interestingly, heme binding to FA1 stabilizes allosterically the B conformation of HSA facilitating the uptake of the heme by target cells by receptor-mediated endocytosis (*9, 18*).

ACKNOWLEDGEMENTS

The authors thank Prof. Martino Bolognesi for helpful discussion and Dr. Federica Cossu for fluorescence measurements.

REFERENCES

1. SAMHSA. Substance Abuse and Mental Health Service Administration. Office of Applied Studies. Results from the 2007 National Survey on Drug Use and Health: National Findings Office of Applied Studies (NSDUH Series H-34. DHHS Publication No. SMA 08–4343). Rockville, MD.
2. Naderi, N., Haghparast, A., Saber-Tehrani, A., Rezaii, N., Alizadeh, A. M., Khani, A., and Motamedi, F. (2008) Interaction between cannabinoid compounds and diazepam on anxiety-like behaviour of mice. *Pharmacol. Biochem. Behav.* **89**, 64–75.
3. Lile, J. A., Kelly, T. H., and Hays, L. R. (2010) The reinforcing, self-reported performance and physiological effects of Delta9-tetrahydrocannabinol, triazolam, hydromorphone, and methylphenidate in cannabis users. *Behav. Pharmacol.* **21**, 29–38.
4. Sudlow, G., Birkett, D. J., and Wade, D. N. (1975) The characterization of two specific drug binding sites on human serum albumin. *Mol. Pharmacol.* **11**, 824–832.
5. Peters, T. Jr. (1996) *All about Albumin: Biochemistry, Genetics and Medical Applications.* Academic Press, Orlando, FL.
6. Ghuman, J., Zunszain, P. A., Petitpas, I., Bhattacharya, A. A., Otagiri, M., and Curry, S. (2005) Structural basis of the drug-binding specificity of human serum albumin. *J. Mol. Biol.* **353**, 38–52.
7. Ascenzi, P., Bocedi, A., Notari, S., Fanali, G., Fesce, R., and Fasano, M. (2006) Allosteric modulation of drug binding to human serum albumin. *Mini Rev. Med. Chem.* **6**, 483–489.
8. Ascenzi, P. and Fasano, M. (2009) Serum heme-albumin: an allosteric protein. *IUBMB Life* **61**, 1118–1122.
9. Ascenzi, P. and Fasano, M. (2010) Allostery in a monomeric protein: the case of human serum heme-albumin. *Biophys. Chem.* **148**, 16–22.
10. Fanali, G., Rampoldi, V., di Masi, A., Bolli, A., Lopiano, L., Ascenzi, P., and Fasano, M. (2010) Binding of anti-Parkinson's disease drugs to human serum albumin is allosterically modulated. *IUBMB Life* **62**, 371–376.
11. Sugio, S., Kashima, A., Mochizuki, S., Noda, M., and Kobayashi, K. (1999) Crystal structure of human serum albumin at 2.5 Å resolution. *Protein Eng.* **12**, 439–446.
12. Zunszain, P. A., Ghuman, J., Komatsu, T., Tsuchida, E., and Curry, S. (2003) Crystal structural analysis of human serum albumin complexed with hemin and fatty acid. *BMC Struct. Biol.* **3**, 6.
13. Petitpas, I., Grüne, T., Bhattacharya, A. A., and Curry, S. (2001) Crystal structures of human serum albumin complexed with monounsaturated and polyunsaturated fatty acids. *J. Mol. Biol.* **314**, 955–960.
14. Chuang, V. T. G. and Otagiri, M. (2002) How do fatty acids cause allosteric binding of drugs to human serum albumin? *Pharm. Res.* **19**, 1458–1464.
15. Hamilton, J. A. (2004) Fatty acid interactions with proteins: what X-ray crystal and NMR solution structures tell us. *Prog. Lipid. Res.* **43**, 177–199.
16. Fasano, M., Fanali, G., Leboffe, L., and Ascenzi, P. (2007) Heme binding to albuminoid proteins is the result of recent evolution. *IUBMB Life* **59**, 436–440.
17. Chen, R. F. (1967) Removal of fatty acids from serum albumin by charcoal treatment. *J. Biol. Chem.* **242**, 173–181.
18. Sogami, M. and Foster, J. F. (1968) Isomerization reactions of charcoal-defatted bovine plasma albumin. The N-F transition and acid expansion. *Biochemistry* **7**, 2172–2182.
19. Cabrera-Crespo, J., Goncalves, V. M., Martins, E. A., Grellet, S., Lopes, A. P. et al. (2000) Albumin purification from human placenta. *Biotechnol. Appl. Biochem.* **31**, 101–106.

20. Boffi, A., Das, T. K., Della Longa, S., Spagnuolo, C., and Rousseau, D. L. (1999) Pentacoordinate hemin derivatives in sodium dodecyl sulfate micelles: model systems for the assignment of the fifth ligand in ferric heme proteins. *Biophys. J.* **77**, 1143–1149.
21. Bocedi, A., Notari, S., Menegatti, E., Fanali, G., Fasano, M., and Ascenzi, P. (2005) Allosteric modulation of anti-HIV drug and ferric heme binding to human serum albumin. *FEBS J.* **272**, 6287–6296.
22. Goodsell, D. S. and Olson, A. J. (1990) Automated docking of substrates to proteins by simulated annealing. *Proteins* **8**, 195–202.
23. Goodsell, D. S., Morris, G. M., and Olson, A. J. (1998) Automated docking of flexible ligands: Applications of autodock. *J. Mol. Recogn.* **9**, 1–5.
24. Morris, G. M., Goodsell, D. S., Halliday, R. S., Huey, R., Hart, W. E., Belew, R. K., and Olson, A. J. (1998) Automated Docking Using a Lamarckian Genetic Algorithm and Empirical Binding Free Energy Function. *J. Comput. Chem.* **19**, 1639–1662.
25. Schuettelkopf, A. W. and van Aalten, D. M. (2004) PRODRG: a tool for high-throughput crystallography of protein-ligand complexes. *Acta Crystallogr. D Biol. Crystallogr.* **60**, 1355–1363.
26. Cooper, Z. D. and Haney, M. (2009) Comparison of subjective, pharmacokinetic, and physiological effects of marijuana smoked as joints and blunts. *Drug Alcohol Depend.* **103**, 107–113.
27. Bocedi, A., Notari, S., Narciso, P., Bolli, A., Fasano, M., and Ascenzi, P. (2004) Binding of anti-HIV drugs to human serum albumin. *IUBMB Life* **56**, 609–614.
28. Gjerde, H., Mordal, J., Christophersen, A. S., Bramness, J. G., and Mørland, J. (2010) Comparison of drug concentrations in blood and oral fluid collected with the Intercept sampling device. *J. Anal. Toxicol.* **34**, 204–209.
29. Padgett, C. L. and Slesinger, P. A. (2010) GABAB receptor coupling to G-proteins and ion channels. *Adv. Pharmacol.* **58**, 123–147.
30. Fanali, G., Fesce, R., Agrati, C., Ascenzi, P., and Fasano, M. (2005) Allosteric modulation of myristate and Mn(III)heme binding to human serum albumin. Optical and NMR spectroscopy characterization. *FEBS J.* **272**, 4672–4683.
31. Fanali, G., Bocedi, A., Ascenzi, P., and Fasano, M. (2007) Modulation of heme and myristate binding to human serum albumin by anti-HIV drugs. An optical and NMR spectroscopic study. *FEBS J.* **274**, 4491–4502.
32. Bolli, A., Marino, M., Rimbach, G., Fanali, G., Fasano, M., and Ascenzi, P. (2010) Flavonoid binding to human serum albumin. *Biochem. Biophys. Res. Commun.* **398**, 444–449.
33. Bhattacharya, A. A., Gruene, T., and Curry, S. (2000) Crystallographic analysis reveals common modes of binding of medium and long-chain fatty acids to human serum albumin. *J. Mol. Biol.* **303**, 721–732.
34. Pettersen, E. F., Goddard, T. D., Huang, C. C., Couch, G. S., Greenblatt, D. M., Meng, E. C., and Ferrin, T. E. (2004) UCSF chimera—a visualization system for exploratory research and analysis. *J. Comput. Chem.* **25**, 1605–1612.

Biochemical and Biophysical Research Communications 411 (2011) 185–189

Contents lists available at ScienceDirect

Biochemical and Biophysical Research Communications

journal homepage: www.elsevier.com/locate/ybbrc

Ibuprofen and warfarin modulate allosterically ferrous human serum heme–albumin nitrosylation

Paolo Ascenzi [a,*,1], Yu Cao [a,1], Grazia R. Tundo [b,c], Massimo Coletta [b,c], Gabriella Fanali [d], Mauro Fasano [d]

[a] Department of Biology and Interdepartmental Laboratory for Electron Microscopy, University Roma Tre, Via della Vasca Navale 79, I-00146 Roma, Italy
[b] Department of Experimental Medicine and Biochemical Sciences, University of Roma "Tor Vergata", Via Montpellier 1, I-00133 Roma, Italy
[c] Interuniversity Consortium for the Research on the Chemistry of Metals in Biological Systems, Via Celso Ulpiani 27, I-70126 Bari, Italy
[d] Department of Structural and Functional Biology, Center of Neuroscience, University of Insubria, Via Alberto da Giussano 12, I-21052 Busto Arsizio (VA), Italy

ARTICLE INFO

Article history:
Received 13 June 2011
Available online 24 June 2011

Keywords:
Ferrous human serum heme–albumin
Ibuprofen-dependent HSA–heme–Fe(II) nitrosylation
Warfarin-dependent HSA–heme–Fe(II) nitrosylation
Kinetics
Thermodynamics
Allostery

ABSTRACT

Ferrous human serum heme–albumin (HSA–heme–Fe(II)) displays globin-like properties. Here, the effect of ibuprofen and warfarin on kinetics of HSA–heme–Fe(II) nitrosylation is reported. Values of the second-order rate constant for HSA–heme–Fe(II) nitrosylation (k_{on}) decrease from $6.3 \times 10^6\ M^{-1}\ s^{-1}$ in the absence of drugs, to $4.1 \times 10^5\ M^{-1}\ s^{-1}$ and $4.8 \times 10^5\ M^{-1}\ s^{-1}$, in the presence of saturating amounts of ibuprofen and warfarin, respectively, at pH 7.0 and 20.0 °C. From the dependence of k_{on} on the drug concentration, values of the dissociation equilibrium constant for ibuprofen and warfarin binding to HSA–heme–Fe(II) (i.e., $K = 3.2 \times 10^{-3}$ M and 2.6×10^{-4} M, respectively) were determined. The observed allosteric effects could indeed reflect ibuprofen and warfarin binding to the regulatory fatty acid binding site FA2, which brings about an alteration of heme coordination, slowing down HSA–heme–Fe(II) nitrosylation. Present data highlight the allosteric modulation of HSA–heme–Fe(II) reactivity by heterotropic effectors.

1. Introduction

Human serum albumin (HSA), the most abundant protein in plasma, is characterized by an extraordinary ligand binding capacity. Indeed, HSA provides a depot and carrier for many compounds, affects pharmacokinetics of many drugs, provides the metabolic modification of some ligands, renders potential toxins harmless by transporting them to disposal sites, accounts for most of the antioxidant capacity of the human serum, and displays (pseudo-) enzymatic properties [1–16].

The modular three-dimensional structure of HSA provides a variety of ligand binding sites (Fig. 1). Among others, HSA is able to bind up to nine equivalents of long-chain fatty acids (FAs) at multiple binding sites (labeled FA1 to FA9). FA1 has a strong affinity for the ferric heme (heme-Fe(III)), FA3 and FA4 together contribute to Sudlow's site II (i.e., to the ibuprofen primary site), and FA7 corresponds to Sudlow's site I (i.e., the warfarin binding cleft). Moreover, FA2 and FA6 are secondary ibuprofen sites. Remarkably, the heme pocket (i.e., the FA1 cleft) and sites FA2, FA3-FA4 (i.e., Sudlow's site II), FA6, and FA7 (i.e., Sudlow's site I) are allosterically-coupled, ibuprofen and warfarin acting as prototypical allosteric effectors [4,5,8–16,17–34].

Remarkably, HSA is crucial for heme scavenging, providing protection against free heme oxidative damage, limiting the access of pathogens to heme, and contributing to iron homeostasis by recycling the heme iron [10,15,35–37]. In turn, heme binding confers to HSA globin-like spectroscopic and reactivity properties [9,14,16,30,38]. In particular, heme–albumin (HSA–heme–Fe) has been reported to bind NO and to act as a NO and peroxynitrite scavenger, both HSA–heme ligand binding and detoxification properties are modulated allosterically by drugs [14,16,31,34,39–44].

Here, the effect of ibuprofen and warfarin on kinetics of ferrous HSA–heme (HSA–heme–Fe(II)) nitrosylation is reported. Ibuprofen and warfarin binding to FA2 impair allosterically HSA–heme–Fe(II) nitrosylation by inducing His146–Fe(II) coordination. Present data contribute to the description of the allosteric modulation of HSA–heme–Fe(II) reactivity by heterotropic effectors, highlighting the role of FA2 as the warfarin secondary binding cleft.

2. Materials and methods

HSA (essentially FA free), hemin (protoporphyrin IX-Fe(III)) chloride, ibuprofen, and warfarin were obtained from Sigma-Aldrich

Abbreviations: FA, fatty acid; heme-Fe(III), ferric heme; HSA, human serum albumin; HSA–heme–Fe, Heme–albumin; HSA–heme–Fe(II), ferrous HSA–heme–Fe; HSA–heme–Fe(II)-NO, ferrous nitrosylated HSA–heme–Fe.

* Corresponding author. Fax: +39 06 5733 6321.
E-mail address: ascenzi@uniroma3.it (P. Ascenzi).

[1] These authors contributed equally to this work.

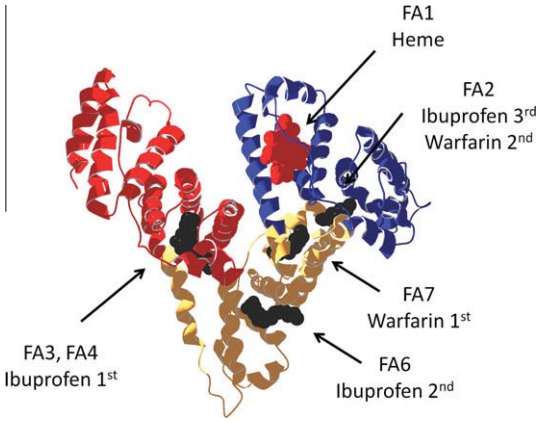

Fig. 1. Ribbon representation of the HSA structure highlighting the modular three-domain architecture (blue: domain I; orange: domain II; red: domain III). Relevant binding sites are labeled as follows: FA1 (heme site, occupied by heme, in red), FA2 (3rd ibuprofen site and 2nd warfarin site, occupied by myristate, in black), FA3 and FA4 (1st ibuprofen site, occupied by two myristates, in black), FA6 (2nd ibuprofen site, occupied by myristate, in black), and FA7 (1st warfarin site, occupied by myristate, in black). The coordinates of HSA complexed with heme and myristate were from PDB entry 1O9X [24]. The picture was drawn with Swiss-PDB-Viewer [52]. (For interpretation of the references to colour in this figure legend, the reader is referred to the web version of this article.)

(St. Louis, MO, USA). NO (from Aldrich Chemical Co., Milwaukee, WI, USA) was purified by flowing it through an NaOH column in order to remove acidic nitrogen oxides. All the other chemicals (from Merck KGaA, Darmstadt, Germany) were of analytical or reagent grade and were used without purification unless stated.

HSA–heme–Fe(II) (2.2×10^{-6} M) was prepared by adding a 1.4-molar excess of HSA to the heme-Fe(II) solution (1.0×10^{-1} M sodium phosphate buffer, pH 7.0), at 20.0 °C [40,41,45].

The NO solution was prepared by keeping in a closed vessel the 1.0×10^{-1} M phosphate buffer solution (pH 7.0) under NO at P = 76.0 mm Hg anaerobically (T = 20.0 °C) [40,41].

The ibuprofen stock solution (2.0×10^{-2} M) was prepared by dissolving the drug in 1.0×10^{-1} M phosphate buffer, at pH 7.0 and 20.0 °C [41]. The warfarin stock solution (2.0×10^{-2} M) was prepared by dissolving the drug in water at pH 10.0, then adjusting pH to 7.0 with HCl [40]. Ibuprofen and warfarin stock solutions were then mixed with the HSA–heme–Fe(II) and NO solutions to obtain the desired final drug concentration.

The NO binding kinetics to HSA–heme–Fe(II) displays two phases, namely a fast ligand-dependent process (amounting to about 80% of the total absorption amplitude) and a slow ligand-independent process (amounting to about 20% of the total absorption amplitude) (see Fig. 1 of the Supplementary data). Kinetics of HSA–heme–Fe(II) nitrosylation were analysed in the framework of the minimum mechanism reported in Scheme 1, focussing only on the predominant fast bimolecular process.

The HSA–heme–Fe(II) nitrosylation process was regarded as irreversible because the rate of the inverse reaction is negligible with respect to values of the pseudo-first order rate constant for ferrous nitrosylated HSA–heme (HSA–heme–Fe(II)-NO) formation (k_{obs}) (see present study and [40,41] for comparison).

Values of k_{obs} for the fast ligand-dependent process were obtained by rapid-mixing the HSA–heme–Fe(II) (final concentration 1.1×10^{-6} M) solution with the NO (final concentration, 5.0×10^{-6}–3.0×10^{-5}) solution under anaerobic conditions, at pH 7.0 (1.0×10^{-1} M sodium phosphate buffer) and 20.0 °C, in the absence and presence of ibuprofen and warfarin (final concentration, 5.0×10^{-5}–1.0×10^{-2} M). Kinetics was monitored

$$\text{HSA-heme-Fe(II)} + \text{NO} \xrightarrow{k_{on}} \text{HSA-heme-Fe(II)-NO}$$

Scheme 1.

between 340 and 460 nm. The dead-time of the rapid-mixing stopped-flow apparatus was 1.4 ms.

Values of k_{obs} for the fast ligand-dependent process were determined from data analysis according to Eq. (1):

$$[\text{HSA—heme—Fe(II)}]_t = [\text{HSA—heme—Fe(II)}]_i \times e^{-k_{obs} \times t} \quad (1)$$

Values of the second-order rate constants for NO binding to HSA–heme–Fe(II) (k_{on}; see Scheme 1) were obtained, in the absence and presence of ibuprofen and warfarin, from the dependence of k_{obs} on the NO concentration (i.e., [NO]) according to Eq. (2):

$$k_{obs} = k_{on} \times [\text{NO}] \quad (2)$$

Values of the dissociation equilibrium constant for ibuprofen and warfarin binding to HSA–heme–Fe(II) (i.e., K) were obtained from the dependence of k_{on} on the drug concentration (i.e., [drug]). Values of K were determined from data analysis, according to Eq. (3):

$$k_{on} = (k^*_{on} - k^0_{on}) - \{((k^*_{on} - k^0_{on}) \times [\text{drug}])/(K + [\text{drug}])\} + k^0_{on} \quad (3)$$

where k^*_{on} is the k_{on} value obtained in the absence of drugs (i.e., under conditions where [drug] = 0), and k^0_{on} is the k_{on} value obtained in the presence of saturating amounts of drugs (i.e., under conditions where [drug] >> K).

Kinetic data were analyzed using the MatLab program (The Math Works Inc., Natick, MA, USA). The results are given as mean values of at least four experiments plus or minus the corresponding standard deviation.

3. Results and discussion

In the absence of drugs, mixing of the HSA–heme–Fe(II) and NO solutions causes a shift of the optical absorption maximum of the Soret band (i.e., λ_{max}) from 418 nm (i.e., HSA–heme–Fe(II)) to 389 nm (i.e., HSA–heme–Fe(II)–NO). In the presence of saturating amounts of ibuprofen and warfarin (1.0×10^{-2} M), mixing of the HSA–heme–Fe(II) and NO solutions causes a shift of λ_{max} from 422 nm (*i.e.*, drug-HSA–heme–Fe(II)) to 418 nm (i.e., drug-HSA–heme–Fe(II)–NO). These spectroscopic observations agree with previous data [19,20,31,46] indicating that the heme–Fe atom of drug-free HSA–heme–Fe(II) and of HSA–heme–Fe(II)–NO is predominantly tetra- and penta-coordinated, respectively, whereas the heme–Fe atom of drug-bound HSA–heme–Fe(II) and of HSA–heme–Fe(II)-NO is predominantly penta- and hexa-coordinated, respectively.

Under all the experimental conditions, the time course for NO binding to HSA–heme–Fe(II) is biphasic (see Fig. 1 of the Supplementary Data). The fast and the slow processes account for about 80% and 20% of the total absorption amplitude, respectively. Noticeably, the fast process displays a typical bimolecular (NO-dependent) behavior and is affected by drug concentration. On the other hand, the slow process is independent of the NO and drug concentration. In this context, data were analysed in the framework of the minimum mechanism reported in Scheme 1, focussing only on the predominant fast bimolecular process.

The time course of the fast bimolecular nitrosylation process of HSA–heme–Fe(II), in the absence and presence of ibuprofen and warfarin, is shown in Figs. 2 and 3 (panel A). Values of the pseudo-first-order rate constant for fast bimolecular nitrosylation of HSA–heme–Fe(II) (i.e., k_{obs}; see Eq. (1)) are wavelength-independent at fixed NO and drug concentration (data not shown).

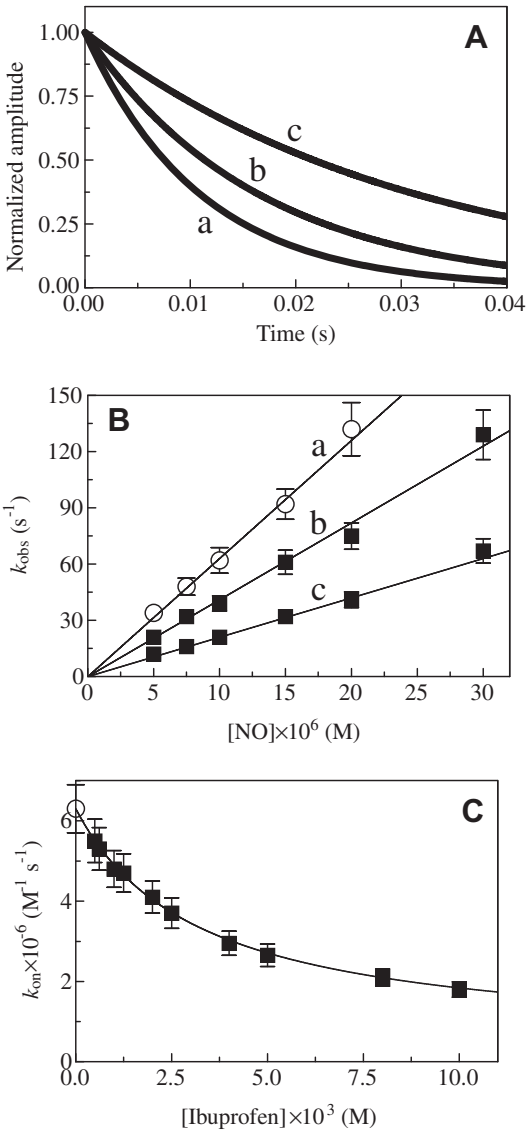

Fig. 2. Effect of ibuprofen on the HSA–heme–Fe(II) nitrosylation. Normalized averaged time courses of NO binding to HSA–heme–Fe(II) in the absence and presence of ibuprofen (A). The ibuprofen concentration was 0.0 M (trace a), 2.0×10^{-3} M (trace b), and 8.0×10^{-3} M (trace c). The time course analysis according to Eq. (1) allowed the determination of the following values of k_{obs}: $9.2 \times 10\ s^{-1}$ (trace a), $6.1 \times 10\ s^{-1}$ (trace b), and $3.2 \times 10\ s^{-1}$ (trace c). The HSA–heme–Fe(II) concentration was 1.1×10^{-6} M. The NO concentration was 1.5×10^{-5} M. Dependence of k_{obs} on the NO concentration in the absence and presence of ibuprofen (B). The ibuprofen concentration was: 0.0 M (a), 2.0×10^{-3} M (b), and 8.0×10^{-3} M (c). The continuous lines were calculated according to Eq. (2) with the following values of $k_{on} = 6.3 \times 10^6\ M^{-1}\ s^{-1}$ (a), $4.1 \times 10^6\ M^{-1}\ s^{-1}$ (b), and $2.1 \times 10^6\ M^{-1}\ s^{-1}$ (c). Dependence of k_{on} on the ibuprofen concentration (C). The continuous line was calculated according to Eq. (3) with the following parameters: $k^*_{on} = 6.3 \times 10^6\ M^{-1}\ s^{-1}$, $k^0_{on} = 4.1 \times 10^5\ M^{-1}\ s^{-1}$, and $K = 3.2 \times 10^{-3}$ M. All data were obtained at pH 7.0 and 20.0 °C. Where not shown, standard deviation is smaller than the symbol. For details, see text.

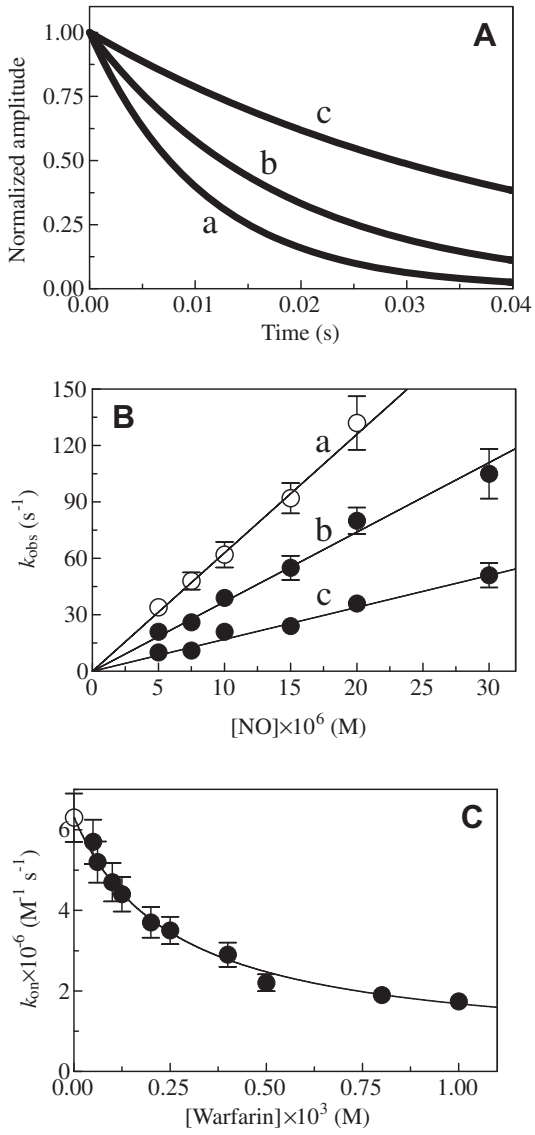

Fig. 3. Effect of warfarin on the HSA–heme–Fe(II) nitrosylation. Normalized averaged time courses of NO binding to HSA–heme–Fe(II) in the absence and presence of warfarin (A). The warfarin concentration was 0.0 M (trace a), 2.0×10^{-4} M (trace b), and 1.0×10^{-3} M (trace c). The time course analysis according to Eq. (1) allowed the determination of the following values of k_{obs}: $9.2 \times 10^1\ s^{-1}$ (trace a), $5.5 \times 10^1\ s^{-1}$ (trace b), and $2.4 \times 10^1\ s^{-1}$ (trace c). The HSA–heme–Fe(II) concentration was 1.1×10^{-6} M. The NO concentration was 1.5×10^{-5} M. Dependence of k_{obs} on the NO concentration in the absence and presence of warfarin (B). The warfarin concentration was: 0.0 M (a), 2.0×10^{-4} M (b), and 1.0×10^{-3} M (c). The continuous lines were calculated according to Eq. (2) with the following values of $k_{on} = 6.3 \times 10^6\ M^{-1}\ s^{-1}$ (a), $3.7 \times 10^6\ M^{-1}\ s^{-1}$ (b), and $1.7 \times 10^6\ M^{-1}\ s^{-1}$ (c). Dependence of k_{on} on the warfarin concentration (C). The continuous line was calculated according to Eq. (3) with the following parameters: $k^*_{on} = 6.3 \times 10^6\ M^{-1}\ s^{-1}$, $k^0_{on} = 4.8 \times 10^5\ M^{-1}\ s^{-1}$, and $K = 2.6 \times 10^{-4}$ M. All data were obtained at pH 7.0 and 20.0 °C. Where not shown, standard deviation is smaller than the symbol. For details, see text.

Values of k_{obs} increase linearly with the NO concentration, in the absence and presence of ibuprofen and warfarin (Figs. 2 and 3, panel B). The analysis of data reported in Figs. 2 and 3 (panel B) according to Eq. (2) allowed the determination of values of the second-order rate constant for HSA–heme–Fe(II) nitrosylation (k_{on}; corresponding to the slope of the linear plots). Remarkably, the *y* intercept of the linear plots (corresponding to the first-order rate constant for NO dissociation from HSA–heme–Fe(II)–NO) is very close to zero, indicating that HSA–heme–Fe(II) nitrosylation can be considered as an irreversible process over the time range explored. Indeed, values of the first-order rate constant for NO dissociation from (drug-)HSA–heme–Fe(II)–NO [40,41] are lower than those of k_{obs} (see Figs. 2 and 3, panels B and C) by 4–6 orders of magnitude.

Values of k_{on} for HSA–heme–Fe(II) nitrosylation decrease from $6.3 \times 10^6\ M^{-1}\ s^{-1}$ in the absence of drugs, to $4.1 \times 10^5\ M^{-1}\ s^{-1}$ and $4.8 \times 10^5\ M^{-1}\ s^{-1}$, in the presence of saturating amounts of ibuprofen and warfarin, respectively. The k^*_{on} value here reported ($= 6.3 \times 10^6\ M^{-1}\ s^{-1}$) is similar to that obtained for NO binding to HSA-tetraphenylporphynatoiron(II) ($= 1.5 \times 10^7\ M^{-1}\ s^{-1}$) [47]. The

analysis of the dependence of k_{on} on the drug concentration (Figs. 2 and 3, panel C), according to Eq. (3), allowed to determine values of the dissociation equilibrium constant for ibuprofen and warfarin binding to HSA–heme–Fe(II) (i.e., $K = 3.2 \times 10^{-3}$ and 2.6×10^{-4} M, respectively).

However, any energy balancing analysis of thermodynamic and kinetic parameters for HSA–heme–Fe(II)(–NO) (de)nitrosylation, in the absence and in the presence of ibuprofen and warfarin, is impaired by the evidence that the coordination state of HSA–heme–Fe(II)(–NO) is altered to a relevant extent upon drug binding. In fact, in the absence of allosteric effectors, HSA–heme–Fe(II)-NO is predominantly five-coordinated. In contrast, HSA–heme–Fe(II)-NO becomes predominantly hexa-coordinated upon addition of ibuprofen and warfarin [19,20,31].

Data reported in Figs. 2 and 3 (panel C) indicate that ibuprofen and warfarin bind to one site of HSA–heme–Fe(II). Warfarin binds to one site of HSA–heme–Fe(II)-NO ($K = 6.2 \times 10^{-5}$ M) [40], of HSA–heme–Fe(III) ($K = 2.1 \times 10^{-5}$ M) [19], and of heme-free HSA ($K = 3.0 \times 10^{-6}$ M) [19] also. In contrast, ibuprofen binds to three independent sites of HSA–heme–Fe(II)–NO ($K_1 = 3.1 \times 10^{-7}$ M, $K_2 = 1.7 \times 10^{-4}$ M, and $K_3 = 2.2 \times 10^{-3}$ M) [41] and of HSA–heme–Fe(III) ($K_1 = 8.0 \times 10^{-8}$ M, $K_2 = 5.0 \times 10^{-5}$ M, and $K_3 = 7.7 \times 10^{-4}$ M) [42]. Moreover, ibuprofen binds to two sites of heme-free HSA ($K_1 = 3.7 \times 10^{-7}$ M and $K_2 = 4.0 \times 10^{-5}$ M) [2,33,48]. These findings indicate that ibuprofen and warfarin bind to several HSA–heme–Fe sites with different affinity. Moreover, the drug affinity for HSA–heme–Fe depends on the redox state and the (un)ligated form of the heme–Fe atom.

The ibuprofen primary binding cleft (i.e., Sudlow's site II) is formed by the FA3 and FA4 sites, the secondary binding pocket corresponds to FA6 [11], and the third low affinity cleft has been identified with the FA2 pocket [26,30,31,34,42]. The warfarin primary binding site (i.e., Sudlow's site I) corresponds to FA7 [11]. A secondary low-affinity warfarin binding pocket has been postulated on the basis of binding experiments to recombinant HSA fragments [49], but not characterized in full-length HSA from both structural and functional viewpoints. By taking into account values of the dissociation equilibrium constants for ibuprofen and warfarin binding to HSA–heme–Fe(II) observed here (i.e., $K = 3.2 \times 10^{-3}$ and 2.6×10^{-4} M, respectively), it is feasible to consider the drug low-affinity site(s) as responsible for the observed effect [31,33,34,41,42].

Although the low-affinity sites for ibuprofen and warfarin binding to HSA were never described by X-ray crystallography, there are evidences from solution studies that ibuprofen binds to three different sites, the weakest one corresponding to FA2 [31,34]. In a similar way, warfarin binds to two different sites, the lowest affinity one being located at the interface between domains IA and II [49], thus corresponding to FA2. Drug binding to FA2 has been postulated to induce a remarkable conformational change(s) in HSA with the consequent reorientation of His146 that was suggested as the putative ligand able to coordinate to the heme iron at the sixth position [31,34]. Remarkably, His146 has been demonstrated to be indispensable for the allosteric transition(s) of HSA upon ligand binding to FA2 [50].

The drug-dependent decrease of k_{on} for NO binding to HSA–heme–Fe(II) (present study) could reflect the tetra- to penta-coordination transition of the heme-Fe(II) atom. Spectroscopic observations here reported, i.e. the large red shift of the Soret band upon drug binding, suggest the drug-dependent His146–Fe(II) coordination, which inhibits HSA–heme–Fe(II) nitrosylation. A similar behavior has been reported for modulation of CO binding to oxygen carriers, such as myoglobin [51]. Remarkably, drugs impair peroxynitrite scavenging by HSA–heme–Fe(III) by inducing the formation of the six-coordinated His146-Fe(III)-Tyr161 species, rendering unreactive the heme–Fe atom [31,42,43].

As a whole, present data reinforce the idea that HSA could be taken as the prototype of monomeric allosteric proteins. Furthermore, HSA–heme represents a unique case within heme–proteins since allosteric effectors modulate both heme binding to HSA and the heme–Fe atom reactivity [14,16].

Acknowledgment

This work was partially supported by a Grant from the University Roma Tre, Roma, Italy, 'CLAR 2010' to P.A.

Appendix A. Supplementary data

Supplementary data associated with this article can be found, in the online version, at doi:10.1016/j.bbrc.2011.06.130.

References

[1] G. Sudlow, D.J. Birkett, D.N. Wade, The characterization of two specific drug binding sites on human serum albumin, Mol. Pharmacol. 11 (1975) 824–832.
[2] T. Peters Jr, All about Album: Biochemistry Genetics and Medical Applications, Academic Press, San Diego and London, 1996.
[3] E. Monzani, B. Bonafé, A. Fallarini, C. Redaelli, L. Casella, L. Minchiotti, M. Galliano, Enzymatic properties of hemalbumin, Biochim. Biophys. Acta 1547 (2001) 302–312.
[4] C. Bertucci, E. Domenici, Reversible and covalent binding of drugs to human serum album methodological approaches and physiological relevance, Curr. Med. Chem. 9 (2002) 1463–1481.
[5] U. Kragh-Hansen, V.T. Chuang, M. Otagiri, Practical aspects of the ligand-binding and enzymatic properties of human serum albumin, Biol. Pharm. Bull. 25 (2002) 695–704.
[6] Y. Sakurai, S.F. Ma, H. Watanabe, N. Yamaotsu, S. Hirono, Y. Kurono, U. Kragh-Hansen, M. Otagiri, in: Esterase-like activity of serum album characterization of its structural chemistry using *p*-nitrophenyl esters as substrates, Pharm. Res. 21 (2004) 285–292.
[7] A. Sułkowska, B. Bojko, J. Równicka, W. Sułkowski, Competition of drugs to serum albumin in combination therapy, Biopolymers 74 (2004) 256–262.
[8] P. Ascenzi, A. Bocedi, S. Notari, E. Menegatti, M. Fasano, Heme impairs allosterically drug binding to human serum albumin Sudlow's site I, Biochem. Biophys. Res. Commun. 334 (2005) 481–486.
[9] A. Bocedi, S. Notari, E. Menegatti, G. Fanali, M. Fasano, P. Ascenzi, Allosteric modulation of anti-HIV drug and ferric heme binding to human serum albumin, FEBS J. 272 (2005) 6287–6296.
[10] M. Fasano, S. Curry, E. Terreno, M. Galliano, G. Fanali, P. Narciso, S. Notari, P. Ascenzi, The extraordinary ligand binding properties of human serum albumin, IUBMB Life 57 (2005) 787–796.
[11] J. Ghuman, P.A. Zunszain, I. Petitpas, A.A. Bhattacharya, M. Otagiri, S. Curry, Structural basis of the drug-binding specificity of human serum albumin, J. Mol. Biol. 353 (2005) 38–52.
[12] P. Ascenzi, A. Bocedi, S. Notari, G. Fanali, R. Fesce, M. Fasano, Allosteric modulation of drug binding to human serum albumin, Mini Rev. Med. Chem. 6 (2006) 483–489.
[13] P.A. Zunszain, J. Ghuman, A.F. McDonagh, S. Curry, Crystallographic analysis of human serum albumin complexed with 4Z, 15E-bilirubin-IXα, J. Mol. Biol. 381 (2008) 394–406.
[14] P. Ascenzi, M. Fasano, Serum heme–album an allosteric protein, IUBMB Life 61 (2009) 1118–1122.
[15] S. Curry, Lessons from the crystallographic analysis of small molecule binding to human serum albumin, Drug Metab. Pharmacokinet. 24 (2009) 342–357.
[16] P. Ascenzi, M. Fasano, Allostery in a monomeric protein: the case of human serum albumin, Biophys. Chem. 148 (2010) 16–22.
[17] A.A. Bhattacharya, S. Curry, N.P. Franks, Binding of the general anesthetics propofol and halothane to human serum albumin: high resolution crystal structures, J. Biol. Chem. 275 (2000) 38731–38738.
[18] A.A. Bhattacharya, T. Grüne, S. Curry, Crystallographic analysis reveals common modes of binding of medium and long-chain fatty acids to human serum albumin, J. Mol. Biol. 303 (2000) 721–732.
[19] S. Baroni, M. Mattu, A. Vannini, R. Cipollone, S. Aime, P. Ascenzi, M. Fasano, Effect of ibuprofen and warfarin on the allosteric properties of haem–human serum albumin: a spectroscopic study, Eur. J. Biochem. 268 (2001) 6214–6220.
[20] M. Mattu, A. Vannini, M. Coletta, M. Fasano, P. Ascenzi, Effect of bezafibrate and clofibrate on the heme-iron geometry of ferrous nitrosylated heme–human serum albumin: an EPR study, J. Inorg. Biochem. 84 (2001) 293–296.
[21] I. Petitpas, A.A. Bhattacharya, S. Twine, M. East, S. Curry, Crystal structure analysis of warfarin binding to human serum albumin: anatomy of drug site I, J. Biol. Chem. 276 (2001) 22804–22809.
[22] V.T. Chuang, M. Otagiri, How do fatty acids cause allosteric binding of drugs to human serum albumin?, Pharm Res. 19 (2002) 1458–1464.

[23] M. Wardell, Z. Wang, J.X. Ho, J. Robert, F. Ruker, J. Ruble, D.C. Carter, The atomic structure of human methemalbumin at 1.9 Å, Biochem. Biophys. Res. Commun. 291 (2002) 813–819.
[24] P.A. Zunszain, J. Ghuman, T. Komatsu, E. Tsuchida, S. Curry, Crystal structural analysis of human serum albumin complexed with hemin and fatty acid, BMC Struct. Biol. 3 (2003) 6.
[25] J.A. Hamilton, Fatty acid interactions with proteins: what X-ray crystal and NMR solution structures tell us, Prog. Lipid Res. 43 (2004) 177–199.
[26] G. Fanali, R. Fesce, C. Agrati, P. Ascenzi, M. Fasano, Allosteric modulation of myristate and Mn(III)heme binding to human serum albumin: optical and NMR spectroscopy characterization, FEBS J. 272 (2005) 4672–4683.
[27] J.R. Simard, P.A. Zunszain, C.E. Ha, J.S. Yang, N.V. Bhagavan, I. Petitpas, S. Curry, J.A. Hamilton, Locating high-affinity fatty acid-binding sites on albumin by x-ray crystallography and NMR spectroscopy, Proc. Natl. Acad. Sci. USA 102 (2005) 17958–17963.
[28] V.T. Chuang, M. Otagiri, Stereoselective binding of human serum albumin, Chirality 18 (2006) 159–166.
[29] J.R. Simard, P.A. Zunszain, J.A. Hamilton, S. Curry, Location of high and low affinity fatty acid binding sites on human serum albumin revealed by NMR drug-competition analysis, J. Mol. Biol. 361 (2006) 336–351.
[30] G. Fanali, A. Bocedi, P. Ascenzi, M. Fasano, Modulation of heme and myristate binding to human serum albumin by anti-HIV drugs. An optical and NMR spectroscopic study, FEBS J. 274 (2007) 4491–4502.
[31] F.P. Nicoletti, B.D. Howes, M. Fittipaldi, G. Fanali, M. Fasano, P. Ascenzi, G. Smulevich, Ibuprofen induces an allosteric conformational transition in the heme complex of human serum albumin with significant effects on heme ligation, J. Am. Chem. Soc. 130 (2008) 11677–11688.
[32] L. Zhu, F. Yang, L. Chen, E.J. Meehan, M. Huang, A new drug binding subsite on human serum albumin and drug-drug interaction studied by X-ray crystallography, J. Struct. Biol. 162 (2008) 40–49.
[33] G. Fanali, G. Pariani, P. Ascenzi, M. Fasano, Allosteric and binding properties of Asp1-Glu382 truncated recombinant human serum albumin: an optical and NMR spectroscopic investigation, FEBS J. 276 (2009) 2241–2250.
[34] A. di Masi, F. Gullotta, A. Bolli, G. Fanali, M. Fasano, P. Ascenzi, Ibuprofen binding to secondary sites allosterically modulates the spectroscopic and catalytic properties of human serum heme–albumin, FEBS J. 278 (2011) 654–662.
[35] Y.I. Miller, N. Shaklai, Kinetics of hemin distribution in plasma reveals its role in lipoprotein oxidation, Biochim. Biophys. Acta 1454 (1999) 153–164.
[36] P. Ascenzi, A. Bocedi, P. Visca, F. Altruda, E. Tolosano, T. Beringhelli, M. Fasano, Hemoglobin and heme scavenging, IUBMB Life 57 (2005) 749–759.
[37] A. Varshney, P. Sen, E. Ahmad, M. Rehan, N. Subbarao, R.H. Khan, Ligand binding strategies of human serum albumin: how can the cargo be utilized?, Chirality 22 (2010) 77–87.
[38] E. Tsuchida, K. Sou, A. Nakagawa, H. Sakai, T. Komatsu, K. Kobayashi, Artificial oxygen carriers, hemoglobin vesicles and albumin–hemes, based on bioconjugate chemistry, Bioconjugate Chem. 20 (2009) 1419–1440.
[39] P. Ascenzi, M. Fasano, Abacavir modulates peroxynitrite-mediated oxidation of ferrous nitrosylated human serum heme–albumin, Biochem. Biophys. Res. Commun. 353 (2007) 469–474.
[40] P. Ascenzi, F. Imperi, M. Coletta, M. Fasano, Abacavir and warfarin modulate allosterically kinetics of NO dissociation from ferrous nitrosylated human serum heme–albumin, Biochem. Biophys. Res. Commun. 369 (2008) 686–691.
[41] P. Ascenzi, A. di Masi, G. De Sanctis, M. Coletta, M. Fasano, Ibuprofen modulates allosterically NO dissociation from ferrous nitrosylated human serum heme–albumin by binding to three sites, Biochem. Biophys. Res. Commun. 387 (2009) 83–86.
[42] P. Ascenzi, A. di Masi, M. Coletta, C. Ciaccio, G. Fanali, F.P. Nicoletti, G. Smulevich, M. Fasano, Ibuprofen impairs allosterically peroxynitrite isomerization by ferric human serum heme–albumin, J. Biol. Chem. 284 (2009) 31006–31017.
[43] P. Ascenzi, A. Bolli, F. Gullotta, G. Fanali, M. Fasano, Drug binding to Sudlow's site I impairs allosterically human serum heme–albumin-catalyzed peroxynitrite detoxification, IUBMB Life 62 (2010) 776–780.
[44] P. Ascenzi, A. Bolli, A. di Masi, G.R. Tundo, G. Fanali, M. Coletta, M. Fasano, Isoniazid and rifampicin inhibit allosterically heme binding to albumin and peroxynitrite isomerization by heme–albumin, J. Biol. Inorg. Chem. 16 (2011) 97–108.
[45] V.G. Kharitonov, V.S. Sharma, D. Magde, D. Koesling, Kinetics of nitric oxide dissociation from five- and six-coordinate nitrosyl hemes and heme proteins. Including soluble guanylate cyclase, Biochemistry 36 (1997) 6814–6818.
[46] M. Fasano, M. Mattu, M. Coletta, P. Ascenzi, The heme–iron geometry of ferrous nitrosylated heme-serum lipoproteins, hemopexin, and albumin: a comparative EPR study, J. Inorg. Biochem. 91 (2002) 487–490.
[47] T. Komatsu, Y. Matsukawa, E. Tsuchida, Reaction of nitric oxide with synthetic hemoprotein, human serum albumin incorporating tetraphenylporphinatoiron(II) derivatives, Bioconjug. Chem. 12 (2001) 71–75.
[48] J.B. Whitlam, M.J. Crooks, K.F. Brown, P.V. Pedersen, Binding of nonsteroidal anti-inflammatory agents to proteins: I. ibuprofen-serum albumin interaction, Biochem. Pharmacol. 28 (1979) 675–678.
[49] M. Dockal, M. Chang, D.C. Carter, F. Rüker, Five recombinant fragments of human serum albumin-tools for the characterization of the warfarin binding site, Protein Sci. 9 (2000) 1455–1465.
[50] K. Kaneko, V.T. Chuang, A. Minomo, K. Yamasaki, N.V. Bhagavan, T. Maruyama, M. Otagiri, Histidine146 of human serum albumin plays a prominent role at the interface of subdomains IA and IIA in allosteric ligand binding, IUBMB Life 63 (2011) 277–285.
[51] M. Coletta, P. Ascenzi, T.G. Traylor, M. Brunori, Kinetics of carbon monoxide binding to monomeric hemoproteins: role of the proximal histidine, J. Biol. Chem. 260 (1985) 4151–4155.
[52] N. Guex, M.C. Peitsch, SWISS-MODEL and the Swiss-PdbViewer: an environment for comparative protein modeling, Electrophoresis 18 (1997) 2714–2723.

J Biol Inorg Chem
DOI 10.1007/s00775-011-0837-0

ORIGINAL PAPER

Evidence for pH-dependent multiple conformers in iron(II) heme–human serum albumin: spectroscopic and kinetic investigation of carbon monoxide binding

Yu Cao · Francesco P. Nicoletti · Giampiero De Sanctis · Alessio Bocedi · Chiara Ciaccio · Francesca Gullotta · Gabriella Fanali · Grazia R. Tundo · Alessandra di Masi · Mauro Fasano · Giulietta Smulevich · Paolo Ascenzi · Massimo Coletta

Received: 18 April 2011 / Accepted: 7 August 2011

Abstract Human serum albumin (HSA), the most prominent protein in plasma, is best known for its exceptional ligand binding capacity. HSA participates in heme scavenging by binding the macrocycle at fatty acid site 1. In turn, heme endows HSA with globin-like reactivity and spectroscopic properties. A detailed pH-dependent kinetic and spectroscopic investigation of iron(II) heme–HSA and of its carbonylated form is reported here. Iron (II) heme–HSA is a mixture of a four-coordinate intermediate-spin species (predominant at pH 5.8 and 7.0), a five-coordinate high-spin form (mainly at pH 7.0), and a six-coordinate low-spin species (predominant at pH 10.0). The acidic-to-alkaline reversible transition reflects conformational changes leading to the coordination of the heme Fe(II) atom by the His146 residue via its nitrogen atom, both in the presence and in the absence of CO. The presence of several species accounts for the complex, multiexponential kinetics observed and reflects the very slow interconversion between the different species observed both for CO association to the free iron(II) heme–HSA and for CO dissociation from CO–iron(II) heme–HSA as a function of pH.

Keywords Iron(II) heme–human serum albumin · Carbon monoxide · Resonance Raman · Kinetics · Allostery

Abbreviations

4cIS	Four-coordinate intermediate spin
5cHS	Five-coordinate high spin
6cLS	Six-coordinate low spin
FA	Fatty acid
HDL	High-density lipoproteins

G. De Sanctis is on sabbatical leave from the University of Camerino, Camerino (MC), Italy.

Electronic supplementary material The online version of this article (doi:10.1007/s00775-011-0837-0) contains supplementary material, which is available to authorized users.

Y. Cao · G. De Sanctis · C. Ciaccio · F. Gullotta · G. R. Tundo · M. Coletta (✉)
Department of Experimental Medicine and Biochemical Sciences,
University of Rome "Tor Vergata",
Via Montpellier 1,
00133 Rome, Italy
e-mail: coletta@seneca.uniroma2.it

Y. Cao · A. di Masi · P. Ascenzi
Department of Biology,
University Roma Tre,
Rome, Italy

F. P. Nicoletti · G. Smulevich
Department of Chemistry "Ugo Schiff",
University of Florence,
Florence, Italy

A. Bocedi
Department of Molecular Genetics and Microbiology,
Duke University,
Durham, NC, USA

C. Ciaccio · F. Gullotta · G. R. Tundo · G. Smulevich · M. Coletta
Interuniversity Consortium on the Research of Chemistry of Metals in Biological Systems, Bari, Italy

G. Fanali · M. Fasano
Department of Structural and Functional Biology,
Center of Neuroscience,
University of Insubria,
Busto Arsizio, VA, Italy

HSA Human serum albumin
LDL Low-density lipoproteins

Introduction

Human serum albumin (HSA), the most prominent protein in plasma (approximately 7.5×10^{-4} M HSA), is best known for its exceptional ligand binding capacity. Among others, HSA appears (1) to be an important determinant of the pharmacokinetic behavior of many drugs, (2) to account for most of the antioxidant capacity of human serum, and (3) to display enzymatic properties [1–11].

HSA is a single nonglycosylated all-α chain protein, constituted by 585 amino acids, containing three homologous domains (labeled I, II, and III). Each domain consists of two separate helical subdomains (named A, encompassing helices h1–h6, and B, encompassing helices h7–h10) connected by random coils. Terminal regions of sequential domains contribute to the formation of interdomain h10–h1 helices linking subdomain IB to subdomain IIA and subdomain IIB to subdomain IIIA, respectively (Fig. 1) [2, 3, 10–17].

The structural organization of HSA provides a variety of ligand binding sites (Fig. 1). According to Sudlow's nomenclature, bulky heterocyclic anions bind preferentially to Sudlow's site I (located in subdomain IIA), whereas Sudlow's site II (located in subdomain IIIA) is preferred by aromatic carboxylates with an extended conformation (Fig. 1) [3, 11, 18–24]. Among others, HSA is able to bind 7 equiv of long-chain fatty acids (FAs) at multiple binding sites (labeled FA1 to FA7) (Fig. 1) [11, 15, 25–28].

HSA undergoes pH- and ligand-dependent reversible conformational transition(s). Between pH 2.7 and 4.3, HSA assumes the fast-migrating form, characterized by an increase in viscosity, much lower solubility, and a significant loss of helical content. Between pH 4.3 and 8.0 and in the absence of ligands, HSA displays the neutral form, which is characterized by the typical heart-shaped structure. At pH > 8.0 and in the absence of ligands, HSA exhibits the basic form, which is characterized by a high affinity for some ligands (e.g., heme). Ligands that bind with the highest affinity to one of the conformational states may allosterically modulate the HSA transition [3, 8, 20, 22, 29–32].

The FA1 binding site has been shown to be the primary binding site of several ligands, including the heme [14, 33]. There is increasing evidence that FA1 has evolved to selectively bind iron(III) heme with high affinity ($K_d \sim 10^{-8}$ M) [14–16, 29, 33]. The tetrapyrrole ring is arranged in a D-shaped cavity delimited by the Tyr138 and Tyr161 residues, which have a π–π stacking interaction with the porphyrin and supply a donor oxygen (from

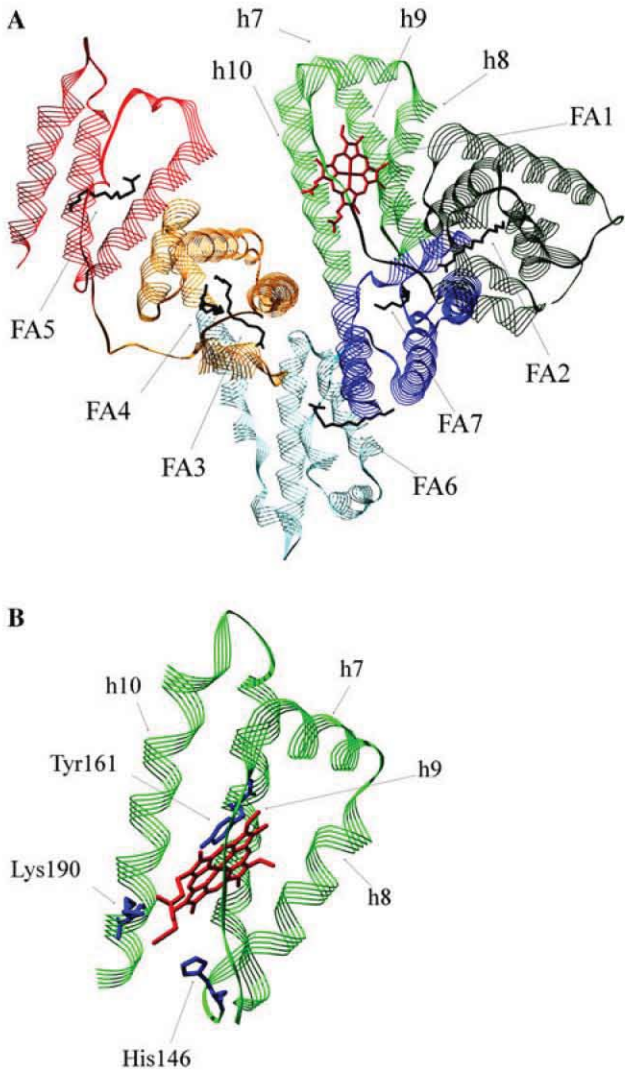

Fig. 1 **a** Human serum albumin (HSA) structure. The six subdomains of HSA are colored as follows: *dark green* subdomain IA, *light green* subdomain IB, *blue* subdomain IIA, *cyan* subdomain IIB, *orange* subdomain IIIA, *red* subdomain IIIB. The heme (*red*) binds to its primary cleft in subdomain IB. Different fatty acid binding sites (from *FA1* to *FA7*) are indicated. Helices h7–h10 are labeled. **b** Zoom of the heme binding pocket. Heme (*red*) is bound to the cleft formed by helices h7–h10. Residues His146, Tyr161, and Lys190 are shown. Atomic coordinates are taken from Protein Data Bank entry 1N5U [14]

Tyr161) for the heme Fe(III) atom. The iron(III) heme propionates protrude from the pocket, pointing toward the interface between domains I and III and are stabilized by salt bridges with His146 and Lys190. A weak coordination between the iron(III) heme and the phenolic oxygen atom of the Tyr161 residue (Fe–O_{Tyr161} distance 2.73 Å) was suggested by crystallography [14, 33] and further confirmed by resonance Raman spectroscopy [34]. Iron(III) heme is secured to HSA by the long IA–IB connecting loop that fits into the cleft opening [14–16, 29, 33, 34]. In turn, heme endows HSA with globin-like reactivity [4, 35–39] and spectroscopic properties [22, 30–32, 34, 40–43].

HSA is crucial for heme scavenging, providing protection against free heme oxidative damage, limiting the access of pathogens to heme, and contributing to iron homeostasis by recycling the heme iron. In fact, during the first seconds after the appearance of heme in plasma, more than 80% of this powerful oxidizer binds to high-density lipoproteins (HDL) and low-density lipoproteins (LDL), and only the remaining 20% binds to HSA and hemopexin. This first kinetic effect, due to the faster heme binding rate for HDL and LDL, is followed by a slower heme transfer to HSA and hemopexin, which have a higher affinity for heme. Heme binding confers on HSA globin-like spectroscopic and reactivity properties [11, 42, 44, 45]; in addition, HSA–heme has been reported to facilitate scavenging of reactive nitrogen species [46, 47]. Furthermore, since the rate of heme transfer from HDL and LDL to HSA and hemoproteins is faster than the heme-induced lipoprotein oxidation [8, 48, 49], the formation of HSA–heme represents a protective event, which prevents the formation of oxidized HDL and LDL, which are the most oxidatively intolerant plasma components. Afterwards, heme transits from HSA to hemopexin, which releases it into hepatic parenchymal cells after internalization of the hemopexin–heme complex by CD91-receptor-mediated endocytosis. Lastly, HSA–heme mutants have been reported to act as O_2 carriers, which may be useful as transfusion alternatives in clinical situations [45]. Remarkably, both heme binding to HSA and HSA–heme spectroscopic and reactivity properties are modulated competitively and allosterically, such that HSA(–heme) could be considered as a prototypical monomeric allosteric protein [11].

Here, a detailed spectroscopic and functional characterization of iron(II) heme–HSA carbonylation in the acidic, neutral, and alkaline pH regions is reported. To have a substantially unique (more than 98%) heme-bound site (i.e., FA1 site, see Fig. 1), we employed substoichiometric amounts of heme (with a heme to HSA ratio of 1:1.7). The kinetics were investigated by a rapid-mixing stopped-flow technique and were analyzed in parallel with CO rebinding data obtained after laser photolysis of CO–iron(II) heme–HSA [50]. The data obtained indicate the presence of multiple iron(II) heme–HSA and CO–iron(II) heme–HSA conformers whose relative amounts are pH-dependent. Indeed, iron(II) heme–HSA is a mixture of a four-coordinate intermediate-spin (4cIS) species which is predominant at pH 5.8 and 7.0, and which coexists with a minor five-coordinate high-spin (5cHS) form, and a six-coordinate low-spin (6cLS) species (predominant at pH 10.0). The acidic-to-alkaline reversible transition reflects conformational changes leading to the coordination of the heme Fe(II) atom by the His146 residue via its nitrogen atom, both in the presence and in the absence of CO. Accordingly, the presence of several species accounts for the complex, multiexponential kinetics of iron(II) heme–HSA carbonylation and CO–iron(II) heme–HSA decarbonylation as a function of pH, reflecting the very slow interconversion between the different species. This investigation may also have some physiopathological significance in view of the large amount of HSA in the bloodstream and of its role as a heme scavenger during hemolytic processes, rendering the levels of heme–HSA relevant under these conditions.

Materials and methods

Materials

HSA (purity 96% or greater, essentially FA free) and hemin [iron(III) protoporphyrin IX; iron(III) heme] chloride were obtained from Sigma-Aldrich (St. Louis, MO, USA). Gaseous CO and ^{13}CO were purchased from Rivoira (Milan, Italy) and FluoroChem (Hadfield, UK), respectively. Sodium dithionite was obtained from Fluka Chemicals (Buchs, Switzerland). All other chemicals were obtained from Merck (Darmstadt, Germany). All chemicals were of analytical or reagent grade and were used without further purification.

Sample preparation

The HSA stock solution was prepared by dissolving HSA in 1.0×10^{-1} M phosphate buffer at pH 7.0 to give a final concentration of 2.0×10^{-3} M. The HSA concentration was determined spectrophotometrically at 280 nm ($\varepsilon_{280\ nm} = 38.2 \times 10^3\ M^{-1}\ cm^{-1}$) [51]. The iron(III) heme stock solution was prepared by dissolving iron(III) heme in 1.0×10^{-1} M NaOH to give a final concentration of approximately 3×10^{-3} M. The iron(III) heme concentration was determined spectrophotometrically at 535 nm, after converting iron(III) heme to the bisimidazolate–iron(III) heme derivative by adding 1.0 M imidazole, in sodium dodecyl sulfate micelles ($\varepsilon_{535\ nm} = 14.5 \times 10^3\ M^{-1}\ cm^{-1}$) [52]. An appropriate amount of the iron(III) heme solution was added to the HSA solution to give a final iron(III) heme to HSA ratio of 1:1.7. The iron(III) heme–HSA concentration was determined spectrophotometrically at 404 nm ($\varepsilon_{404\ nm} = 99.2\ mM^{-1}\ cm^{-1}$). Samples at pH 5.8 and 10.0 were prepared by diluting the iron(III) heme–HSA stock solution at pH 7.0 in the appropriate 1.0×10^{-1} M phosphate or glycine buffer, respectively, and then waiting for 1 h. Iron(II) heme–HSA samples were prepared by addition of a freshly prepared sodium dithionite stock solution (1.1×10^{-1} M) to the deoxygenated iron(III) heme–HSA solution (5% v/v final concentration of sodium dithionite). CO–iron(II) heme–HSA was prepared by degassing the iron(III) heme–HSA solution by flushing it first with N_2, then

with CO or ^{13}CO and subsequently reducing the iron(III) heme–HSA by addition of a freshly prepared sodium dithionite stock solution (1.1×10^{-1} M) (5% v/v final concentration of sodium dithionite). The concentration of iron(II) heme–HSA and CO–iron(II) heme–HSA used for electronic absorption and resonance Raman spectroscopy ranged between 2.0×10^{-5} and 1.5×10^{-3} M. For kinetic experiments, 1.0×10^{-5} M iron(II) heme–HSA and CO–iron(II) heme–HSA sample solutions were used.

Spectroscopic characterization

Electronic absorption spectra of iron(III) heme–HSA, iron(II) heme–HSA, and CO–iron(II) heme–HSA were measured with a double-beam Cary 5 spectrophotometer (Varian, Palo Alto, CA, USA) using a 5-mm NMR tube or a 1-mm cuvette, and a 600 nm/min scan rate. The resonance Raman spectra of iron(II) heme–HSA were obtained using a 5-mm NMR tube and by excitation with the 413.1-nm line of a Kr^+ laser (Innova 300 C, Coherent, Santa Clara, CA, USA) and the 441.6-nm line of a HeCd laser (IK4121RG, Kimmon, Tokyo, Japan). Backscattered light from a slowly rotating NMR tube was collected and focused into a triple spectrometer (consisting of two Acton Research SpectraPro 2300i spectrometers and a SpectraPro 2500i spectrometer in the final stage with a 1,800 or 3,600 grooves per millimeter grating) working in the subtractive mode, equipped with a liquid-N_2-cooled CCD detector. The spectral resolution of the resonance Raman spectra cited in the figure captions is that calculated theoretically on the basis of the optical properties of the spectrometer. However, for the moderately broad experimental resonance Raman bands observed in the present study (approximately 10 cm^{-1}), the effective spectral resolution will, in general, be lower. To improve the signal-to-noise ratio, a number of spectra were accumulated and summed only if no spectral differences were noted. To minimize the heme Fe(II) atom oxidation under laser irradiation, samples at pH 5.8 were cooled by a gentle flow of N_2 gas passed through liquid N_2. The resonance Raman spectra were calibrated with indene, CCl_4, dimethyl sulfoxide, and pyridine as standards to an accuracy of ± 1 cm^{-1} for intense isolated bands. Electronic absorption spectra and resonance Raman spectra of heme–HSA derivatives were obtained at 25 °C between pH 5.8 and 10.0.

Kinetics of CO binding to iron(II) heme–HSA

The kinetics of CO dissociation from CO–iron(II) heme–HSA and of CO association to iron(II) heme–HSA were studied at 25 °C and between pH 4.8 and 10.5, employing a rapid-mixing stopped-flow apparatus (Applied Photophysics, Salisbury, UK) (time resolution 1 ms).

Kinetics of CO dissociation from CO–iron(II) heme–HSA

CO dissociation kinetics were studied by mixing a CO-saturated iron(II) heme–HSA solution [the final CO–iron(II) heme–HSA concentration was 5.0×10^{-6} M], in the presence of sodium dithionite (final concentration 1.1×10^{-2} M), with a degassed buffered solution containing $NaNO_2$ (final concentration 5.0×10^{-3} M) [53].

Kinetics of CO association to iron(II) heme–HSA

CO association kinetics were studied by mixing an unliganded iron(II) heme–HSA solution [the final iron(II) heme–HSA concentration was 3.0×10^{-6} M], in the presence of sodium dithionite (final concentration 1.1×10^{-2} M), with a degassed buffered solution equilibrated with CO (the final ligand concentration ranged between 1.5×10^{-5} and 5.0×10^{-4} M) [53].

Data analysis

Kinetic progress curves of CO dissociation from CO–iron(II) heme–HSA and of CO association to iron(II) heme–HSA were analyzed according to Eq. 1:

$$A_{\text{obs}} = A_0 \pm \sum_{i-1}^{i-n} \Delta A_i \cdot \exp(-{}^{i}k \cdot t), \tag{1}$$

where A_{obs} is the observed absorbance at 414 nm after a given time interval, A_0 is the absorbance at $t = 0$, n is the number of exponentials, ΔA_i is the absorbance change associated with the ith exponential, ${}^{i}k$ is the rate constant of the ith exponential (either CO association or CO dissociation rate constant), and t is the time; the sign $\pm$ is related to the possibility that during the reaction the absorbance can either increase or decrease.

The pH dependence of the observed rate constants was analyzed according to Eq. 2:

$$k_{\text{obs}} = \frac{\sum_{i-0}^{i-n} {}^{i}k \cdot \prod_{r-0}^{r-i} K_r \cdot [\text{H}^+]^r}{\sum_{i-0}^{i-n} \prod_{r-0}^{r-i} K_r \cdot [\text{H}^+]^r}, \tag{2}$$

where k_{obs} is the rate constant (either CO association or CO dissociation) at a given pH value, ${}^{i}k$ is the rate constant of the ith protonated species (with ${}^{0}k$ corresponding to the rate constant of the unprotonated form at very alkaline pH values), K_r is the proton binding affinity for the rth protonated group (with $K_0 = 1$), and $[\text{H}^+]$ is the proton concentration.

The population percentage is defined at each pH value by the relative amplitude (i.e., ΔA) of one exponential with respect to the total amplitude of the kinetic progress curve (expressed as the sum of all ΔA). It is expressed through Eq. 3:

$$ {}^{i}P = \frac{\Delta A_i}{\sum_{m-1}^{m-n} \Delta A_m}, \quad (3) $$

where ${}^{i}P$ is the relative percentage of species i, m (1, 2, 3, …, n) is the degree of the species (or exponential) under consideration, n is the total number of species observed, and ΔA_i is the optical amplitude of the exponential corresponding to species i.

The pH-dependent behavior of each species i was analyzed according to Eq. 4:

$$ P_{\text{obs}} = P_0 \pm \Delta P_1 \cdot \frac{K_1 \cdot [\text{H}^+]}{1 + K_1 \cdot [\text{H}^+] + K_1 \cdot K_2 \cdot [\text{H}^+]^2} \pm \Delta P_2 \cdot \frac{K_1 \cdot K_2 \cdot [\text{H}^+]^2}{1 + K_1 \cdot [\text{H}^+] + K_1 \cdot K_2 \cdot [\text{H}^+]^2}, \quad (4) $$

where P_{obs} is the observed percentage of each species i at a given pH value, P_0 is the percentage of species i in the unprotonated form (i.e., at very alkaline pH values), ΔP_1 and ΔP_2 are the percentage variations of species i upon the first and the second protonation, respectively, K_1 and K_2 are the binding affinity equilibrium constants for the first and the second protonating group, respectively (such that $\text{p}K_1 = \log K_1$ and $\text{p}K_2 = \log K_2$), and $[\text{H}^+]$ is the proton concentration.

Results

Spectroscopic properties of iron(II) heme–HSA

In agreement with previous results [34, 38], the UV–vis spectrum of iron(II) heme–HSA at pH 7.0 is characterized by a broad Soret band centered at 418 nm, with two shoulders at 405 and 424 nm, and β and α bands at 536 and 572 nm, respectively (Fig. 2a). The 413.1-nm excitation resonance Raman spectrum (Fig. 2b), in resonance with the Soret band at 418 nm, shows the presence of a predominant 4cIS Fe(II) species (ν_4 at 1,370 cm^{-1}, ν_3 at 1,502 cm^{-1}, ν_2 at 1,580 cm^{-1}, ν_{10} at 1,635 cm^{-1}) in equilibrium with a 5cHS Fe(II) species (ν_4 at 1,358 cm^{-1}, ν_3 at 1,472 cm^{-1}, ν_2 at 1,557 cm^{-1}, ν_{10} at 1,602 cm^{-1}). This latter form has been proposed to correspond to a 5cHS species containing a tyrosinate (possibly Tyr161) [14] coordinated to the iron(II) heme, whereas the formation of a 4cIS species is a consequence of the weakness of the heme Fe(II)–O_{Tyr} bond [34]. A small amount of a 6cLS Fe(II) species (Soret band at 424 nm, α band at 559 nm, and ν_3 at 1,492 cm^{-1}) is also observed.

When the pH is decreased from 7.0 to 5.8, the relative intensities of the resonance Raman bands change (Fig. 2b), clearly indicating that the amount of the 4cIS form increases and the amount of the 6cLS species diminishes as the Soret band sharpens at 424 nm (Fig. 2a); it is not clear if any change in the amount of the 5cHS species occurs. At pH values lower than 5.8, the iron(II) heme–HSA complex is not stable enough for spectroscopic characterization and, in agreement with previous findings [4], free heme was detected.

At pH 10.0, the 6cLS species becomes the predominant form and the 4cIS and 5cHS species remain in trace amounts. The UV–vis spectrum of the 6cLS species (Fig. 2a) resembles very closely that obtained upon complexation of iron(II) heme with 2-methylimidazole [34] as well as that of iron(II) *Herbaspirillum seropedicae* truncated hemoglobin [54]. Therefore, we assign the 6cLS form to a iron(II) heme coordinated to the oxygen atom of Tyr161 and the nitrogen atom of His146. This hypothesis agrees with our previous finding that an allosteric conformational transition, induced by ibuprofen binding, moves the His146 residue close to the heme Fe(III) atom. This residue is about 9 Å from the heme iron; therefore, significant changes in the heme cavity site can be foreseen [34]. The crystal structure of iron(III) heme–HSA in the presence of ibuprofen is not available, but a model study, made by energy minimization of the heme structure within the heme binding cleft of the HSA–ibuprofen complex [24], has revealed an appreciable tilt of α-helix h10 and a reorientation of α-helix h7 [34]. Accordingly, we suggest that at alkaline pH the formation of the His146–Fe(II)–Tyr161 6cLS species derives from a shift of α-helix h8 (as a consequence of the tilt of α-helix h10 and of the reorientation of α-helix h7); this leads to a rotation of the His146 residue toward the heme Fe(II) atom (Fig. 1).

Spectroscopic properties of CO–iron(II) heme–HSA

On the basis of the findings that a conformational change(s) occurs in iron(II) heme–HSA upon a change in pH [altering the ligand coordination state of iron(II) heme–HSA], we extended the previous study on the CO–iron(II) heme–HSA adduct at pH 7.0 [34] to different pH values in order to gain insight into the pH-dependent conformational changes occurring at the heme binding site (i.e., at FA1). In fact, heme-bound CO is a sensitive probe for investigating distal and proximal effects on ligand binding of heme proteins since back-donation from the heme Fe(II) atom $d\pi$ orbitals to the CO π^* orbitals is modulated by polar interactions between the oxygen atom of the iron(II) heme bound CO and distal polar residues, and by a *trans*-ligand effect, i.e., variations in the donor strength of the *trans* ligand. As the back-donation increases, the Fe–C bond strengthens and the CO bond weakens, thereby increasing the ν(Fe–CO) vibrational frequencies and decreasing the ν(CO) frequencies [55–57].

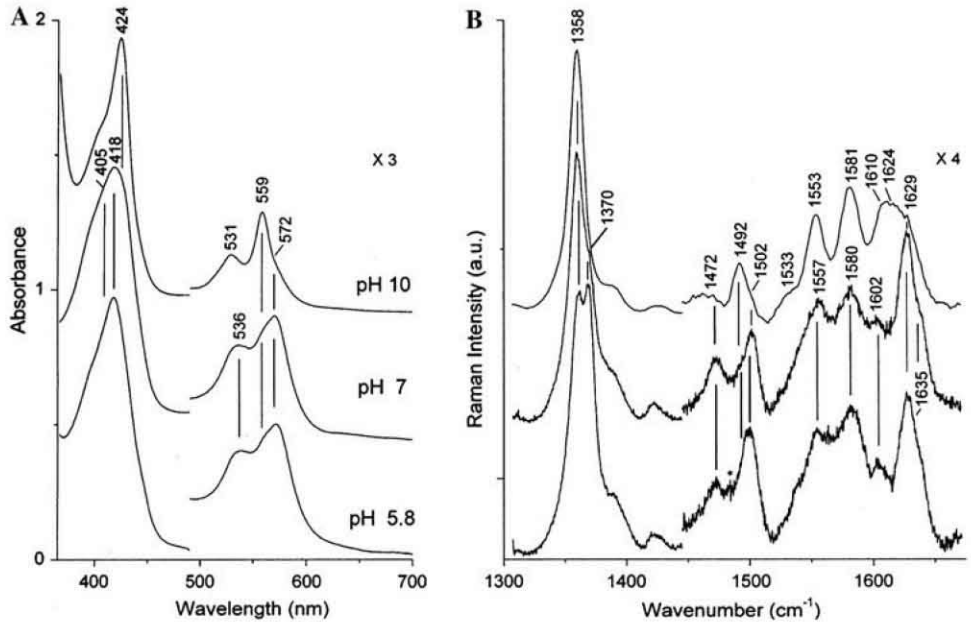

Fig. 2 Electronic absorption (**a**) and resonance Raman (**b**) spectra of iron(II) heme–HSA at pH 5.8, 7.0, and 10.0 at 25 °C. The experimental conditions were as follows: **a** 600 nm/min scan rate, **b** 413.1-nm excitation wavelength, 1.1-cm ^{1} spectral resolution (pH 7.0 and 5.8), 3.8-cm ^{1} spectral resolution (pH 10.0); at pH 5.8, 2-mW laser power at the sample, average of 30 spectra with 120-s integration time; at pH 7.0, 17-mW laser power at the sample, average of six spectra with 300-s integration time; at pH 10.0, 10-mW laser power at the sample, average of four spectra with 120-s integration time. The intensities are normalized to that of the ν_4 band. The *asterisk* indicates the small amount of the iron(III) heme–HSA form due to the easy oxidation of the sample at pH 5.8. Spectra have been shifted along the ordinate axis to allow better visualization

As previously reported [34, 37], upon addition of CO to iron(II) heme–HSA at pH values between 5.8 and 7.0, the electronic absorption spectrum is characterized by a sharp Soret band centered at 416 nm and β and α bands at 536 and 569 nm, respectively (Fig. S1). The blueshift of the Soret absorption band, as compared with that of the Fe(II)–CO complexes of heme proteins having an imidazole as the fifth axial ligand ($\lambda_{max} = 420$ nm), has been interpreted as a CO–iron(II) heme adduct with a *trans* ligand weaker than His, or no ligand at all [34]. At pH 10.0, the 4-nm redshift of the Soret band (Fig. S1) strongly suggests a conformational transition which allows the weak *trans* CO–iron(II) heme ligand to be replaced by an amino acid residue coordinating the heme Fe(II) atom with a nitrogen atom. Accordingly, the resonance Raman spectra of CO–iron(II) heme–HSA at pH 7.0 and 10.0 (Fig. 3) clearly show a change in the relative intensity of the ν(Fe–CO) and ν(CO) stretching modes (Table 1). At pH 10.0, the strong bands at 524 cm^{-1} [ν(Fe–CO)] and at 1,960 cm^{-1} [ν(CO)], observed at pH 7.0 [34], decrease in intensity; concomitantly, a band at 498 cm^{-1} [ν(Fe–CO)] becomes clearly evident. The corresponding ν(CO) stretch could possibly be assigned to the shoulder at 1,970 cm^{-1}. It must be noted that a very weak band at 498 cm^{-1} is also present in a very low amount at pH 7.0. Accordingly, a change of the excitation wavelength from 413.1 to 441.6 nm, i.e., in resonance with the Soret band at 420 nm (Fig. S1), leads to a substantial enhancement of the 498-cm^{-1} resonance Raman band relative to the 524-cm^{-1} band (Fig. S2).

For a large class of CO adducts of ferrous heme proteins and heme model compounds containing an imidazole as the fifth heme Fe(II) atom axial ligand, a linear correlation between the frequencies of the ν(Fe–CO) and ν(CO) stretching modes has been found. The correlation plots have a negative slope and depend on the extent of π back-bonding. Furthermore, since Fe–CO back-bonding is also modulated by variations in the donor strength of the *trans* axial ligand, changes in the *trans* ligand donor strength shift the correlation line and give rise to parallel lines at higher or lower positions in the correlation plot [55–57].

In the inset in Fig. 3, a plot of the ν(Fe–CO) and ν(CO) frequencies for CO adducts of a variety of ferrous heme proteins and heme model compounds having either a His residue as the fifth axial ligand or a weaker/absent *trans* ligand is shown [57]. The ν(Fe–CO) stretching mode at 524 cm^{-1} and the ν(CO) stretch at 1,960 cm^{-1} of the CO–iron(II) heme–HSA complex at pH 7.0 are located above the His line of the ν(Fe–CO)/ν(CO) back-bonding correlation, since the proximal ligand is either weak [55] or absent [56]. This result is consistent with the presence of a Tyr residue as the axial ligand. However, the correlation plot cannot effectively separate a five-coordinate CO–iron(II) heme system from a six-coordinate species with a weak proximal ligand, such as water or Tyr [57, 58]. The ν(Fe–CO)/ν(CO)

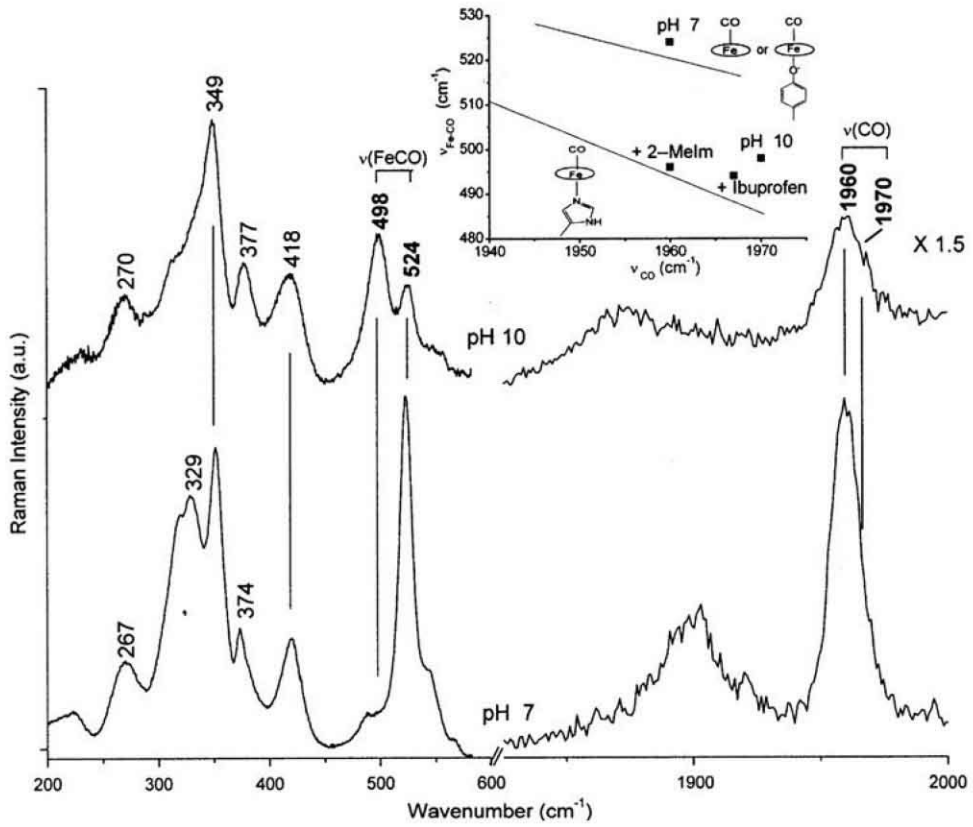

Fig. 3 Resonance Raman spectra of CO–iron(II) heme–HSA at pH 7.0 and 10.0, at 25 °C. The experimental conditions were as follows: 413.1-nm excitation wavelength; 1- and 3.3-cm $^{-1}$ spectral resolution for the low-frequency and high-frequency regions, respectively; at pH 7.0, 15-mW laser power at the sample, average of 32 spectra with 140-s integration time (low-frequency region), average of three spectra with 600-s integration time (high-frequency region); at pH 10.0, 2-mW laser power at the sample, average of six spectra with 1,500-s integration time (low-frequency region), average of eight spectra with 600-s integration time (high-frequency region). The intensities are normalized to that of the ν_4 band (not shown). Spectra have been shifted along the ordinate axis to allow better visualization. The *inset* shows the correlation plot of the ν(Fe–CO) versus ν(CO) frequencies observed in the CO complexes of iron(II) heme–HSA under various experimental conditions. The *lower line* indicates the back-bonding correlation line for six-coordinate CO–heme proteins with imidazole as the sixth ligand [57]. The *upper line* represents five-coordinate, with no *trans* internal axial ligand, or six-coordinate iron(II) carbonylated heme proteins with weak *trans* internal axial ligands. Data and references are given in Table 1. The respective *trans* ligands are shown. *2–MeIm*: 2-methylimidazole

stretch values of the alkaline form at pH 10.0 fall on the His ν(Fe–CO)/ν(CO) back-bonding correlation line (Fig. 3), closer to the values of the iron(II) heme–HSA complex in the presence of 2-methylimidazole or ibuprofen, in which the *trans* axial ligand is an imidazole or His, respectively [34]. These data confirm that at alkaline pH a major conformational change(s) occurs in the heme pocket of CO–iron(II) heme–HSA, allowing the His146 residue to coordinate the heme Fe(II) atom via its nitrogen atom, both in the presence and in the absence of CO.

Kinetics of CO binding to iron(II) heme–HSA

Kinetics of CO dissociation from CO–iron(II) heme–HSA

Figure S3 shows the time course of CO dissociation from CO–iron(II) heme–HSA upon replacement of CO with NO at two widely different pH values, namely, pH 4.8 (Fig. S3a) and pH 10.0 (Fig. S3b), followed by observation of the absorbance changes at 414 nm. At pH $\leq$ 7.0 this reaction can be described by Eq. 1 with three exponentials (i.e., $n = 3$, see Fig. S3a), whereas at alkaline pH only two exponentials are required (i.e., $n = 2$, see Fig. S3b). This indicates that two or three CO–iron(II) heme–HSA species are present at the respective pH values, and they interchange very slowly. The pH dependence of the CO dissociation rate constants, corresponding to the various exponentials, is reported in Fig. 4a. It displays a proton-linked behavior for the two faster exponentials, characterized by the two pK_a values reported in Table 2. On the other hand, the complex behavior observed for the relative percentage of absorption amplitudes of different exponentials (see Fig. 4b) clearly indicates that the two main exponentials refer to two pH-dependent structural

Table 1 Vibrational frequencies (cm ^{1}) of the Fe(II)–CO stretching modes in the CO adducts of selected iron porphyrins and heme proteins

Protein	ν(Fe–CO)	ν(CO)	Axial ligation	Reference
6c CO complexes with a weak *trans* ligand or 5c complexes with no ligand				
Iron(II) heme–HSA + ibuprofen	525 (519)	1,962 (1,924)	CO–Fe	[34]
Iron(II) heme–HSA + 2-MeIm	524 (520)	1,960 (1,912)	CO–Fe–O_{Tyr}	[34]
Iron(II) heme–HSA (pH 7.0)	524 (520)	1,960 (1,912)	CO–Fe–O_{Tyr}	[34]
$HasA_{SM}$	532 (523)	1,954 (1,905)	CO–Fe–O_{Tyr}	[63]
Human HO-1 (H25Y)	529 (524)	1,962 (1,917)	CO–Fe–OH_2	[64]
Iron(II) heme–CO in PBS (pH 6.9)	525	1,962	CO–Fe	[34]
Sperm whale Mb (pH 2.6)	526		CO–Fe–OH_2	[65]
6c CO complexes with imidazole *trans* ligand and apolar distal environment				
Iron(II) heme–HSA (pH 10.0)	498 (494)	1,970 (1,927)	CO–Fe–N_{His}	This work
Iron(II) heme–HSA + ibuprofen	494 (488)	1,967 (1,924)		[34]
Iron(II) heme–HSA + 2-MeIm	496 (492)	1,960 (1,912)	CO–Fe–N_{His}	[34]
Fe(PPDME)(Im)	495	1,960	CO–Fe–N_{His}	[66]
Sperm whale Mb				
pH 4.1	488	1,967	CO–Fe–N_{His}	[65]
pH 2.6	491		CO–Fe–N_{His}	[67]

The frequencies obtained with ^{13}CO are given in parentheses

6c six coordinate, *5c* five coordinate, *HSA* human serum albumin, *2-MeIm* 2-methylimidazole, *$HasA_{SM}$* hemophore HasA from *Serratia marcenscens*, *HO-1* heme oxygenase 1, *PBS* phosphate-buffered saline, *Mb* myoglobin, *PPDME* protoporphyrin IX dimethyl ester, *Im* imidazole

arrangements of CO–iron(II) heme–HSA. The resulting pK_a values are reported in Table 2. The third exponential, which is always less than 10% of the total amplitude, is characterized by a very slow pH-independent rate (see Fig. 4a) that disappears at pH $\geq$ 7.0. This suggests that it possibly corresponds to CO dissociation from aggregated free heme (also detected by the spectroscopic analysis, see earlier).

Kinetics of CO association to iron(II) heme–HSA

Figure S4 shows the time course of CO binding to iron(II) heme–HSA at two widely different pH values, namely, pH 4.8 (Fig. S4a) and pH 10.0 (Fig. S4b), followed by the observation of absorbance changes at 414 nm. At both pH values, CO binding to iron(II) heme–HSA is characterized by a multiexponential behavior, suggesting the existence of several structural arrangements of the heme pocket that likely interchange at a rate much slower than CO binding. This latter feature is supported by the experimental evidence that a pH jump of iron(II) heme–HSA from pH 7.0 to either pH 5.2 or pH 9.1 displays a very slow rate (see Fig. S5) for the pH-linked conformational change(s), indicating that this process is characterized by a rate $j < 10^{-3}$ s^{-1}. Therefore, the CO binding kinetic progress curve represents a "snapshot" of the different CO-binding iron(II) heme–HSA species present in the reaction mixture. As a consequence, the amplitude of the exponentials describing the time courses reflects the relative percentage of iron(II) heme–HSA species, such that the percentage of each species i (i.e., P_i) at a given pH value and CO concentration can be quantified according to Eq. 3.

Figure S4 shows the markedly different kinetic pattern of iron(II) heme–HSA carbonylation at pH 4.8 and 10.0. At pH 4.8 (Fig. S4a) we observe only a small percentage of the fast CO-binding iron(II) heme–HSA species, followed by a much larger amount of a slow reacting form(s). Conversely, at pH 10.0 (Fig. S4b), the amount of the iron(II) heme–HSA species which reacts fast with CO is much greater than the amount of the slow reacting form(s). In particular, according to Eq. 1 the analysis of the CO binding kinetics at 414 nm indicates that at pH $\leq$ 7.0 (at least) four exponentials (i.e., $n = 4$) are required to fit the progress curves, whereas at pH $\geq$ 7.0, three exponentials (i.e., $n = 3$) may be sufficient.

The analysis of individual kinetic progress curves at various CO concentrations and pH values allowed us to characterize the CO dependence and the proton linkage of all CO binding rates. This first step of data analysis is reported in Fig. 5 for three representative pH values, namely, pH 4.8 (Fig. 5a), pH 7.0, (Fig. 5b), and pH 10.0 (Fig. 5c). The rate of the first exponential is always dependent on the CO concentration (see Fig. 5), indicating that it refers to CO binding to a species where either the heme Fe(II) atom is five coordinate or the endogenous coordinating ligand dissociates at a rate much faster than the pseudo-first-order rate of CO binding. Therefore, this process can be analyzed by employing Eq. 5 [53]:

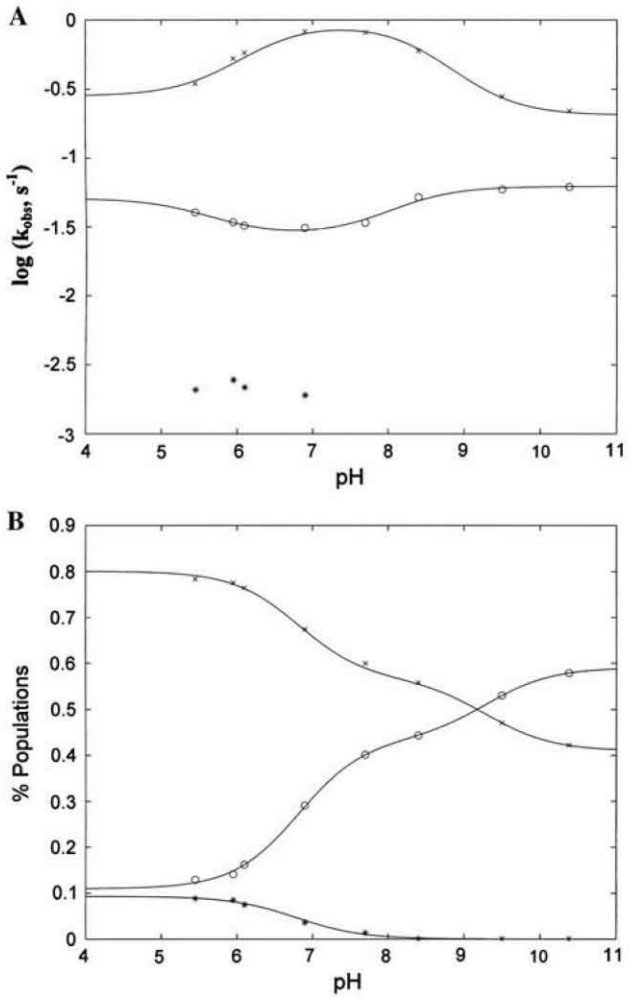

Fig. 4 pH dependence of CO dissociation rates from CO–iron(II) heme–HSA, at 25.0 °C. (**a**) pH dependence of the CO dissociation rate constants for species 1 (*open circles*), 2 (*crosses*), and 3 (*asterisks*). The *lines* were obtained by the nonlinear least-squares fitting of data, according to Eq. 2; values of pK_a are reported in Table 2. (**b**) pH dependence of the percentage of CO–iron(II) heme–HSA populations as derived from the percentage of different exponentials. The *lines* were obtained by the nonlinear least-squares fitting of data, according to Eq. 4; values of pK_a are reported in Table 2. The attribution of rate constants was based on the corresponding percentage of populations

$$k_{obs} = k_{on} \cdot [CO] + k_{off}, \tag{5}$$

where k_{obs} is the observed rate constant at a given CO concentration, k_{on} is the second-order CO association rate constant, and k_{off} is the first-order CO dissociation rate constant. The continuous lines in Fig. 5 refer to the non-linear least-squares fitting of data according to Eq. 5 for iron(II) heme–HSA carbonylation at pH 4.8 (Fig. 5a), pH 7.0 (Fig. 5b), and pH 10.0 (Fig. 5c). We conducted the analysis by imposing one of the k_{off} values obtained from direct measurements of CO dissociation; the best fit (reported in Fig. 5) was obtained by employing greater

Table 2 Values of pK_1 and pK_2 for the pH dependence of CO–iron(II) heme–HSA species (calculated according to Eq. 4) and of the kinetics of CO dissociation from CO–iron(II) heme–HSA (i.e., k_{obs} obtained by NO replacement experiments and calculated according to Eq. 2)

	pK_1	pK_2
CO–iron(II) heme–HSA species (see Fig. 4b)		
1	8.9 ± 0.2	6.6 ± 0.2
2	8.9 ± 0.2	6.6 ± 0.2
3	6.8 ± 0.2	
Rate constants for CO dissociation from CO–iron(II) heme–HSA species (see Fig. 4a)		
1	8.5 ± 0.2	6.3 ± 0.2
2	8.2 ± 0.2	5.5 ± 0.2

valuess (see Fig. 4a) obtained from the direct measurement for k_{off} at the corresponding pH value.

The second exponential displays a peculiar behavior, since its value depends on CO at low ligand concentration and levels off at high CO concentrations, indicating the existence of a rate-limiting step (see Fig. 5). This feature suggests that this CO binding process concerns a form characterized by an hexacoordinating ligand which must be displaced to permit CO binding to iron(II) heme–HSA, according to Scheme 1 [59]:

$$\text{L–Fe(II)-heme–HSA} \underset{k_{+L}}{\overset{k_{-L}}{\rightleftarrows}} \text{Fe(II)-heme–HSA} + \text{L} + \text{CO} \underset{k_{off}}{\overset{k_{on}}{\rightleftarrows}} \text{CO–Fe(II)-heme–HSA}$$

Scheme 1 Reaction scheme for the process characterized by a rate-limiting step

where L–Fe(II)-heme–HSA is the 6cLS species, Fe(II)-heme–HSA is the 5cHS species, CO–Fe(II)-heme–HSA is the CO-bound species, k_{-L} is the rate constant for the dissociation of the six-coordinate internal ligand, k_{+L} is the rate for the association of the hexacoordinating internal ligand, which competes with the association rate constant for CO binding (i.e., k_{on}), and k_{off} is the CO dissociation rate constant. According to Scheme 1, the observed rate constant k_{obs} corresponds to Eq. 6a:

$$k_{obs} = \frac{k_{-L} \cdot k_{on} \cdot [CO] + k_{off} \cdot k_{+L}}{k_{off} \cdot [CO] + k_{+L}}. \tag{6a}$$

Whenever $k_{on}[CO] \ll k_{+L}$, Eq. 6a reduces to Eq. 6b:

$$k_{obs} = \frac{k_{-L} \cdot k_{on} \cdot [CO]}{k_{+L}} + k_{off}. \tag{6b}$$

Whenever $k_{on}[CO] \gg k_{+L}$, Eq. 6a reduces to Eq. 6c:

$$k_{obs} = k_{-L} + \frac{k_{off} \cdot k_{+L}}{k_{on} \cdot [CO]}, \tag{6c}$$

which is essentially independent of CO concentration. It is important to underline that only k_{-L} and k_{off} are defined unequivocally by the application of Eqs. 6a, 6b, and 6c.

Fig. 5 CO concentration dependence of the observed carbonylation rate constants of iron(II) heme–HSA at pH 4.8 (**a**), 7.0 (**b**), and 10.0 (**c**), at 25.0 °C. The *continuous lines* were obtained by the nonlinear least-squares fitting of data to species 1 according to Eq. 5 [giving k_{on} of 6.1(±0.8) × 10^6 M^{-1} s^{-1} at pH 4.8, 4.2(±0.6) × 10^6 M^{-1} s^{-1} at pH 7.0, and 1.3(±0.3) × 10^7 M^{-1} s^{-1} at pH 10.0]. The *dashed lines* were obtained by the nonlinear least-squares fitting of data to species 2 according to Eq. 6a. The rate constants referring to species 3 and 4 are CO-independent

These equations also allowed the parameter k_{on}/k_{+L} to be determined, representing the binding competition between CO and the hexacoordinating internal ligand for the heme Fe(II) atom [59].

The CO dependence of the second exponential suggests that it refers to an iron(II) heme–HSA species where the hexacoordinating internal ligand dissociates and reassociates fast enough to show a CO dependence of the carbonylation rate at low CO concentrations, but it becomes CO-independent at high CO concentrations (see Fig. 5). This feature suggests that for this species $k_{on}[CO] \cong k_{+L}$, such that at lower CO concentrations $k_{on}[CO] < k_{+L}$ (i.e., the system follows the behavior indicated by Eq. 6b), whereas at high CO concentrations $k_{on}[CO] > k_{+L}$ (i.e., the system is described by Eq. 6c). The dashed lines in Fig. 5 correspond to the nonlinear least-squares fitting of data for the second exponential according to Eqs. 6a, 6b, and 6c. In this case the best fit (reported in Fig. 5) was obtained by employing the smaller values of k_{off} obtained from the direct measurement of this parameter at the corresponding pH value (see Fig. 4a).

The rate(s) of the third and fourth (when present) exponential(s) is (are) always independent of the CO concentration (see Fig. 5). Also in these cases Scheme 1 can be applied; however, the CO independence of the rate constants over the whole concentration range investigated clearly indicates that these processes refer instead to hexacoordinating species which dissociate and reassociate with a much smaller rate constant, so $k_{on}[CO]$ is always much greater than both k_{+L} and k_{-L}.

Additional information can be obtained from the analysis of the CO dependence of the optical absorption amplitudes of CO–iron(II) heme–HSA species, since they should refer to the CO binding equilibrium between different species. Obviously, in the case of the simple binding process, as for the first exponential (see Eq. 5), the CO dependence is related to the intrinsic CO affinity equilibrium constant K_{CO} (which is equal to $\frac{k_{on} \times [CO]}{k_{off}}$). On the other hand, for the other exponentials, where Scheme 1 must be applied, the CO dependence refers instead to the observed CO affinity equilibrium constant K_{obs} (which is equal to $\frac{k_{-L} \cdot k_{on} \times [CO]}{k_{+L} \cdot k_{off}} = \frac{K_{CO}}{K_L}$), which represents the ratio between the intrinsic CO affinity equilibrium constant K_{CO} and the affinity equilibrium constant for the hexacoordinating internal ligand K_L (which is equal to $\frac{k_{+L}}{k_{-L}}$).

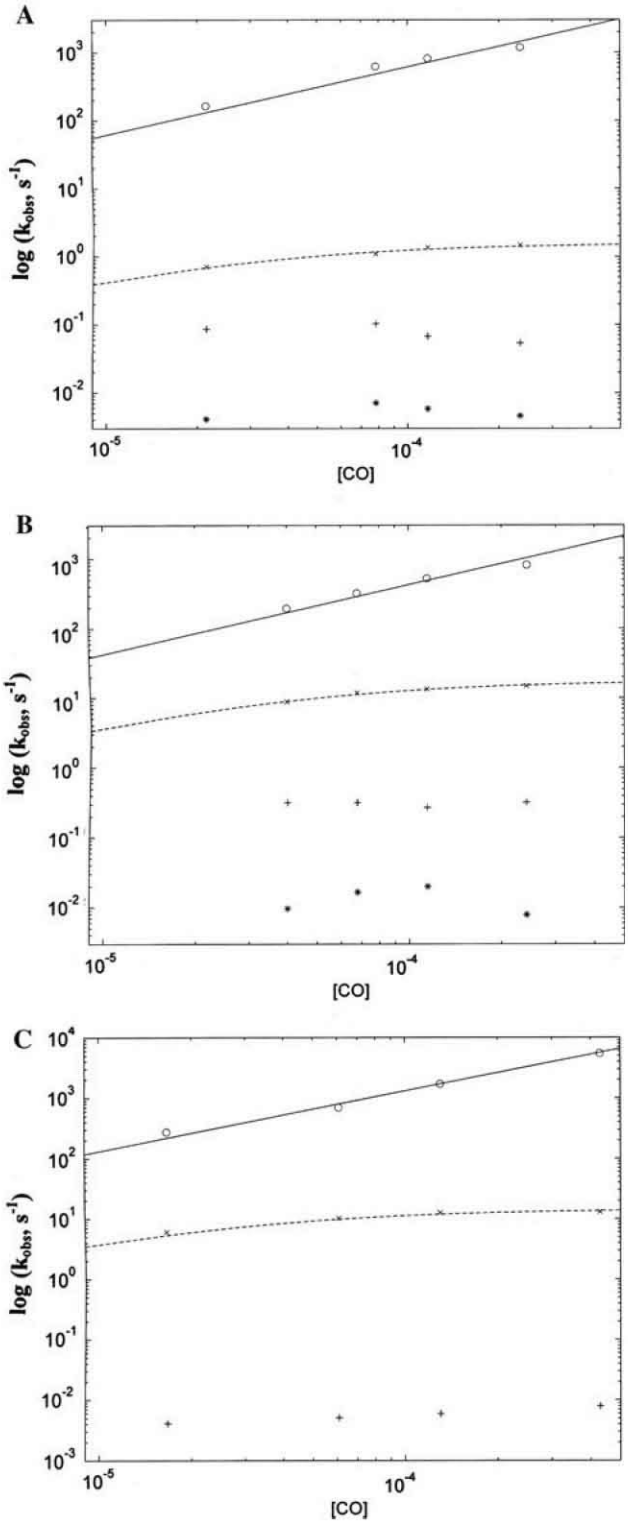

Figure S6 displays the CO dependence of the optical absorption amplitudes of various species at three indicative pH values, namely, pH 4.8 (Fig. S6a), pH 7.0 (Fig. S6b), and pH 10.0 (Fig. S6c). It is immediately evident that the values of the amplitudes of the first exponential are

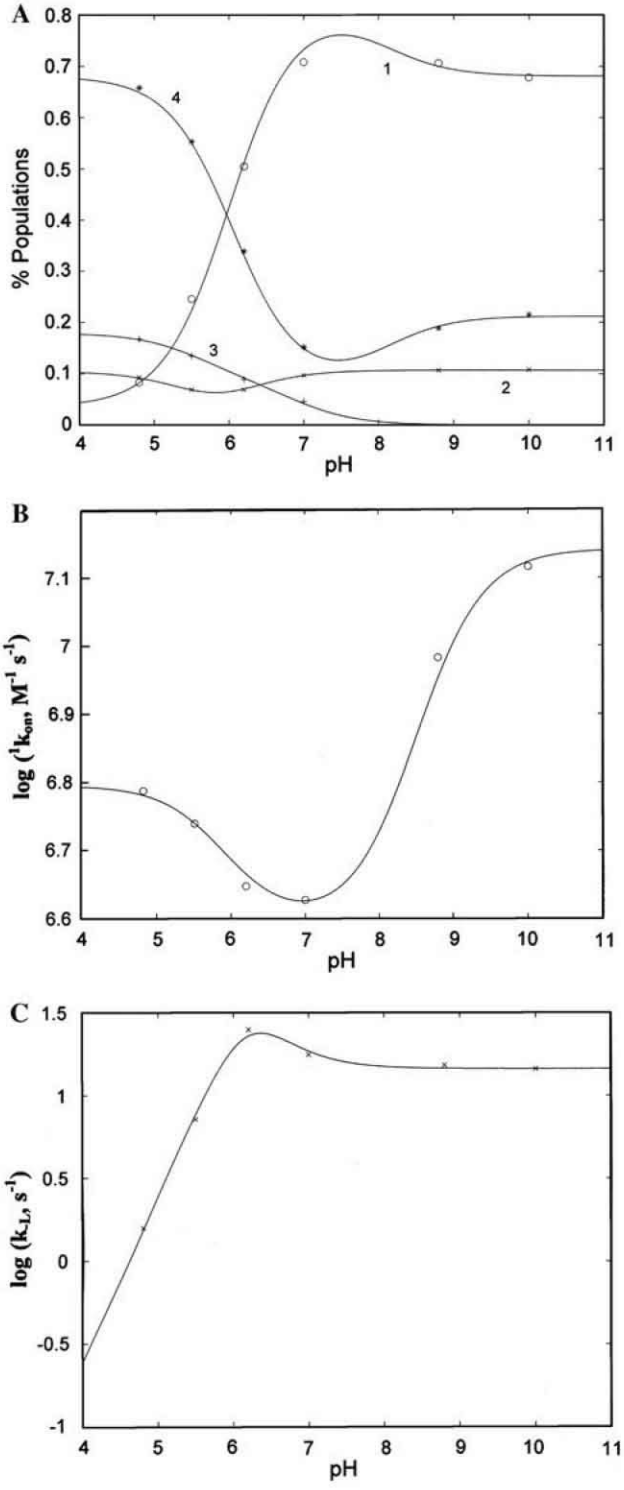

Fig. 6 pH dependence of unligated iron(II) heme–HSA and CO–iron(II) heme–HSA populations. (**a**) pH dependence of the percentage of unligated iron(II) heme–HSA as derived from the percentage of different exponentials. The *lines* were obtained by the nonlinear least-squares fitting of data, according to Eq. 4; the pK_a values are reported in Table 3. The assignment of species 1 to 4 is given in the text. (**b**) pH dependence of the CO association rate constants for species 1. The *line* was obtained by the nonlinear least-squares fitting of data, according to Eq. 2; the pK_a values are reported in Table 3. (**c**) pH dependence of the rate-limiting-step kinetic constant k_{L} (see Eq. 6c). The *line* was obtained by the nonlinear least-squares fitting of data, according to Eq. 2; the pK_a values are reported in Table 3

CO-independent at all the pH values investigated over the CO concentration range between 1.5×10^{-5} and 5.0×10^{-4} M, indicating that CO affinity is high enough to completely saturate all the five-coordinate heme species even at the lowest CO concentration. The same holds for the intermediate species and only the slowest CO binding forms (corresponding to the fourth exponential at pH $\leq$ 7.0 and to the third exponential at pH $\geq$ 7.0) are CO-concentration-dependent (see Fig. S6). The requirement of higher CO concentrations for the formation of the CO–iron(II) heme–HSA adduct indeed suggests a fairly high affinity for the hexacoordinating endogenous ligand (thus efficiently competing with CO). This feature, which possibly indicates the occurrence of different endogenous hexacoordinating ligands, was analyzed according to Eq. S1.

In this way, we obtained the value of ΔA_{tot} for the species that displays a CO dependence of the optical absorption amplitudes (for the CO-independent species the experimental values already correspond to their respective ΔA_{tot}). Therefore, applying Eq. 3 (where each $A_i = \Delta A_{tot}$ for a given form i), we calculated the pH dependence of the species distribution (Fig. 6a). The inspection of Fig. 6a allowed us to highlight that (1) the population percentage characterized by the first exponential (i.e., 5cHS) increases markedly from pH 4.8 to pH 7.0, then decreases somewhat going from pH 7.0 to pH 10.0; (2) the percentage of the species characterized by the second exponential (about 10% of the total population) seems to remain fairly constant over the whole pH range investigated; (3) the percentage of the species characterized by the third exponential decreases upon raising the pH from 4.8 to 7.0, and eventually becomes too small to be detected at pH $>$ 7.0; (4) the percentage of the slowest CO binding form (corresponding to the fourth exponential at pH $\leq$ 7.0 and to the third exponential at pH $>$7.0) decreases markedly on increasing the pH from 4.8 to pH 7.0 (in a fashion inversely mirroring the behavior of the 5cHS species), then slightly increases between pH 7.0 and pH 10.0. The pH-dependent behavior of each species, i, was analyzed according to Eq. 4.

Figure 6b and c shows the pH dependence of the rate constants for CO binding to iron(II) heme–HSA; the data were analyzed according to Eq. 2. In particular, for the first exponential we indicate the pH dependence of the bimolecular rate constant for CO binding to the 5cHS species (see Fig. 6b), whereas for the second exponential we

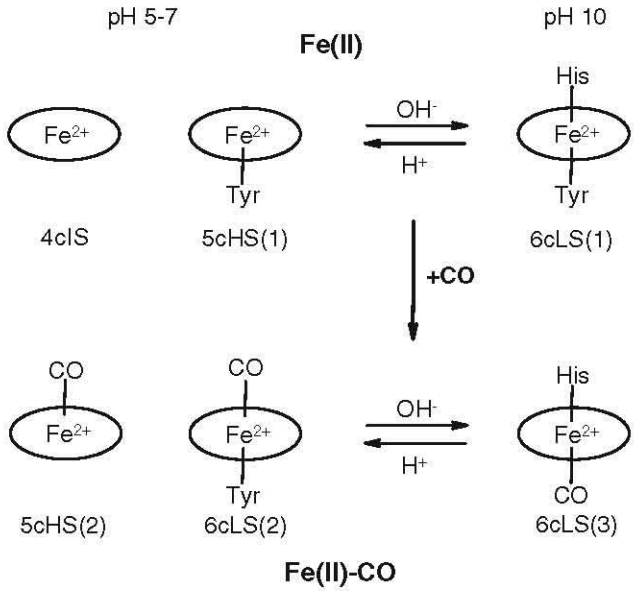

Fig. 7 The heme iron coordination of the iron(II) heme–HSA (*top*) and CO–iron(II) heme–HSA (*bottom*) species. *Bottom* the (Fe^{2+}–CO) and (CO–Fe^{2+}–Tyr) species cannot be distinguished by resonance Raman spectroscopy. *4cIS* four-coordinate intermediate spin, *5cHS* five-coordinate high spin, *6cLS* six-coordinate low spin

indicate the pH dependence of the rate-limiting values corresponding to k_{-L} (see above) (see Fig. 6c). All the pK_a values are reported in Table 2.

Discussion

In iron(II) heme–HSA the presence of many pH-dependent differently coordinated species (see Figs 2, 3) represents a complex scenario. In fact, the pH-dependent kinetics for CO dissociation from the CO–iron(II) heme–HSA complex and the CO binding to iron(II) heme–HSA appears quite complex, displaying several exponentials, whose percentage contribution to the total optical density change varies with pH (see Figs 4b, 6a). This feature, which reflects the very slow interconversion rates between the different species (see Fig. S5), mirrors the exchange of the axial coordination, which takes place at different pH values, as illustrated in Fig. 7.

The unliganded and the CO–iron(II) heme–HSA forms show a different pH-dependent transition between different coordination geometries, as demonstrated by the comparison between Figs. 4b and 6a and from the different pK_a values (see Tables 2, 3). Therefore, upon CO binding at different pH values, the different axial coordination likely contributes to the kinetic behavior observed. Thus, we cannot rule out that one of the kinetic patterns corresponding to the slowest CO-independent exponentials indeed reflects a change in the coordinating residue rather than CO binding.

Table 3 Values of pK_1 and pK_2 for the pH-dependence of iron(II) heme–HSA species (as calculated according to Eq. 4), of the kinetics of CO binding to five-coordinate high-spin (*5cHS*) iron(II) heme–HSA (i.e., k_{on}, as calculated according to Eq. 2), and of the kinetics of dissociation of the weakly bound endogenous ligand from species 2 (i.e., k_{-L}, as calculated from Eq. 2)

	pK_1	pK_2
Iron(II) heme–HSA species (see Fig. 6a)		
1	8.1 ± 0.2	6.0 ± 0.2
2	6.2 ± 0.2	5.5 ± 0.2
3	6.9 ± 0.2	5.6 ± 0.2
4	8.1 ± 0.2	6.1 ± 0.2
Kinetics of CO binding to 5cHS iron(II) heme–HSA species (see Fig. 6b)		
k_{on} (M^{-1} s^{-1})	8.8 ± 0.2	5.8 ± 0.2
Kinetics of dissociation of the weakly bound endogenous ligand from species 2 of iron(II) heme–HSA (see Fig. 6c)		
k_{-L} (s^{-1})	5.5 ± 0.2	6.8 ± 0.2

Focusing on the CO-bound forms, the increase in pH brings about the progressive decrease of the fastest CO-dissociating form and the appearance of a slower transition characterized by two pK_a values (6.6 ± 0.2 and 8.9 ± 0.2) (see Fig. 4b; Table 2). These two pK_a values might correspond to (1) a transition (characterized by pK_a = 6.6 ± 0.2) between a CO-bound five-coordinate form [without an internal *trans* axial ligand, indicated as 5cHS(2) in Fig. 7] and a CO-bound six-coordinate form [i.e., the 6cLS(2) form in Fig. 7], where the *trans* axial ligand is Tyr161 (this transition is silent in resonance Raman spectroscopy); and (2) a transition (characterized by pK_a = 8.9 ± 0.2) between the 6cLS(2) species and another CO-bound six-coordinate form where the *trans* axial ligand is His146 [6cLS(3) species, Fig. 7]. The first pK_a value could be attributed to the deprotonation of the Tyr161 phenolic group that is strongly polarized by the proximity of the iron atom, whereas the second constant is associated with the neutral-to-basic conformational transition [34]. In this case, a dramatic reorientation of the h8 helix could induce the His146 side chain to protrude into the heme cavity *trans* to Tyr161. This reorientation leads to two different 6cLS species, namely, (1) the 6cLS(3) species in the CO-bound form where His146 coordinates Fe(II) axially and CO replaces Tyr161, and (2) the 6cLS(1) form (Fig. 7) in the iron(II) heme–HSA complex where both His146 and Tyr161 are axially coordinated to Fe(II). Therefore, if the second transition corresponds to the substitution of Tyr161 by His146 as a *trans* axial coordinating residue, the corresponding pK_a value (which cannot be attributed to the protonation/deprotonation of a His) must refer to the protonation of another residue(s) involved in the modulation of iron(II) heme coordination and in the neutral-to-basic transition (e.g., Lys190 and/or Arg114). In this

respect, it is interesting to underline that the substitution of Lys190 by Arg eliminates the heterogeneity of CO rebinding after photolysis to iron(II) heme–HSA [39], clearly indicating that Lys190 plays a major role in the conformation of the heme inside the FA1 site through its interaction with heme propionates. A third exponential is observed at pH $\leq$ 8.0 (see Fig. 4b) and is likely related to the presence of aggregated free CO-bound iron(II) heme, whose dissociation is very slow and pH-independent (see Fig. 4a).

In the case of the CO reaction with iron(II) heme–HSA, the predominance at low pH values of a very slow CO-independent binding process (Fig. 6a) indicates that either (1) the CO access to the heme pocket of the 4cIS species is very difficult, possibly impaired by a high energy barrier which can be overcome at a very slow rate, or (2) bimolecular CO binding to the 4cIS species (which is very fast, see Fig. 6b) initially leads to a five-coordinate CO-bound species [i.e., 5cHS(2) species in Fig. 7], followed by a very slow process (likely characterized by a large conformational change) involving the binding of an endogenous axial ligand *trans* to the CO in the 5cHS(2) form. The final form is, therefore, a 6cLS species, whose axial ligand is likely a Tyr residue [i.e., the 6cLS(2) species in Fig. 7]. These two species cannot be distinguished by resonance Raman spectroscopy.

As the pH is raised above 6.0, the species characterized by a bimolecular CO-dependent binding process becomes predominant. This form likely corresponds to the 5cHS(1) species (Fig. 7), where Tyr161 is the iron(II) heme axial ligand, as suggested by resonance Raman spectroscopy (see Fig. 2) and the relatively high pK_a values of the transitions (i.e., pK_a = 6.0 $\pm$ 0.2 for process 1 and pK_a = 6.1 $\pm$ 0.2 for process 4; see Fig. 6a, Table 3). In other words, this process should mirror the progressive predominance of species 5cHS(1) (Fig. 7), which simply reacts with CO, giving rise to the 6cLS(2) form (Fig. 7) without forming an intermediate. The fast bimolecular rate constant suggests the presence of a weak proximal bond in the 5cHS(1) species, compatible with the Fe(II)–O_{Tyr161} bond (Fig. 7). This bimolecular rate constant is somewhat smaller than that at pH < 5.5 (see Fig. 6b), which corresponds to the reaction of CO with the 4cIS form to give the 5cHS(2) species (see Fig. 7). It is important to underline that CO binding at pH 7.0 to site-directed mutants of iron(II) heme–HSA, where Tyr161 had been substituted by either Leu or Phe [45] displays only small differences for the bimolecular rate constant of species 1 with respect to our wild type [i.e., $^1k_{on} = 4.2(\pm0.6) \times 10^6\ M^{-1}\ s^{-1}$ for the wild type, whereas $^1k_{on} = 2.0(\pm0.3) \times 10^6\ M^{-1}\ s^{-1}$ for the double mutant I142H/Y161L and $^1k_{on} = 6.8(\pm0.8) \times 10^6\ M^{-1}\ s^{-1}$ for the double mutant I142H/Y161F]. Although some caution is required for comparison with these double mutants, since the presence of His142 might lead to an alternative axial coordination of the heme with His142, this result seems to indicate that the removal of Tyr161 does not bring about any dramatic alteration of the bimolecular CO binding process.

The behavior of species 2 (Fig. 6a), which amounts to about 10% of the total iron(II) heme–HSA molecules, is characterized by a CO-dependent rate constant at low CO concentrations, which becomes independent of CO at higher ligand concentrations. The occurrence of a rate-limiting step suggests that CO binding displaces an endogenous ligand that is coordinated in the unliganded form, but this ligand dissociates at a rate similar to that of the pseudo-first-order CO binding rate; thus, the observation of the rate-limiting step depends on the CO concentration. The rate-limiting constant shows a slight increase as the pH is lowered from 10.0 to 6.0, but a marked decrease as the pH is lowered further (Fig. 6c). The resulting pK_a values (see Table 3 for CO binding to species 2) indicate that the rate-limiting constant is somewhat increased owing to the protonation of a group characterized by pK_a = 5.5 $\pm$ 0.2, but the effect is overwhelmed by a remarkable decrease due to the protonation of a group with pK_a = 6.8 $\pm$ 0.2. Therefore, species 2 may correspond to the 6cLS(1) form (Fig. 7), the axial ligands being His146 and Tyr161, and the rate-limiting step for CO binding to iron(II) heme–HSA at alkaline pH should correspond to the dissociation of Tyr161. This being the case, the relatively fast dissociation rate of this endogenous axial ligand at alkaline pH suggests that this Tyr residue (i.e., Tyr161) is a weakly bound axial ligand. The rate-limiting constant then slightly increases at lower pH (Fig. 6c) owing to the easier protonation of Tyr161 (possibly characterized by pK_a = 5.5 $\pm$ 0.2); at pH $\leq$ 6.5 a different rate-limiting step for CO binding becomes predominant, resulting in a much slower rate for the displacement of the internal ligand.

Finally, the two very small CO-independent rate constants are much less interesting. Species 3 (Fig. 6a) likely corresponds to free iron(II) heme (detected by resonance Raman spectroscopy). It binds CO very slowly and its CO-independent rate constant is limited by the dissociation of the stacked hemes. The other slow process (species 4 in Fig. 6a), whose population depends on pH in a fashion inversely mirroring that of species 1, is probably due to a slow process involving the substitution of the axial coordinating ligand. Upon CO binding, species 6cLS(2) converts to the 6cLS(3) form (see above). Therefore, as in unliganded iron(II) heme–HSA, an increase of pH brings about an increase of the population of the 5cHS(1) species at the expense of the 4cIS state. Similarly, following CO binding, a change from the 6cLS(2) to the 6cLS(3) species is observed (see Fig. 7).

In conclusion, the kinetics of CO dissociation from CO–iron(II) heme–HSA and CO association to iron(II)

heme–HSA clearly reveal a complex network of ligand-linked interactions between the heme and the neighboring residues of the FA1 site. Moreover, many residues must be called into play to regulate the access and exit pathways of diatomic ligands (such as CO) to this site and to participate in the stabilization of the axial coordination of the heme and, thus, of its reactivity with the ligand(s). In addition, the growing importance of the diatomic ligand CO as a gas transducer involved in the signaling related to reactive oxygen species [60] renders these kinetic investigations of physiopathological relevance. Thus, the role played by heme–HSA in the detoxification process is significantly enhanced by the fact that the amount of heme–HSA increases significantly under pathological conditions [9, 10, 61, 62] owing to the function of HSA as a heme scavenger from HDL and LDL, impairing their oxidation [8, 48, 49].

Furthermore, this behavior, which underlies the occurrence of multiple conformations of iron(II) heme–HSA, may have great impact on the function of heme–HSA as a metabolite and drug transporter, since this proton-linked modulation is reflected in its capability of interacting with molecules circulating in the bloodstream, as previously demonstrated [3, 8, 20, 22, 29–32]. Therefore, HSA, not only acting as a heme carrier but also displaying transient heme-based properties, represents a case for "chronosteric effects" [62], which opens the scenario toward the possibility of a time- and metabolite-dependent multiplicity of roles for HSA.

Acknowledgments This work was supported by local Italian grants (ex 60%) to G.S., P.A. (CLAR 2009), and M.C.

References

1. Kragh-Hansen U (1981) Pharmacol Rev 33:17–53
2. Carter DC, Ho JX (1994) Adv Protein Chem 45:153–203
3. Peters T Jr (1996) In all about albumin: biochemistry genetics and medical applications. Academic Press, San Diego
4. Monzani E, Bonafé B, Fallarini A, Redaelli C, Casella L, Minchiotti L, Galliano M (2001) Biochim Biophys Acta 1547:302–312
5. Curry S (2002) Vox Sang 83(Suppl. 1):315–319
6. Kragh-Hansen U, Chuang VT, Otagiri M (2002) Biol Pharm Bull 25:695–704
7. Sakurai Y, Ma SF, Watanabe H, Yamaotsu N, Hirono S, Kurono Y, Kragh-Hansen U, Otagiri M (2004) Pharm Res 21:285–292
8. Ascenzi P, Bocedi A, Visca P, Altruda F, Tolosano E, Beringhelli T, Fasano M (2005) IUBMB Life 57:749–759
9. Fasano M, Curry S, Terreno E, Galliano M, Fanali G, Narciso P, Notari S, Ascenzi P (2005) IUBMB Life 57:787–796
10. Ascenzi P, Bocedi A, Notari S, Fanali G, Fesce R, Fasano M (2006) Mini Rev Med Chem 6:483–489
11. Ascenzi P, Fasano M (2010) Biophys Chem 148:16–22
12. He X, Carter DC (1992) Nature 358:209–215
13. Sugio S, Kashima A, Mochizuki S, Noda M, Kobayashi K (1999) Protein Eng 12:439–446
14. Wardell M, Wang Z, Ho JX, Robert J, Rüker F, Ruble J, Carter DC (2002) Biochem Biophys Res Commun 291:813–819
15. Simard JR, Zunszain PA, Hamilton JA, Curry S (2006) J Mol Biol 361:336–351
16. Fasano M, Fanali G, Leboffe L, Ascenzi P (2007) IUBMB Life 59:436–440
17. Ascenzi P, Fasano M (2009) IUBMB Life 61:1118–1122
18. Sudlow G, Birkett DJ, Wade DN (1975) Mol Pharmacol 11:824–832
19. Diana FJ, Veronich K, Kapoor AL (1989) J Pharm Sci 78:195–199
20. Yamasaki K, Maruyama T, Yoshimoto K, Tsutsumi Y, Narazaki R, Fukuhara A, Kragh-Hansen U, Otagiri M (1999) Biochim Biophys Acta 1432:313–323
21. Dockal M, Chang M, Carter DC, Rüker F (2000) Protein Sci 9:1455–1465
22. Baroni S, Mattu M, Vannini A, Cipollone R, Aime S, Ascenzi P, Fasano M (2001) Eur J Biochem 268:6214–6220
23. Petitpas I, Bhattacharya AA, Twine S, East M, Curry S (2001) J Biol Chem 276:22804–22809
24. Ghuman J, Zunszain PA, Petitpas I, Bhattacharya AA, Otagiri M, Curry S (2005) J Mol Biol 353:38–52
25. Bhattacharya AA, Curry S, Franks NP (2000) J Biol Chem 275:38731–38738
26. Bhattacharya AA, Grüne T, Curry S (2000) J Mol Biol 303:721–732
27. Curry S (2009) Drug Metab Pharmacokinet 24:342–357
28. Simard JR, Zunszain PA, Ha CE, Yang JS, Bhagavan NV, Petitpas I, Curry S, Hamilton JA (2005) Proc Natl Acad Sci USA 102:17958–17963
29. Fasano M, Baroni S, Vannini A, Ascenzi P, Aime S (2001) J Biol Inorg Chem 6:650–658
30. Mattu M, Vannini A, Coletta M, Fasano M, Ascenzi P (2001) J Inorg Biochem 84:293–296
31. Fasano M, Mattu M, Coletta M, Ascenzi P (2002) J Inorg Biochem 91:487–490
32. Fanali G, De Sanctis G, Gioia M, Coletta M, Ascenzi P, Fasano M (2009) J Biol Inorg Chem 14:209–217
33. Zunszain PA, Ghuman J, Komatsu T, Tsuchida E, Curry S (2003) BMC Struct Biol 3:6
34. Nicoletti FP, Howes BD, Fittipaldi M, Fanali G, Fasano M, Ascenzi P, Smulevich G (2008) J Am Chem Soc 130:11677–11688
35. Dill K, Alonso DOV, Hutchinson K (1989) Biochemistry 28:5439–5449
36. Komatsu T, Matsukawa Y, Tsuchida E (2000) Bioconjug Chem 11:772–776
37. Kamal JK, Behere DV (2002) J Biol Inorg Chem 7:273–283
38. Komatsu T, Ohnichi N, Nakagawa A, Zunszain PA, Curry S, Tsuchida E (2005) J Am Chem Soc 127:15933–15942
39. Komatsu T, Nakagawa A, Curry S, Tsuchida E, Murata K, Nakamura N, Ohno H (2009) Org Biomol Chem 7:3836–3841
40. Monzani E, Curto M, Galliano M, Minchiotti L, Aime S, Baroni S, Fasano M, Amoresano A, Salzano AM, Pucci P, Casella L (2002) Biophys J 83:2248–2258
41. Fanali G, Fesce R, Agrati C, Ascenzi P, Fasano M (2005) FEBS J 272:4672–4683
42. Fanali G, Bocedi A, Ascenzi P, Fasano M (2007) FEBS J 274:4491–4502
43. Fanali G, Pariani G, Ascenzi P, Fasano M (2009) FEBS J 276:2241–2250
44. Bocedi A, Notari S, Menegatti E, Fanali G, Fasano M, Ascenzi P (2005) FEBS J 272:6287–6296
45. Tsuchida E, Sou K, Nakagawa A, Sakai H, Komatsu T, Kobayashi K (2009) Bioconjug Chem 20:1419–1440
46. Ascenzi P, Fasano M (2007) Biochem Biophys Res Commun 353:469–474

47. Ascenzi P, di Masi A, Coletta M, Ciaccio C, Fanali G, Nicoletti FP, Smulevich G, Fasano M (2009) J Biol Chem 284:31006–31017
48. Miller YI, Shaklai N (1999) Biochim Biophys Acta 1454:153–164
49. Tolosano E, Fagoonee S, Morello N, Vinchi F, Fiorito V (2010) Antioxid Redox Signal 12:305–320
50. Marden MC, Hazard ES, Leclerc L, Gibson QH (1989) Biochemistry 28:4422–4426
51. Kharitonov VG, Sharma VS, Magde D, Koesling D (1997) Biochemistry 36:6814–6818
52. Boffi A, Das TK, Della Longa S, Spagnuolo C, Rousseau DL (1999) Biophys J 77:1143–1149
53. Antonini E, Brunori M (1971) Hemoglobin and myoglobin in their reactions with ligands. North-Holland, Amsterdam
54. Razzera G, Vernal J, Baruh D, Serpa VI, Tavares C, Lara F, Souza EM, Pedrosa FO, Almeida FC, Terenzi H, Valente AP (2008) J Biol Inorg Chem 13:1085–1096
55. Ray GB, Li XY, Ibers JA, Sessler JL, Spiro TG (1994) J Am Chem Soc 116:162–176
56. Vogel KM, Kozlowski PM, Zgierski MZ, Spiro TG (2000) Inorg Chim Acta 297:11–17
57. Spiro TG, Wasbotten IH (2005) J Inorg Biochem 99:34–44
58. Ye X, Yu A, Georgiev GY, Gruia F, Ionascu D, Cao W, Sage JT, Champion PM (2005) J Am Chem Soc 127:5854–5861
59. Coletta M, Angeletti M, De Sanctis G, Cerroni L, Giardina B, Amiconi G, Ascenzi P (1996) Eur J Biochem 235:49–53
60. Piantadosi CA (2008) Free Radic Biol Med 45:562–569
61. Müller-Eberhard U, Javid J, Liern HH, Hanstein A, Hanna M (1968) Blood 32:811–815
62. Fasano M, Fanali G, Fesce R, Ascenzi P (2008) Human serum heme-albumin: an allosteric "chronosteric" protein. In: Bolognesi M, Di Prisco G, Verde C (Eds.) Dioxygen Binding and Sensing Proteins. Protein Reviews, Vol 9, pp 121–131. Springer, Heidelberg
63. Lukat-Rodgers GS, Rodgers KR, Caillet-Saguy C, Izadi-Pruneyre N, Lecroisey A (2008) Biochemistry 47:2087–2098
64. Liu Y, Moenne-Loccoz P, Hildebrand DP, Wilks A, Loehr TM, Mauk AG, Ortiz de Montellano PR (1999) Biochemistry 38:3733–3743
65. Sage J, Morikis D, Champion PM (1991) Biochemistry 30:1227–1237
66. Ling JH, Li TS, Olson JS, Bocian DF (1994) Biochim Biophys Acta 1188:417–421
67. Ramsden J, Spiro TG (1989) Biochemistry 28:3125–3128

9. Conclusion and Perspectives

The allosteric modulation of reactivity and ligand binding properties of HSA is relevant from both physiological and pathological viewpoints [1]. Indeed, both heme binding to HSA and heme-based reactivity of HSA-heme-Fe are modulated by endogenous and exogenous ligands [1-5].

Endogenous and exogenous ligands affect heme binding to the FA1 site by competitive inhibition. Moreover, FAs and drugs impair allosterically heme binding to the FA1 site by association to the FA2, FA6, and FA7 (*i.e.*, Sudlow's site I) clefts [1-5].

The modulation of heme binding to HSA by drugs is pivotal in the pharmacological therapy management. Indeed, the increase of the heme plasma level under pathological conditions (reaching ca. 4×10^{-5} M [6,7]), such as severe hemolytic anemia, crash syndrome, and post-ischemic reperfusion, could induce the release of HSA-bound endogenous and exogenous ligands (*e.g.*, metabolites and drugs) increasing their bio-availability, with the concomitant intoxication of the patient. As expected, the toxic plasma heme concentration could increase in patients after drug administration. Indeed, accounting for both the affinity constants of drug binding to HSA and to HSA-heme-Fe, and the plasma levels of drugs bound to FA7 (and even to other functionally linked sites FA2 and FA6), the molar fraction of the drug-bound HSA could decrease from 50-90% to 10-50% in the presence of specific ligands [1,2,5,8-10].

HSA-heme-Fe displays globin-like reactivity and spectroscopic properties. In particular, both HSA-heme-Fe(II) and HSA-heme-Fe(III) species bind NO [11-14]. Moreover, NO facilitates the reduction of the heme-Fe(III) atom with the concomitant formation of the HSA-heme-Fe(II)-NO species [13]. Furthermore, HSA-heme-Fe(II) undergoes reversible carbonylation [15]. On the other hand, HSA-heme-Fe(II) does not

undergo oxygenation since the heme-Fe(II)-atom is oxidized by O_2 [16].

Both endogenous and exogenous ligands modulate the heme-Fe-based reactivity of HSA-heme-Fe [5]. Indeed, drug binding to the FA7 primary site (*i.e.*, Sudlow's site I) and to the FA2 and FA6 clefts inhibits allosterically both HSA-heme-Fe(II) nitrosylation and denitrosylation process [11,12,14]. Moreover, drug (*i.e.*, ibuprofen and warfarin) binding to HSA-heme-Fe impair allosterically the detoxification of reactive nitrogen and oxygen species (*i.e.*, NO and peroxynitrite) [17-20].

Drug-dependent modulation of HSA-heme-Fe-based scavenging of reactive nitrogen and oxygen species could be relevant under physiological and pathological conditions [1,21,22]. HSA-heme-Fe(III) displays scavenging and detoxification functions by facilitating the conversion of NO to NO_2^- and NO_3^- and the isomerization of peroxynitrite to NO_3^- [17-20]. HSA-heme-Fe(III) also exhibits weak peroxidase and catalase activity, participating to the anti-oxidative homeostasis of the blood which contains little enzymes having related functions [23].

Remarkably, NO and peroxynitrite scavenging by HSA-heme-Fe could occur in patients affected with a variety of severe hematologic diseases characterized by massive intravascular hemolysis, and displaying high HSA-heme-Fe plasmatic levels [6,7]. Although the in vivo concentration of NO and peroxynitrite is openly debated, their levels have been reported to be much higher than micromolar concentration, at least over brief periods of time (see [18]). Moreover, the plasma level of prototypical drugs ibuprofen and warfarin is ca. 10^{-6} to 10^{-4} M (see [18]). Remarkably, concentrations of HSA-heme-Fe, reactive nitrogen species, and drugs used for in vitro studies overlap levels observed in vivo (see [1]).

The ligand- (*e.g.*, FA- and drug-) dependent conformational changes of HSA(-heme-Fe) are at the root of allosteric properties. The reversible N-to-B allosteric transition of

HSA is pivotal for binding, transport, and release at the disposal sites of endogenous and exogenous ligands. Ligand binding to the FA7 primary cleft (*i.e.*, Sudlow's site I) and to the secondary FA2 and FA6 sites impairs the FA1 binding capacity, stabilizing the N conformation of HSA. According to linked functions, ligand binding to FA1 stabilizes the B conformation of HSA, inhibiting ligand association to several clefts including the FA7 site [5].

It is currently accepted that the reversible N-to-B allosteric transition is characterized essentially by the distortion and the remarkable rotation of 16° of the long helix that connects domains I and II, with the consequent reorientation of amino acid side chains that form ligand binding cavities in domains I and II the modulatory site (Fig. 8). Actually, binding of long chain FAs to FA2 attracts Tyr150 and Arg257, two key residues positioned in the center of the apolar chamber of the FA7 cleft, towards the carboxylate moiety of the FA, rendering the drug pocket FA7 more hydrophobic [4]. On the other hand, the reorientation of Tyr150 drives the interaction of Phe149 with the heme, thus making a stabilizing π-π interaction and accounting for the allosteric modulation observed in solution studies [5]. This effect is not observed for short chain FAs that preferably bind to the FA3-FA4 cleft displacing the specific ligands (*e.g.*, ibuprofen) without inducing HSA allosteric rearrangement(s) [5]. Interestigly, His146 has been proposed to be the axial-ligand of the heme-Fe(III) atom upon ibuprofen binding, instead of Tyr150 in ligand-free HSA-heme-Fe(III) [24].

In order to give a precise molecular description of the allosteric properties of HSA, and hopefully make a good use of it in pharmaceutical industry, the characterization of natural and artificial mutants is pivotal to identify the key residues involved in ligand binding and controlling the conformational transition(s) [1].

Remarkably, the multiple metal binding properties of HSA seems to have a relevant role in the development of neuropathologies. Indeed, it has been reported that HSA can be

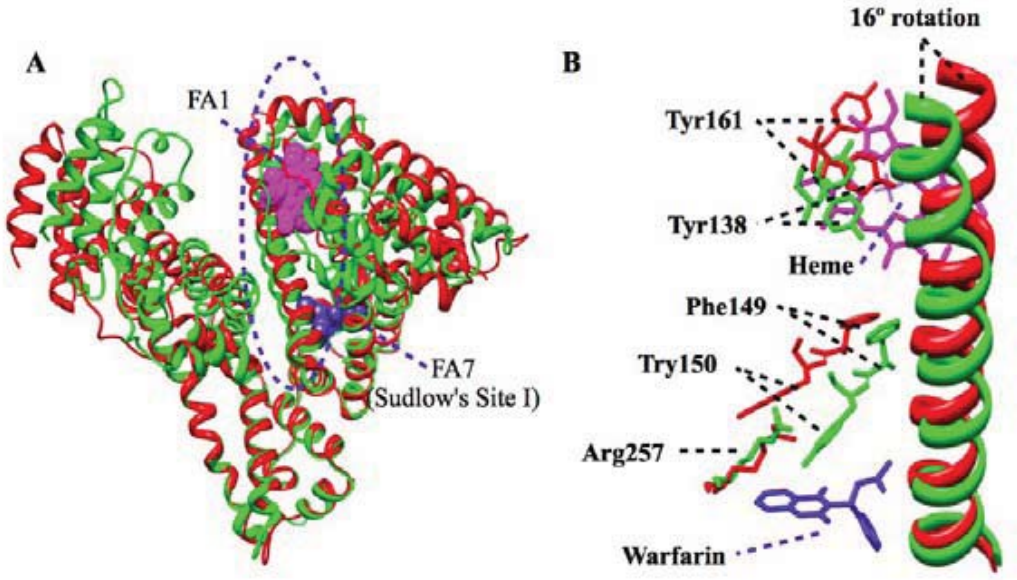

Fig. 8. The overlay structures of heme- and warfarin-bound HSA (panel A) and of the inter-domain helix connecting domains I and II (panel B). Heme- and warfarin-bound HSA are colored in red and green, respectively. The atomic coordinates have been retrieved from PDB entries 1O9X and 2BXD [27,28]. The picture was drawn with Chimera [29].

synthesized in human microglia cells [25]. HSA can bind Cu(II) and amyloid β-peptides (Aβ) in the cerebrospinal fluid, thus avoiding the progression of Aβ aggregation, probably playing a protective role against to Cu(II)/Aβ toxicity in the extracellular brain compartment [26].

Beyond the structural and functional viewpoints, the incredible versatility of HSA is of great challenge in evolution biology, physiology, and pathology. Although HSA is one of the most investigated proteins, some questions are in order. Is HSA essential? How can humans almost totally lacking HSA safely survive? Why many of the functions performed by HSA may be assumed by other plasma proteins? Answers to these and other questions could unveil several still unrecognized physiological roles of HSA. Here, structure-function relationships of HSA are reported and discussed with an emphasis to issues related to human health [1].

Lastly, the present data describe a curious situation where heme binding to a non-classical heme-protein (*i.e.*, HSA) confers (although transiently) ligand binding and (pseudo-)enzymatic properties. Moreover, HSA(-heme-Fe) properties appear to be affected by third components. Note that the effects arising from heme binding to HSA might have some role in the regulation of biological functions. Since these actions are dependent on the transient interaction of a ligand (*e.g.*, heme) with a carrier (*e.g.*, HSA), they have been called “chronosteric” effects (see [1]).

References

1. Fanali, G., di Masi, A., Trezza, V., et al., 2012. Human serum albumin: from bench to bed. Mol. Aspects Med., in press.
2. Fasano, M., Curry, S., Terreno, E., et al., 2005. The extraordinary ligand binding properties of human serum albumin. IUBMB Life 57, 787-796.

3. Ghuman, J., Zunszain, P.A., Petitpas, I., et al., 2005. Structural basis of the drug-binding specificity of human serum albumin. J. Mol. Biol. 353, 38-52.
4. Curry, S., 2009. Lessons from the crystallographic analysis of small molecule binding to human serum albumin. Drug. Metab. Pharmacokinet. 24, 342-357.
5. Ascenzi, P., and Fasano, M., 2010. Allostery in a monomeric protein: the case of human serum albumin. Biophys. Chem. 148, 16-22.
6. Muller-Eberhard, U., Javid, J., Liem, H.H., et al., 1968. Plasma concentrations of hemopexin, haptoglobin and heme in patients with various hemolytic diseases. Blood 32, 811-815.
7. Miller, Y.I., Shaklai, N., 1999. Kinetics of hemin distribution in plasma reveals its role in lipoprotein oxidation. Biochim. Biophys. Acta 1454, 153-164.
8. Ascenzi, P., Bocedi, A., Notari, S., et al., 2005. Heme impairs allosterically drug binding to human serum albumin Sudlow's site I. Biochem. Biophys. Res. Commun. 334, 481-486.
9. Bocedi, A., Notari, S., Menegatti, E., et al., 2005. Allosteric modulation of anti-HIV drug and ferric heme binding to human serum albumin. FEBS J. 272, 6287-6296.
10. Ascenzi, P., Bocedi, A., Notari, S., et al., 2006. Allosteric modulation of drug binding to human serum albumin. Mini Rev. Med. Chem. 6, 483-489.
11. Ascenzi, P., Imperi, F., Coletta, M., et al., 2008., Abacavir and warfarin modulate allosterically kinetics of NO dissociation from ferrous nitrosylated human serum heme-albumin. Biochem. Biophys. Res. Commun. 369, 686-691.
12. Ascenzi, P., di Masi, A., De Sanctis, G., et al., 2009. Ibuprofen modulates allosterically NO dissociation from ferrous nitrosylated human serum heme-albumin by binding to three sites. Biochem. Biophys. Res. Commun. 387, 83-86.

13. Ascenzi, P., Cao, Y., di Masi, A., et al., 2010. Reductive nitrosylation of ferric human serum heme-albumin. FEBS J. 277, 2474-2485.
14. Ascenzi, P., Cao, Y., Tundo, G.R., et al., 2011. Ibuprofen and warfarin modulate allosterically ferrous human serum heme-albumin nitrosylation. Biochem. Biophys. Res. Commun. 411, 185-189.
15. Cao, Y., Nicoletti, F.P., De Sanctis, G., et al., 2011. Evidence for pH-dependent multiple conformers in iron(II) heme-human serum albumin: spectroscopic and kinetic investigation of carbon monoxide binding. J. Biol. Inorg. Chem. doi: 10.1007/s00775-011-0837-0.
16. Tsuchida, E., Sou, K., Nakagawa, A., et al., 2009. Artificial oxygen carriers, hemoglobin vesicles and albumin-hemes, based on bioconjugate chemistry. Bioconjugate Chem. 20, 1419-1440.
17. Ascenzi, P., and Fasano, M., 2007. Abacavir modulates peroxynitrite-mediated oxidation of ferrous nitrosylated human serum heme-albumin. Biochem. Biophys. Res. Commun. 353, 469-474.
18. Ascenzi, P., di Masi, A., Coletta, M., et al., 2009. Ibuprofen impairs allosterically peroxynitrite isomerization by ferric human serum heme-albumin. J. Biol. Chem. 284, 31006-31017.
19. Ascenzi, P., Bolli, A., Gullotta, F., et al., 2010. Drug binding to Sudlow's site I impairs allosterically human serum heme-albumin-catalyzed peroxynitrite detoxification. IUBMB Life 62, 776-780.
20. Ascenzi, P., Bolli, A., di Masi, A., et al., 2011. Isoniazid and rifampicin inhibit allosterically heme binding to albumin and peroxynitrite isomerization by heme-albumin. J. Biol. Inorg. Chem. 16, 97-108.
21. Pacher, P., Beckman, J.S., and Liaudet, L., 2007, Nitric oxide and peroxynitrite in health and disease. Physiol Rev. 87, 315-424.

22. Trujillo, M., Ferrer-Sueta, G., and Radi, R., 2008, Peroxynitrite detoxification and its biologic implications. Antioxid. Redox Signal. 10, 1607-1620.
23. Monzani, E., Bonafè, B., Fallarini, A., et al., 2001. Enzymatic properties of hemalbumin. Biochim. Biophys. Acta 1547, 302-312.
24. Nicoletti, F.P., Howes, B.D., Fittipaldi, M., et al., 2008. Ibuprofen induces an allosteric conformational transition in the heme complex of human serum albumin with significant effects on heme ligation. J. Am. Chem. Soc. 130 11677-11688.
25. Ahn, S.M., Byun, K., Cho, K., et al., 2008. Human microglial cells synthesize albumin in brain. PLoS One. 3, e2829.
26. Rózga, M., and Bal, W. 2010. The Cu(II)βA human serum albumin model of control mechanism for copper-related amyloid neurotoxicity. Chem. Res. Toxicol. 23, 298-308.
27. Ghuman, J., Zunszain, P.A., Petitpas, I., et al., 2005. Structural basis of the drug-binding specificity of human serum albumin. J. Mol. Biol. 353, 38-52.
28. Wardell, M., Wang, Z., Ho, J.X., et al., 2002. The atomic structure of human methemalbumin at 1.9 Å. Biochem. Biophys. Res. Commun. 291, 813-819.
29. Pettersen, E.F., Goddard, T.D., Huang, C.C., et al., 2004. UCSF Chimera - a visualization system for exploratory research and analysis. J. Comput. Chem. 25, 1605-1612.

10. Acknowledgements

I am deeply grateful to Prof. Massimo Coletta (University of Roma “Tor Vergata”, Roma, Italy), Prof. Mauro Fasano and Dr. Gabriella Fanali (University of Insubria, Busto Arsizio, VA, Italy) for their patient and inspiring tutoring. My sincere thanks to University of Roma Tre that makes possibile these dynamic and wonderful years.